MULTIPHASE FLOW HANDBOOK

SECOND EDITION

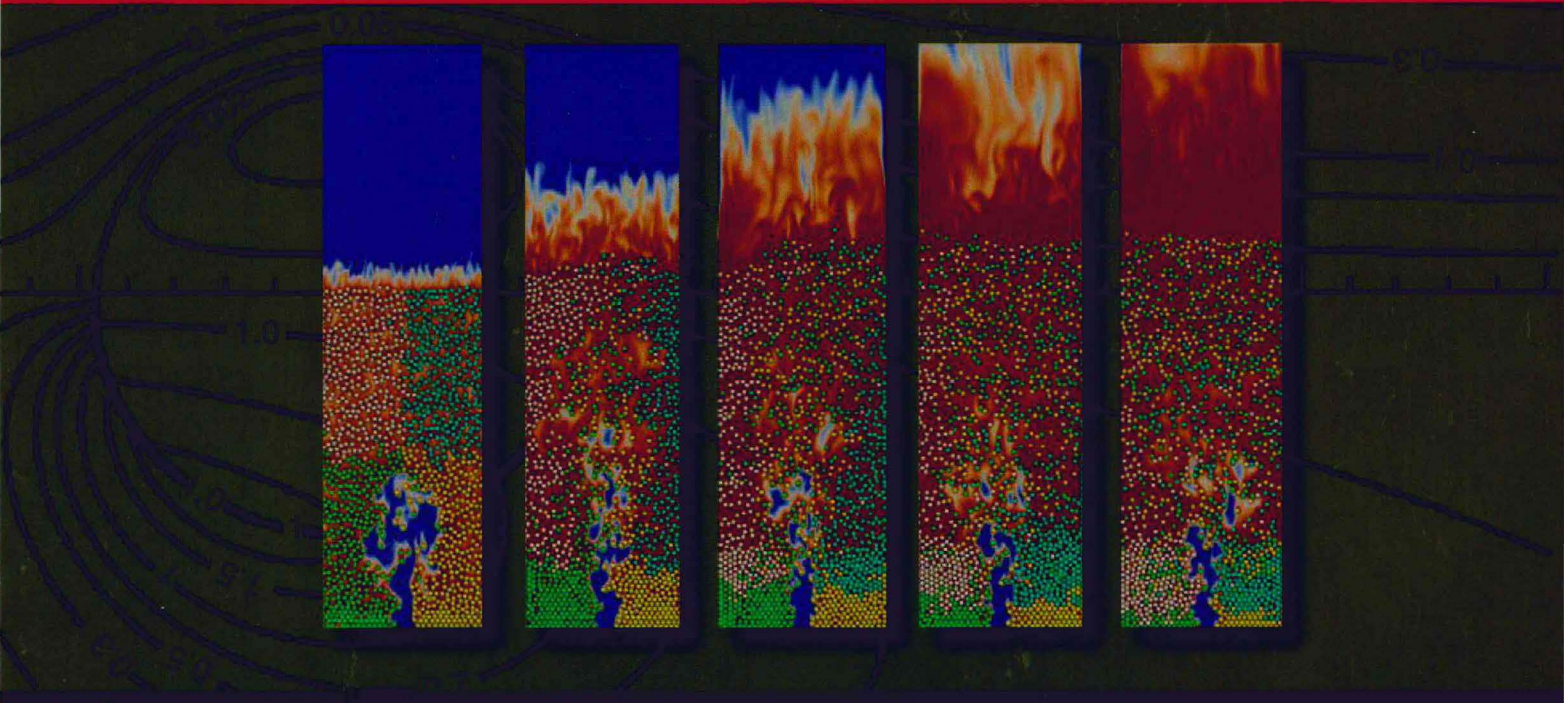

EDITED BY

Efstathios E. Michaelides

Clayton T. Crowe

John D. Schwarzkopf

CRC Press
Taylor & Francis Group

Contents

3

Gas–Liquid Flow in Ducts

Afshin J. Ghajar and Swanand M. Bhagwat

3.1 Introduction

The phenomenon of gas–liquid two-phase flow embraces several applications pertinent to oil and gas industry, process engineering, heat exchangers (evaporators and condensers), cooling of nuclear reactors, etc. Gas–liquid two-phase flows are classified as one-component and two-component two-phase flow. One-component two-phase flow consists of the two phases of a single chemical species such as steam water and refrigerant vapor–liquid flow used in nuclear and refrigeration applications, whereas two-component two-phase flow consists of the two phases of two chemically different species such as air–water and air–oil. The two-component two-phase flow is often referred to as nonboiling two-phase flow and is usually encountered in industrial applications such as artificial lift systems and simultaneous transportation of oil and natural gas from remote extraction locations to the processing units. Chemical operations requiring flow of two chemical species together for enhanced mass transfer, as in the case of ozone treatment of water, also rely on the two-component two-phase flow phenomenon. For the purpose of flow assurance and designing, sizing, and optimization of industrial processes and equipments handling two-phase flow, the determination of the void fraction, total two-phase pressure drop, and heat transfer is crucial. In particular, for nonboiling two-phase flow applications, the total two-phase pressure drop based on flow patterns, void fraction, and pipe geometry influences the design of a two-phase flow system. Knowledge of nonboiling heat transfer in two-component two-phase flows is equally important to estimate and prevent advent of wax deposition in subsea pipeline carrying hydrocarbons. The two-phase flow literature reports a plethora of correlations for the determination of flow patterns, void fraction, two-phase pressure drop, and nonboiling heat transfer correlations; however, the validity of a majority of these correlations is restricted over a narrow range of two-phase flow conditions. Consequently, it is quite a challenging task for the end user to select an appropriate correlation/model for the type of two-phase flow under consideration. Selection of a correct correlation also requires some fundamental understanding of the two-phase flow physics and the underlying principles/assumptions/limitations associated with these correlations. Thus, it is of significant interest for a design engineer to have knowledge of the flow patterns and their transitions and their influence on two-phase flow variables. To address some of these issues and facilitate selection of appropriate two-phase flow models, this chapter presents a succinct review of the flow patterns, void fraction, pressure drop, and nonboiling heat transfer phenomenon and recommend some of the well-scrutinized modeling techniques. Additionally, this chapter provides three illustrative

Table 3.1 Basic Definitions of Interest to Two-Phase Flow

Parameter	Definition	Description
x	$\frac{\dot{m}_G}{\dot{m}_G+\dot{m}_L}$	Two-phase flow quality
α_G	$\frac{A_G}{A}$ or $1-\frac{A_L}{A}$, $\frac{V_G}{V}$ or $1-\frac{V_L}{V}$	Void fraction
λ	$\frac{U_{SG}}{U_{SG}+U_{SL}}$ or $\left[1+\frac{1-x}{x}\left(\frac{\rho_G}{\rho_L}\right)\right]^{-1}$	Gas volumetric flow fraction
U_{SG}	$\frac{Gx}{\rho_G}$ or $\frac{\dot{m}_G}{A\rho_G}$	Superficial gas velocity (m/s)
U_{SL}	$\frac{G(1-x)}{\rho_L}$ or $\frac{\dot{m}_L}{A\rho_L}$	Superficial liquid velocity (m/s)
U_G	$\frac{U_{SG}}{\alpha_G}$ or $\frac{\dot{m}_G}{A_G\rho_G}$	Actual gas velocity (m/s)
U_L	$\frac{U_{SL}}{1-\alpha_G}$ or $\frac{\dot{m}_L}{A_L\rho_L}$	Actual liquid velocity (m/s)
U_M	$U_{SL}+U_{SG}$ or $U_L(1-\alpha_G)+U_G\alpha_G$	Two-phase mixture velocity (m/s)
S	$\frac{U_G}{U_L}$ or $\left(\frac{x}{1-x}\right)\left(\frac{1-\alpha_G}{\alpha_G}\right)\left(\frac{\rho_L}{\rho_G}\right)$	Slip ratio
Re_{SL}	$\frac{\rho_L U_{SL} D}{\mu_L}$ or $\frac{G(1-x)D}{\mu_L}$	Superficial liquid Reynolds number
Re_{SG}	$\frac{\rho_G U_{SG} D}{\mu_G}$ or $\frac{GxD}{\mu_G}$	Superficial gas Reynolds number

example problems focused on some iterative methods for the determination of void fraction and pressure drop and the use of Reynolds analogy–based and empirical heat transfer correlations for the calculation of nonboiling two-phase heat transfer.

3.1.1 Basic Concepts and Definitions

The gas–liquid two-phase flow is realistically a 3D flow with flow conditions and fluid properties varying with respect to the pipe cross section, length, and time. A valid assumption of 1D two-phase flow to a great extent simplifies several two-phase flow variables and modeling techniques. At the outset, this section introduces some of the primary variables used throughout this chapter and adopted by different two-phase flow models. The parameters listed in Table 3.1 are defined in context to single-phase flow of gas and liquid phase and their simple relationships that represent some two-phase flow variables. The two-phase flow quality (x) is defined using the mass flow rate of the gas ($\dot{m}_G$) and liquid ($\dot{m}_L$) phase and is similar to the thermodynamic quality based on enthalpy balance only when thermodynamic equilibrium exists between the two phases. Based on the measurement technique such as cross-sectional or volumetric method, void fraction (α_G) is defined as the ratio of pipe cross section/volume of pipe occupied by the gas to the total cross section/volume of the pipe. The gas volumetric flow fraction (λ) is essentially the homogeneous void fraction under the assumption of no slippage between the two phases. The phase superficial velocity (U_{SG} or U_{SL}) is defined assuming the phase mass flow rate/mass flux (G) through the entire pipe cross section (A). Actual phase velocity (U_G or U_L) is based on the phase mass flow rate through the pipe cross-sectional area (A_G or A_L) occupied by that phase. The two-phase mixture velocity is simply the summation of the superficial velocity of each phase. The slip ratio (S) is the ratio of actual gas-phase velocity to actual liquid-phase velocity. Finally, the phase superficial Reynolds number (Re_{SL} or Re_{SG}) is based on the phase superficial velocity, phase density (ρ_L or ρ_G), and phase dynamic viscosity (μ_L or μ_G).

3.2 Flow Patterns, Flow Maps, and Transition Theories

The physical structure of two-phase flow known as "flow pattern" is most fundamental among all two-phase flow variables and also forms the basis of two-phase flow modeling methods. Unlike single-phase flow theory, two-phase flow cannot be distinguished as laminar, transitional, or turbulent but rather is classified on the basis

of several user-defined flow patterns. In this section, a brief information about the flow patterns occurring in different pipe orientations, their mapping technique using physically measurable quantities, and mathematical models to estimate their existence is laid out.

3.2.1 Flow Patterns

The flow patterns observed in gas–liquid two-phase flow are quite intriguing in nature and depend on the alignment of one phase with respect to the other across the pipe cross section. The morphological variations in the structure of flow patterns are essentially due to the significantly different physical properties of the two phases such as viscosity and density, compressible nature of the gas phase, and the interaction between gravity, inertia, and buoyant forces. Correct understanding of the physical structure of flow patterns and their transition is instrumental in the general understanding of the mechanism of mass, momentum, and energy transfer in two-phase flow. This preliminary section of this chapter is aimed at describing the physical structure of some key flow patterns illustrated in Figure 3.1 and their physical variations as a function of varying two-phase flow conditions:

Bubbly flow: Bubbly flow often called as dispersed bubbly flow is characterized by the flow of small gas bubbles dispersed in continuous liquid medium. The size (much smaller than the pipe diameter), shape (typically spherical or oblong), and distribution (uniform, center peaked, or wall peaked) of bubble density depend upon the pipe geometry and inclination, fluid properties, and phase flow rates. For nonvertical pipe orientations, bubbly flow appears in the form of small bubbles oriented in the vicinity of pipe upper wall. With increase in liquid-phase flow rates, bubbles tend to get dispersed evenly across the pipe cross section to appear in the form of dispersed bubbly flow. In addition to the dispersed form, bubbly flow may also appear in the form of elongated or agglomerated bubbles during the transition from bubbly to slug or dispersed bubbly to slug/intermittent flows. This physical form of bubbly flow is often identified as bubbly–slug flow.

Slug flow: Slug flow is characterized by the alternate flow of gas and liquid slugs. The size (elongated and comparable to pipe diameter), shape (usually bullet shaped with hemispherical nose and a blunt tail), and frequency of slugs depend upon the pipe geometry, pipe orientation, and fluid properties. For horizontal and nonvertical upward pipe inclinations, gas slug is in the vicinity of the pipe upper wall while it is symmetrically distributed around the pipe axis in vertical flow orientation. The translational velocity of the gas slug along the pipe axis is a function of pipe orientation such that the upward pipe inclinations aid the slug motion, while the downward pipe inclinations oppose the slug motion. The length of the gas slugs reduces, while their frequency increases with increase in the liquid flow rate. The opposite is true for a fixed liquid flow rate and decreasing gas flow rates.

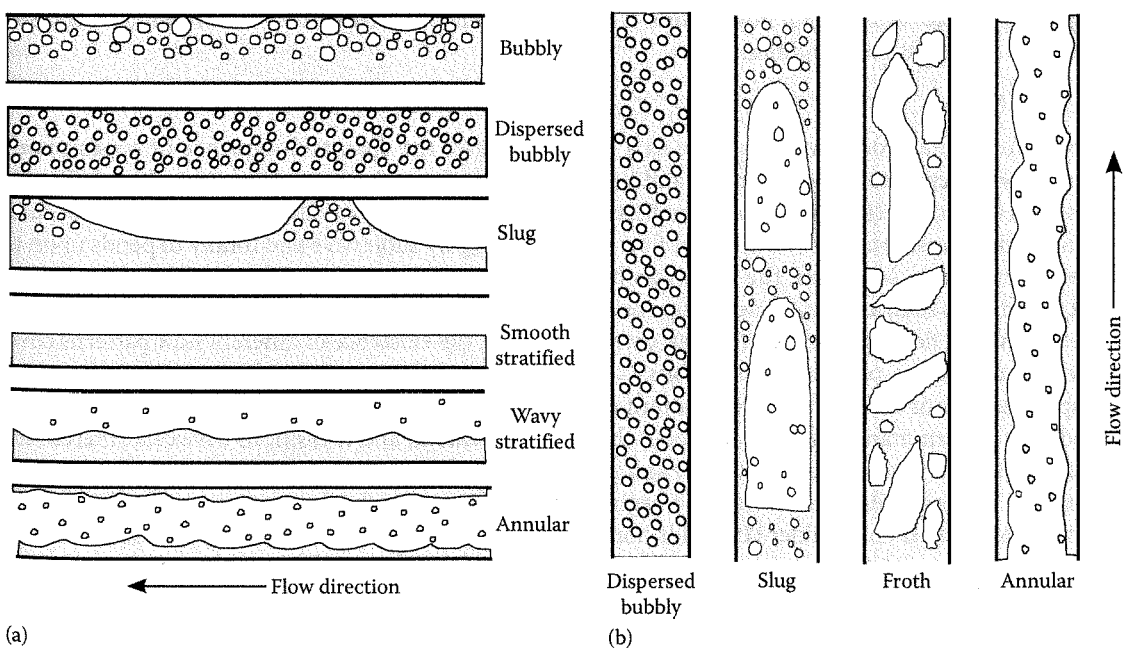

Figure 3.1

Flow patterns in (a) horizontal and (b) vertical upward gas–liquid two-phase flows.

Intermittent flow: The intermittent two-phase flow that typically exists at moderate gas and liquid flow rates is a representation of two-phase flow having chaotic, pulsating, and indefinite phase alignment characteristics. Different subcategories of key flow patterns such as slug wavy, annular wavy, churn, and froth flow exhibit disorderliness, intermittency, and indefinite flow structure, and hence, it is appropriate to club these all different subflow patterns together to call as intermittent flow. This approach of calling certain flow patterns as intermittent flow has been adopted by many researchers to reduce the ambiguity in identifying the transition boundaries between key flow patterns.

Stratified flow: Stratified flow exists in the form of gas and liquid layers flowing parallel to each other such that the pipe bottom wall is in contact with liquid phase, while the upper wall is in contact with the gas phase. Stratified flow in general can be classified as smooth stratified and wavy stratified flow. Smooth stratified flow appears at low liquid and low gas flow rates and is characterized by the complete separation of the two phases sharing a smooth and stable interface, whereas at high gas flow rates, the wavy stratified flow exists and it is characterized by the wavy, dynamic, and rough gas–liquid interface. At relatively high gas and liquid flow rates, the interfacial instability generates disturbance waves at the interface that grow and tend to touch the pipe wall giving an appearance of rolling wave. This type of stratified flow is recognized as rolling wave flow; however, the general flow structure still resembles the stratified flow pattern. A specific case of stratified flow identified as "falling film flow" is observed in vertical downward two-phase flow. The falling film flow is characterized by the downward flow of thin liquid film in contact with the pipe wall. Due to the physical resemblance of this flow pattern with the annular flow, some researchers have classified this flow pattern as a subregion of annular flow. However, there is a significant difference in these two-flow patterns in terms of the intensity of gas core turbulence, interfacial shear, thickness of liquid film, and the amount of liquid entrainment.

Annular flow: Annular flow appears in the form of a turbulent gas core surrounded by the thin/thick (depending upon liquid flow rates) and wavy liquid film. The liquid film distribution in annular flow is affected by the pipe orientation such that for horizontal flow, the asymmetric liquid film is thick at pipe bottom while it is evenly distributed around the circumference in case of vertical two-phase flow. Depending upon the gas and liquid flow rates, the gas–liquid interface may be stable or perturbed by small amplitude waves causing the liquid droplets to detach from liquid film and enter into the turbulent gas core known as the liquid entrainment phenomenon. The amplitude and frequency of interfacial disturbance waves and the amount of liquid entrainment depend on the phase flow rates, fluid properties, pipe geometry, and pipe inclination. A special form of annular flow also known as annular mist flow exists when most of the liquid phase initially flowing in the form of film is entrained into the central gas core by the shearing action of the fast-moving gas core. This type of flow pattern is mostly encountered in applications involving high system pressure and high heat flux conditions.

3.2.2 Flow Maps

The flow pattern maps or flow maps serve as a tool to estimate the span and sequence of appearance of different flow patterns with change in gas and liquid flow rates for a given set of flow conditions. The flow patterns and their transitions are defined qualitatively based on visual observations, and hence, the accurate mapping of the transition between different flow patterns is highly subjective and totally depends upon the observer's perception. Moreover, the transition between different flow patterns is gradual and sensitive to several parameters such as pipe diameter, pipe orientation, and fluid properties making it extremely difficult to have a universal flow pattern map that can correctly predict the existence of different flow patterns covering a wide range of two-phase flow conditions.

Despite the lack of the universal flow pattern map, it is important to consider some of the existing most referred flow pattern maps to get an idea about the sequence, extent, and transitions between different flow patterns. These flow pattern maps may serve as a guideline in understanding the appearance of flow patterns as a function of gas and liquid flow rates. To begin with, let us consider the flow pattern maps of Mandhane et al. (1974) and Taitel and Dukler (1976) for horizontal two-phase flow. The flow map of Mandhane et al. (1974) shown in Figure 3.2 is developed based on the two-phase flow parameters listed as follows:

$12.7 \leq D \leq 165.1$ mm	$0.0003 \leq \mu_L \leq 0.09$ Pa s
$705 \leq \rho_L \leq 1009$ kg/m^3	$10^{-5} \leq \mu_G \leq 2.2 \times 10^{-5}$ Pa s
$0.8 \leq \rho_G \leq 51$ kg/m^3	$0.024 \leq \sigma \leq 0.1$ N/m

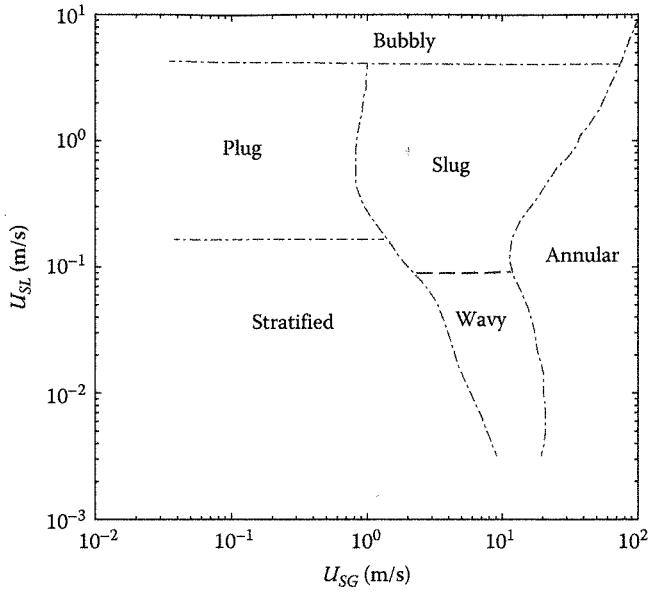

Figure 3.2

Flow pattern map for horizontal flow. (Adapted from Mandhane, J.M. et al., *Int. J. Multiphase Flow*, 1, 537, 1974.)

It is evident that the flow map of Mandhane et al. (1974) considers the existence of bubbly/dispersed bubbly flow to be insensitive to the change in liquid flow rate. Moreover, their flow pattern map shows a common transition boundary between slug and annular flow patterns. Based on the experience, it can be said that the slug flow in the vicinity of annular flow may not exhibit true slug flow characteristics and may appear in the form of agitated two-phase flow without any particular flow structure. Although the flow pattern map of Mandhane et al. (1974) is based on data consisting of a wide range of liquid-phase densities, their flow pattern map is claimed to be more accurate for air–water two-phase flow and is limited to horizontal pipe orientation.

The flow map of Taitel and Dukler (1976) shown in Figure 3.3 is based on mechanistic modeling of two-phase flow patterns and is presented in nondimensional form using the parameter X and parameters F and T of Lockhart and Martinelli (1949) shown in Equations 3.1 through 3.3. The parameter X of Lockhart and

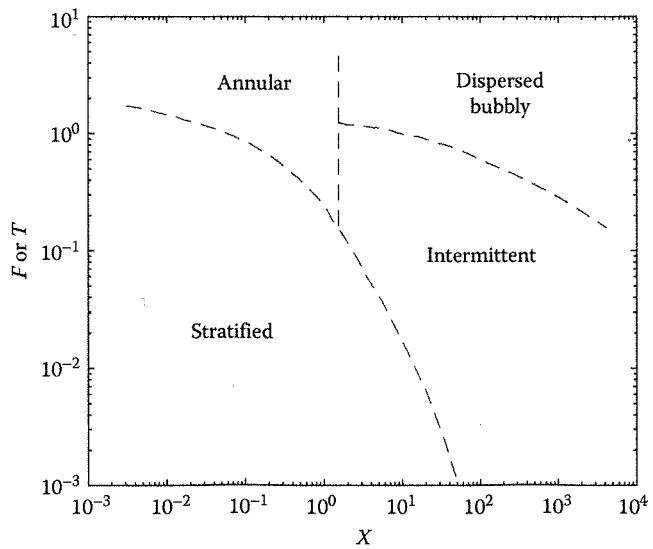

Figure 3.3

Flow pattern map for horizontal flow. (Adapted from Taitel, Y. and Dukler, A.E., *AIChE J.*, 22, 47, 1976.)

Martinelli (1949) is the square root of the ratio of the frictional pressure drop assuming single-phase flow of liquid ($(dp/dz)_L$) and gas ($(dp/dz)_G$) through the pipe, while parameter F is a modified Froude number based on superficial gas velocity (U_{SG}) and accounts for the effect of pipe orientation (θ) and phase densities (ρ_L and ρ_G). For the calculation of single-phase pressure drop, please refer to Section 3.4.7.1. The parameters $F-X$ are used to determine annular, stratified, and intermittent flows, while $T-X$ are used to determine the existence of dispersed bubbly flow. Unlike the flow map of Mandhane et al. (1974), Taitel and Dukler (1976) classify plug/slug/wavy flow patterns as intermittent flow. The flow pattern transition boundaries shown in Figure 3.3 are valid for horizontal two-phase flow. For other pipe orientations, these transition lines could be generated using the transition theories proposed by Taitel and Dukler (1976):

$$X = \sqrt{\frac{(dp/dz)_L}{(dp/dz)_G}} \tag{3.1}$$

$$F = \sqrt{\frac{\rho_G}{\rho_L - \rho_G}} \frac{U_{SG}}{\sqrt{gD}\cos\theta} \tag{3.2}$$

$$T = \sqrt{\frac{(dp/dz)_L}{(\rho_L - \rho_G) g \cos\theta}} \tag{3.3}$$

In case of vertical upward two-phase flow, the flow pattern map of Hewitt and Roberts (1969) developed for air–water two-phase flow and pipe diameters within the range of $10 \leq D \leq 30$ mm provides guidelines on the existence of different flow patterns and transition between them. The flow map of Hewitt and Roberts (1969) shown in Figure 3.4 is plotted using momentum flux of each phase. This flow map is also verified against the high-pressure steam–water data and is found to give satisfactory prediction of the flow patterns. With reference to the horizontal and vertical flow maps, the flow map (in terms of transition boundary between different flow patterns) is systematically affected by the change in upward pipe inclinations. Flow pattern maps for upward pipe inclinations shown in Figure 3.5 are based on the experimental observations and data collected at the Two-Phase Flow Lab, Oklahoma State University (OSU). It is evident from this

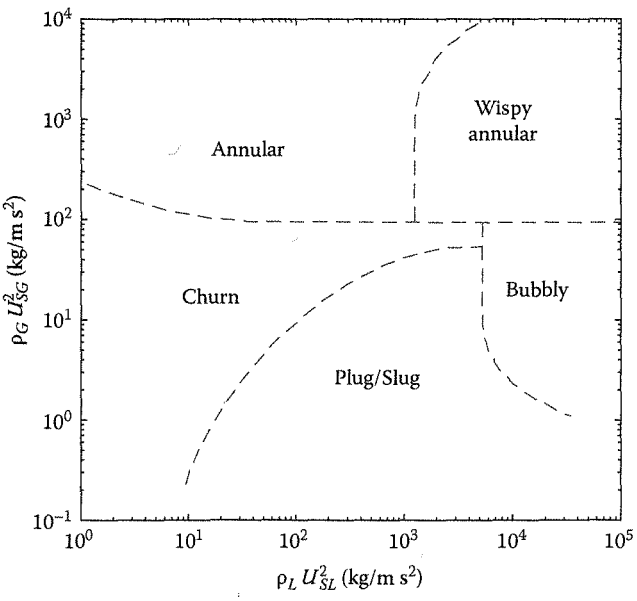

Figure 3.4

Flow pattern map for vertical upward flow. (Adapted from Hewitt, G.F. and Roberts, D.N., Studies of two phase flow patterns by simultaneous x-ray and flash photography, Technical Report AERE-M 2159, Atomic Energy Research Establishment, 1969.)

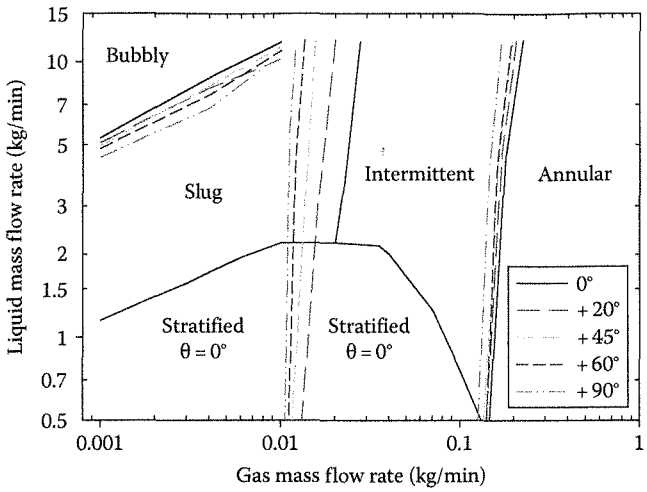

Figure 3.5

Flow pattern map for horizontal and upward inclined two-phase flows. (Based on flow visualization done at the Two-Phase Flow Lab, OSU, Stillwater, OK.)

figure that increase in the pipe orientation from horizontal toward vertical upward direction causes early transition from bubbly to slug flow and shifts the slug/intermittent flow transition line toward lower gas flow rates. The transition boundary between intermittent and annular flow regimes is virtually unaffected by the change in pipe orientation. Note that stratified flow exists in horizontal pipe orientations. For all upward pipe inclinations, this region of stratified flow is replaced by slug and intermittent flow patterns. In comparison to flow map for upward pipe inclinations, the flow pattern map for gas–liquid two-phase flow in downward pipe inclinations is of particular interest due to buoyancy-dominated two-phase flow regions in these orientations. Figure 3.6 shows representative flow pattern maps for different downward pipe inclinations based on flow visualization done at the Two-Phase Flow Lab, OSU. It is found that the effect of change in downward pipe orientation is significant on the transition between stratified–slug and stratified–intermittent flow patterns. The transition from stratified to slug flow regime shifts toward higher liquid flow rates with increase in downward pipe inclinations approximately up to $\theta = -45°$ from horizontal and then again decreases toward lower liquid flow rates thereafter.

It is quite interesting that unlike other pipe inclinations, in steeper downward orientations, two-phase flow pattern that exists inside a pipe for a fixed gas and liquid flow rates may exhibit a transient behavior. This small region where flow patterns tend to change with time is indicated in Figure 3.6. It is also seen that this transient nature of two-phase flow aggravates with increase in downward pipe inclination and propagates toward slightly higher gas flow rates. The transient behavior of flow patterns exists for steeper orientations and is always found to be in the vicinity of bubbly, slug, and stratified flow patterns. The visual observation of this transient nature of flow patterns can also be confirmed by analyzing the two-phase pressure drop signal in time domain as shown in Figure 3.7. A plausible explanation for the transient behavior of flow patterns can be given by considering the two-phase flow physics in downward pipe inclinations. A pressure drop signal in this unsteady region recorded over a period of time shows significant fluctuations. A visual observation of the flow pattern in the transparent test section during the pressure drop data acquisition can confirm the transient nature of two-phase flow that exhibits combined behavior of bubbly, slug, and stratified flows. It is seen that these flow patterns repeat one after another continuously without establishing one fixed flow pattern. For the case of stratified flow with very little gas flow rate, the liquid phase accelerates downstream under the influence of gravity, while the gas phase is believed to either stay virtually stationary or move upstream under the influence of buoyancy. As the liquid phase travels downstream, it further accelerates and creates unstable gas–liquid interface. These instabilities tend to grow at the gas–liquid interface and splash liquid on the pipe upper wall and further try to bridge the entire pipe cross section to trap a gas pocket in the form of slug flow. Slug flow pattern favors dominant buoyancy forces, and consequently, a pseudostationary elongated gas pocket (gas slug) is observed in the pipe. Meanwhile, the liquid phase coming from upstream direction gets accumulated on the top of pseudostationary slug that further slips past the elongated gas bubble and eventually forces the gas bubble to move in the downstream

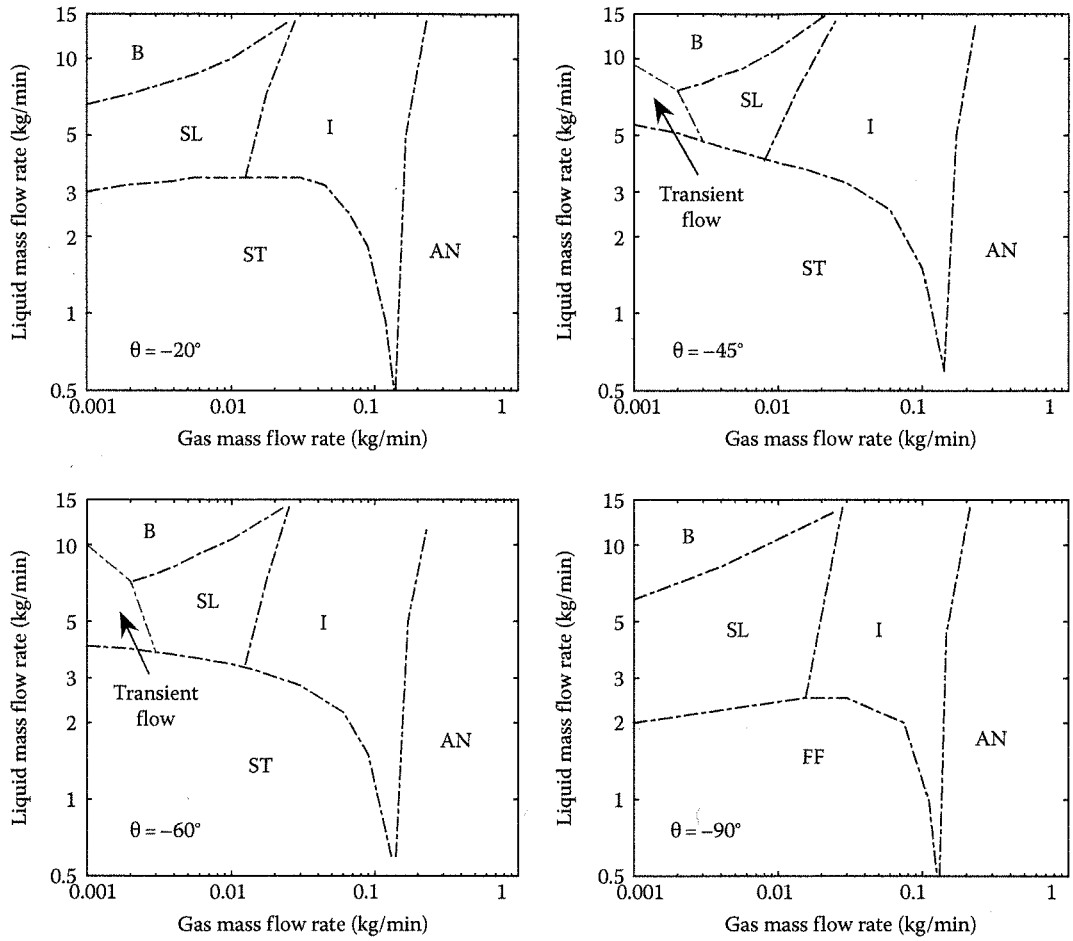

Figure 3.6

Flow pattern map for downward inclined two-phase flow. (Based on flow visualization done at the Two-Phase Flow Lab, OSU, Stillwater, OK.) (B, bubbly; SL, slug; I, intermittent; ST, stratified; FF, falling film; AN, annular.)

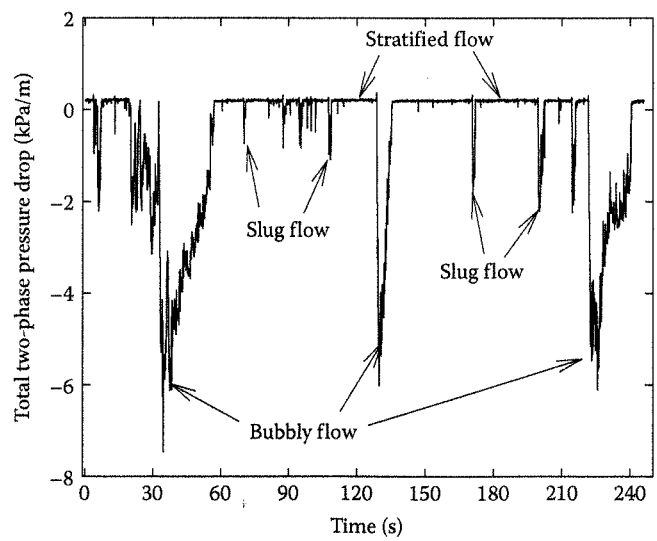

Figure 3.7

Variation in two-phase pressure drop due to transient nature of two-phase flow. (Based on data collected at the Two-Phase Flow Lab, OSU, Stillwater, OK.)

direction. During this process, the liquid phase churns the elongated gas bubbles causing it to disintegrate and move further in the form of small bubbles. After the gas pocket is pushed downstream, the incoming two-phase flow is again in the form of stratified flow pattern, and this process repeats continuously showing stratified, bubbly, and slug flow patterns periodically.

Considering the several forms of flow pattern maps reported earlier, it appears that it is difficult to have an exact agreement between the shape and trends of transition lines between specific flow patterns represented in different flow maps. This is partly because of the different coordinate systems adopted to generate flow maps and variations in the definitions of flow patterns adopted by different researchers. However, in a broad sense these flow pattern maps show agreement between the qualitative range (low, moderate, high) of gas and liquid flow rates that represent certain flow patterns. For instance, the bubbly flow appears at low gas and high liquid flow rates, intermittent and slug flow appears at moderate gas and liquid flow rates, and annular flow exists for low liquid and high gas flow rates. Another important issue that must be brought to the reader's attention is the "gradual" transition between different flow patterns. For the purpose of clarity, the transition boundaries between flow patterns are shown as thin lines; however, in reality, the transition region may be spread over a range of gas and liquid flow rates. In general, keeping in mind the uncertainty, sensitivity, and qualitative identification of flow patterns, following facts and limitations about the flow pattern maps must be perceived:

1. It is difficult to have a universal flow pattern map that can accurately predict the transition of one flow pattern to another for a wide range of two-phase flow conditions.
2. Unlike represented in most flow pattern maps, the transition from one flow pattern to another is always gradual and cannot be presented in the form of a thin continuous line.
3. Correct identification of a flow pattern in the vicinity of the transition line depends on the judgment of an individual.

3.2.3 Flow Pattern Transitions

The two-phase flow literature reports both mechanistic and empirical models to predict transition between different flow patterns. However, these transition models are developed based on the visual observations, limited data bank, and several simplifying assumptions that render uncertainty in their practical applications specifically if the two-phase flow under consideration is on the verge of transition. The following section provides some of the existing flow pattern transition models available in the two-phase flow literature. Considering the vague definition of intermittent flow pattern, the transition models listed here are only for well-defined flow regimes such as bubbly, slug, stratified, and annular flows.

3.2.3.1 Transition between Bubbly and Slug Flows

The transition from bubbly to slug flow occurs when bubbles no longer move independently and tend to coalesce to form a larger bubble usually known as the Taylor bubble. The transition from bubbly to slug flow can be achieved with the decrease in liquid flow rate at a constant gas flow rate or with increase in gas flow rate at a constant liquid flow rate. In general, the two-phase flow literature shows that this transition from bubbly to slug flow occurs for void fraction in the range of 0.25–0.3. The transition from bubbly to slug flow will occur if Equation 3.4 suggested by Taitel et al. (1980) is satisfied. This relationship is obtained by assuming that the maximum void fraction during transition from bubbly to slug flow is approximately 0.25 and that the bubble velocity is equal to the slip velocity ($U_b \cong U_G - U_L$). The bubble velocity at different pipe inclinations represented by Equation 3.5 is the modified form of Haramathy (1960) equation for bubble rise velocity suggested by Taitel et al. (1980) and Barnea (1987):

$$U_{SL} \leq 3U_{SG} - 1.32\left(\frac{\sigma g(\rho_L - \rho_G)}{\rho_L^2}\right)^{0.25} \sin\theta \Big\} (+60° \leq \theta \leq +90°) \tag{3.4}$$

$$U_b = 1.53\left[\frac{g\sigma(\rho_L - \rho_G)}{\rho_L^2}\right]^{0.25} \sqrt{1-\alpha_G}\,\sin\theta \tag{3.5}$$

Note that Equation 3.4 is recommended for use for near vertical pipe orientations ($+60° \leq \theta \leq +90°$) since as per Taitel et al. (1980) and Barnea (1987) it is difficult for bubbly flow to exist in horizontal and near

horizontal pipe orientations. Moreover, Taitel et al. (1980) also reported that the bubbly flow would exist if the pipe diameter of two-phase flow under consideration follows

$$D > 19\left(\frac{(\rho_L - \rho_G)\sigma}{\rho_L^2 g}\right)^{0.5} \tag{3.6}$$

Following a similar concept, Mishima and Ishii (1984) presented a model to predict transition between bubbly and slug flows (valid for vertical upward flow) of the form shown in Equation 3.7. The transition from bubbly to slug flow would occur if Equation 3.7 is satisfied. The parameter C_o is expressed as $C_o = 1.2 - 0.2\sqrt{\rho_G/\rho_L}$ such that for near atmospheric operating conditions $C_o \approx 1.2$. The bubble velocity equation (Equation 3.8) used by Mishima and Ishii (1984) is similar to Equation 3.5, however with different multiplying factors and exponents:

$$U_{SL} \leq \left(\frac{3.33}{C_o} - 1\right)U_{SG} - \frac{0.76}{C_o}\left(\frac{\sigma g \Delta\rho}{\rho_L^2}\right)^{0.25}\Bigg\}(\theta = +90°) \tag{3.7}$$

$$U_b = 1.41\left[\frac{g\sigma(\rho_L - \rho_G)}{\rho_L^2}\right]^{0.25}(1-\alpha_G)^{1.75} \tag{3.8}$$

For vertical upward flow, a comparison between Equations 3.4 and 3.7 shows that transition from bubbly to slug flow will occur at relatively lower U_{SL} using the criteria of Mishima and Ishii (1984). This discrepancy is essentially due to their assumption of $\alpha_G \approx 0.3$ during the transition and a slightly different form of bubble velocity (U_b) used by Mishima and Ishii (1984). As mentioned earlier, bubbly flow pattern can be further classified as bubbly–slug and dispersed bubbly flow. Thus, the bubbly flow predicted by Equations 3.4 and 3.7 may contain both bubbly–slug and dispersed bubbly two-phase flow. Unlike bubbly (elongated bubbly/slug bubbly) flow, the dispersed form of bubbly flow is known to exist in the entire range of pipe orientations, and its existence could be determined using the transition model of Barnea (1986). The model of Barnea (1986, 1987) requires calculation of three different diameters, namely, maximum bubble diameter ($d_{\max}$), critical bubble diameter above which bubble is deformed (d_{def}), and critical bubble diameter below which migration of bubbles is prevented (d_{migr}). These different bubble diameters could be determined from Equations 3.9 through 3.11, respectively. Thus, according to Barnea (1986), dispersed bubbly flow would exist if both $d_{\max} < d_{def}$ and $d_{\max} < d_{migr}$ conditions are satisfied. For these conditions typically at high liquid flow rates, dispersed bubbly flow exists since the turbulent fluctuations are capable to break down bubbles to spherical shape and also suppress the bubble coalesce that leads to slug formation.

$$d_{\max} = \left[0.725 + 4.15\left(\frac{U_{SG}}{U_M}\right)^{0.5}\right]\left(\frac{\sigma}{\rho_L}\right)^{0.6}\left(\frac{2f_M U_M^3}{D}\right)^{-0.4} \tag{3.9}$$

$$d_{def} = 2\left[\frac{0.4\sigma}{(\rho_L - \rho_G)g}\right]^{0.5} \tag{3.10}$$

$$d_{migr} = 0.375\left(\frac{f_M U_M^2 \rho_L}{g\cos\theta(\rho_L - \rho_G)}\right) \tag{3.11}$$

In Equation 3.9, f_M is friction factor based on two-phase mixture velocity U_M and can be calculated using any single-phase friction factor correlation. Considering the packing density and packing configuration of bubbles, Barnea (1986) showed that this transition model for dispersed bubbly flow is valid for void fraction in the range of $0 < \alpha_G \leq 0.52$. For dispersed bubbly flow, the slippage at gas–liquid interface is quite small and it can be assumed that $\alpha_G \approx \lambda$. Thus, the transition from dispersed bubbly to slug or intermittent flow would occur at $\lambda = U_{SG}/U_M > 0.52$.

3.2.3.2 Transition between Stratified and Nonstratified Flows

The stratified flow pattern exists only in horizontal and downward pipe inclinations, and hence, the transition model for estimating the existence of stratified flow is required to be used for this limited range of pipe orientations. The most referred transition model in the two-phase flow literature to separate out stratified flow from nonstratified flow is that of Taitel and Dukler (1976). Their transition model is based on the momentum balance between the two phases, assumes a smooth and flat gas–liquid interface such that $f_i/f_G \approx 1$, and gives the transition line equation that requires the use of a graphical solution. As per the model of Taitel and Dukler (1976), stratified flow will exist if Equation 3.12 is satisfied where F is defined by Equation 3.2:

$$F^2\left[\frac{1}{(1-\tilde{h}_L)^2}\frac{\tilde{U}_G\sqrt{1-(2\tilde{h}_L-1)^2}}{\tilde{A}_G}\right]<1 \tag{3.12}$$

The nondimensional parameters $\tilde{A}_G$ and $\tilde{U}_G=(\pi/4)/\tilde{A}_G$ are the function of nondimensional liquid height ($\tilde{h}_L=h_L/D$). The nondimensional pipe cross-sectional area occupied by the gas phase is calculated using Equation 3.13. As shown in Figure 3.8, the nondimensional liquid height $\tilde{h}_L$ is obtained through the graphical solution of $\tilde{h}_L$ versus X for different values of Y. The parameters X and Y are obtained from the following equations, respectively:

$$\tilde{A}_G=0.25\left[\cos^{-1}(2\tilde{h}_L-1)-(2\tilde{h}_L-1)\sqrt{1-(2\tilde{h}_L-1)^2}\right] \tag{3.13}$$

$$Y=\frac{(\rho_L-\rho_G)g\sin\theta}{(dp/dz)_G} \tag{3.14}$$

The application of Taitel and Dukler (1976) transition model to predict stratified flow is rather tedious due to the use of a graphical solution to determine nondimensional liquid height $\tilde{h}_L$ and consequently other parameters such as $\tilde{U}_G$ and $\tilde{A}_G$. The use of a graphical solution to determine h_L/D could be circumvented by adopting an iterative solution technique. For more details, refer to Taitel and Dukler (1976).

Taitel and Dukler (1976) further attempted to classify stratified flow as smooth stratified and wavy stratified flows. They suggested that the transition between smooth and wavy stratified flow is associated with the phenomenon of wave generation at the gas–liquid interface and that the smooth stratified flow exists

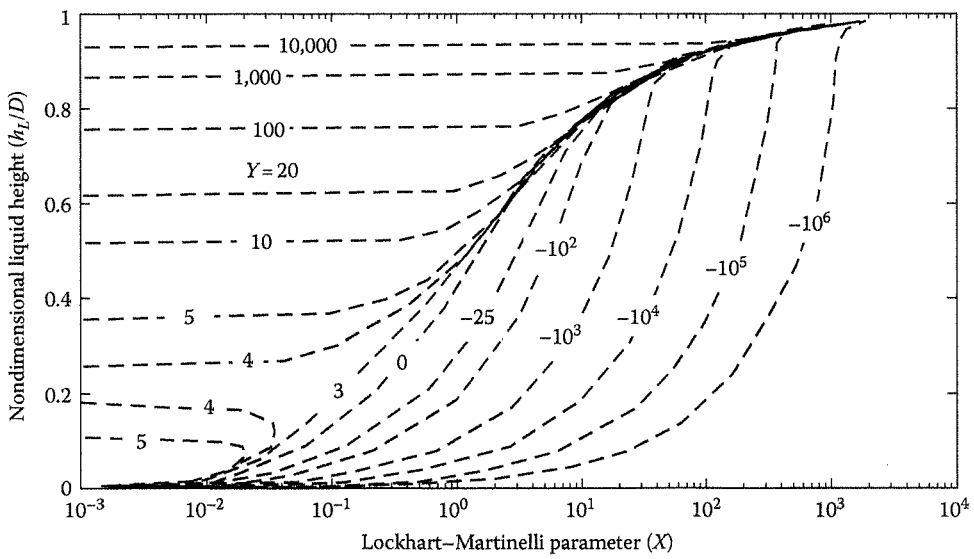

Figure 3.8

Graphical solution to determine the liquid-level height in stratified flow. (Adapted from Taitel, Y. and Dukler, A.E., *AIChE J.*, 22, 47, 1976.)

for superficial gas velocities (U_{SG}) that satisfy Equation 3.15. In practice, smooth stratified flow exists for a very narrow range of two-phase flow conditions and is of less practical significance compared to other flow patterns.

$$U_{SG,t} \geq \left(\frac{4\nu_L g \Delta\rho \cos\theta}{0.01\rho_L U_L} \right)^{0.5} \tag{3.15}$$

A simplifying approximation to the Taitel and Dukler (1976) model has been presented by Cheng et al. (1988). They approximated the trend of Equation 3.12 and presented a criterion given by Equation 3.16 to identify the existence of stratified flow pattern in horizontal pipes in terms of the parameter of Lockhart and Martinelli (1949) applicable for turbulent–turbulent gas–liquid two-phase flow where Fr is the modified Froude number given by Equation 3.17:

$$Fr_{SG} \leq \left(\frac{1}{0.65 + 1.11 X_{tt}^{0.6}} \right)^2 \tag{3.16}$$

$$Fr_{SG} = \frac{Gx}{\sqrt{gD\rho_G(\rho_L - \rho_G)}} = \frac{U_{SG}}{\sqrt{gD}} \sqrt{\frac{\rho_G}{\rho_L - \rho_G}} \tag{3.17}$$

Combining these equations gives the criteria for the existence of stratified flow in terms of two-phase mixture mass flux. Equation 3.18 represents the maximum value of two-phase mixture mass flux (for a given quality and fluid properties), below which stratified flow will always exist and is recommended for use only in case of horizontal two-phase flow:

$$G_{\max} = \frac{\sqrt{gD\rho_G(\rho_L - \rho_G)}}{x} \left(\frac{1}{0.65 + 1.11 X_{tt}^{0.6}} \right)^2 \Bigg\} (\theta = 0°) \tag{3.18}$$

Using the concept of growth of disturbance waves on the gas–liquid interface of stratified flow, Mishima and Ishii (1980) presented a criterion to determine the limit of stratified flow in horizontal two-phase flow. Note that the use of this correlation also requires the determination of liquid height that could be obtained using graphical solution given by Figure 3.8.

$$U_G - U_L = 0.487 \sqrt{\frac{g(D_h - h_L)(\rho_L - \rho_G)}{\rho_G}} \Bigg\} (\theta = 0°) \tag{3.19}$$

The recent work of Bhagwat and Ghajar (2015a) expressed by Equation 3.20 provides an empirical correlation to predict the existence of stratified flow in horizontal and downward pipe inclinations. Similar to the approach of Cheng et al. (1988), the correlation of Bhagwat and Ghajar (2015a) attempts to approximate the trends of Taitel and Dukler (1976) in terms of nondimensional parameters of Fr_{SG} and X and is developed based on the experimental data in horizontal and downward pipe inclinations. The Froude number in Equation 3.20 is similar to that given by Cheng et al. (1988) in Equation 3.17. The variables C_1, C_2, C_3, and C_4 required to solve Equation 3.20 are expressed by Equations 3.21 through 3.24. The nondimensional pipe diameter (D^+) is the normalized pipe diameter defined by $D^+ = D/0.0254$:

$$Fr_{SG} \leq (0.6 + C_2)\exp(-C_1 C_2 X^{C_3}) X^{-C_4} \Bigg\} \begin{array}{l} 12 < D < 150 \text{ mm} \\ 750 \leq \rho_L \leq 1420 \text{ kg/m}^3 \\ 1.2 \leq \rho_G \leq 35 \text{ kg/m}^3 \\ 0° \geq \theta > -90° \\ 0.0002 \leq \mu_L \leq 0.08 \text{ Pa s} \end{array} \tag{3.20}$$

$$C_1 = 1.3\ln(D^+) + 2.5 \tag{3.21}$$

$$C_2 = \frac{C_4^{0.65}}{\left[1 + 2\sin(2|\theta|) \times (1 + 10\tanh(1/|\theta|))\right]} \tag{3.22}$$

$$C_3 = \begin{cases} 0.65(D^+)^{-0.15}((\rho_L - \rho_G)/1000) & : \rho_L < 1000\ \text{kg/m}^3 \\ 0.65(D^+)^{-0.15} & : \rho_L \geq 1000\ \text{kg/m}^3 \end{cases} \tag{3.23}$$

$$C_4 = 0.2\sqrt{1/D^+} \tag{3.24}$$

Variables C_1 and C_2 account for the combined effect of pipe diameter and pipe orientation on the shift in transition line. The shift in transition line by including these variables is in accordance with the observations of Nguyen (1975), Barnea et al. (1982), Crawford et al. (1985), and Ghajar and Bhagwat (2014a) that the increase in downward pipe inclination shifts the transition between stratified and nonstratified flow patterns toward higher values of liquid flow rates or alternatively toward higher values of X. Variable C_3 ensures that the transition line between stratified and nonstratified flows is shifted toward higher values of X with a decrease in liquid-phase density. The variables C_1, C_2, C_3, and C_4 are adjusted such that C_1, C_2, and C_3 control the slope of transition line in the buoyancy-driven region (large values of X), while C_4 controls the slope of transition line in inertia-driven region (small values of X).

A graphical comparison between Taitel and Dukler (1976), Cheng et al. (1988), and Bhagwat and Ghajar (2015a) for horizontal two-phase flow is shown in Figure 3.9. Note that Bhagwat and Ghajar (2015a) model given by Equation 3.20 is of empirical form and merely attempts to mimic the trends of Taitel and Dukler (1976) model using $Fr_{SG} - X$ coordinates. Nevertheless, considering the practical difficulty of using a graphical/iterative solution involved in Taitel and Dukler (1976) model, Equation 3.20 may be regarded as a quick method for hand calculations and to get an estimate of the existence of stratified flow in horizontal and downward pipe inclinations.

3.2.3.3 Transition between Annular and Nonannular Flows

Typically, annular flow shares the transition boundary with intermittent (churn/annular wavy) flow patterns. Moreover, in case of horizontal and downward pipe inclinations, the annular flow also shares a transition

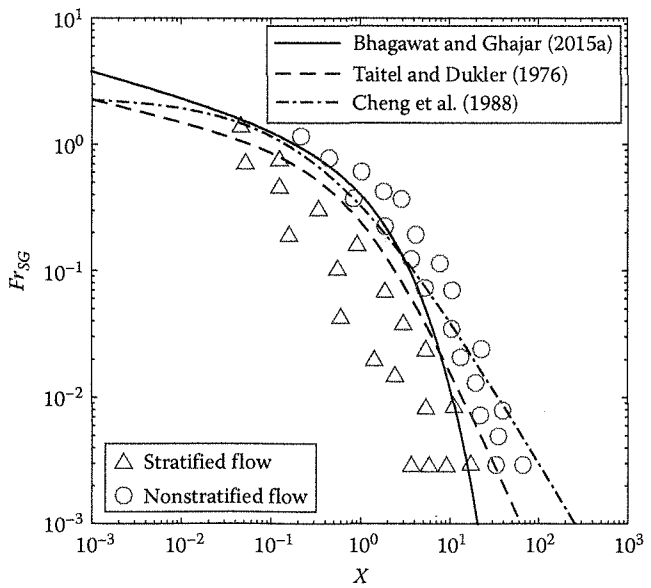

Figure 3.9

Trends of different stratified flow transition models for horizontal flow.

boundary with stratified flow pattern. In annular flow regime, the inertial forces greatly exceed the effect of gravitational forces, and hence, it is usually assumed that the change in pipe orientation will have little effect on the transition between annular and other flow regimes. However, pipe diameter and fluid properties do affect the transition to annular flow regime, and hence, it is desired to have a transition equation for annular flow regime as a function of both pipe diameter and fluid properties. One such transition criterion proposed by Weisman and Kang (1981) is expressed by Equation 3.25 and can be used for all pipe orientations. This criterion, however, at high liquid flow rates is found to incorrectly classify some region of the intermittent flow pattern as annular flow:

$$U_{SL} \geq U_{SG}\left[1.9\left(\frac{gD}{U_{SG}^2}\right)^{0.18}\left(\frac{g\Delta\rho\sigma}{U_{SG}\rho_G^2}\right)^{0.2}\right]^8 \tag{3.25}$$

Another simple yet practical approach to predict the transition to annular flow regime is based on nondimensional gas velocity (Froude number) corresponding to the point of pressure gradient minimum (concept discussed in Section 3.4.6). The two-phase flow literature for vertical upward flow reports that the pressure gradient minimum corresponds to the transition between churn/intermittent and annular flow regimes and the corresponding nondimensional gas velocity satisfies Equation 3.26. Based on the flow visualization and pressure drop measurements carried out at the Two-Phase Flow Lab, OSU, it is found that the criteria given by Equation 3.26 for transition to annular flow regime are a good approximation for the entire range of pipe orientations. The right-hand side of Equation 3.26 gives a range between which the nondimensional gas velocity can vary and for simplicity a value of 1.0 can be used. It also implies that the transition to annular flow regime would be independent of liquid velocity. Based on experience, it is recommended that in conjunction with Equation 3.26, additional simple criteria of $\alpha_G > 0.75$ can be used to confirm the existence of annular flow regime:

$$\frac{U_{SG}}{\sqrt{gD}}\sqrt{\frac{\rho_G}{(\rho_L-\rho_G)}} \geq 0.9-1.1 \tag{3.26}$$

Taitel et al. (1980) present a criterion for transition from dispersed bubbly to annular flow regimes. Their transition criteria based on force balance between the drag on liquid droplet and its weight lead to

$$\frac{U_{SG}\sqrt{\rho_G}}{(g\Delta\rho\sigma)^{0.25}} \geq 3.1 \tag{3.27}$$

A quick comparison between Equations 3.26 and 3.27 shows that the superficial gas velocity (U_{SG}) predicted by Equation 3.27 will always be higher than that predicted by Equation 3.26. This is possibly because Equation 3.26 gives transition to annular flow regime from churn/intermittent flow regimes at lower liquid flow rates, while Equation 3.27 predicts transition from dispersed bubbly flow at high liquid flow rates and hence would need higher gas flow rates for transition to annular flow regime. In addition to the transition theories, here we present in Table 3.2 a thumb rule based on the range of void fraction and qualitative range of gas and liquid flow rates associated with different flow patterns. It must be mentioned that this qualitative and quantitative range of two-phase flow variables is an approximate range based on experience and may give slight deviations compared to the real two-phase flow scenario.

Table 3.2 Thumb Rule for Qualitative Classification of Flow Patterns

	Mass/Volumetric Flow Rate		
Void Fraction (α_G)	Gas Phase	Liquid Phase	Flow Regime
Low ($\alpha_G \leq 0.25$)	Low	Moderate/High	Bubbly
Low to moderate ($0 \leq \alpha_G \leq 0.5$)	Low	High	Dispersed bubbly
Moderate ($0.25 < \alpha_G \leq 0.75$)	Low	Low/Moderate	Slug
Moderate ($0.25 < \alpha_G \leq 0.75$)	Moderate	Low/Moderate	Intermittent
Moderate to high ($0.3 < \alpha_G \leq 0.9$)	Low/Moderate	Low	Stratified
High ($0.75 < \alpha_G < 1$)	High	Low	Annular

3.3 Void Fraction

Void fraction (α_G) also referred to as liquid holdup ($\alpha_L = 1 - \alpha_G$) is defined based on its measurement technique such as local void fraction (using single-point probes), segmental void fraction (using gamma ray absorption method), cross-sectional void fraction (using capacitance probe), and volumetric void fraction (using quick closing valves). It must be noted that irrespective of the measurement technique $\alpha_G + \alpha_L = 1$. Among these different methods, typically the cross-sectional ($\alpha_G = A_G/A$) and volumetric ($\alpha_G = V_G/V$) types of void fraction measurement are most preferred and of practical importance. Under the adiabatic two-phase flow condition over a short pipe length, it can be assumed that the two-phase flow structure remains unaltered throughout the pipe length and cross-sectional void fraction can be equated to volumetric void fraction. The void fraction as a stand-alone physical parameter is typically of no use unless embedded in other constitutive equations to calculate parameters such as actual phase velocity, two-phase mixture density, and hence hydrostatic two-phase pressure drop and heat transfer, liquid height in stratified flow, and liquid film thickness in annular flow regime. Acknowledging the importance of void fraction in practical applications, this section first presents parametric analysis of the void fraction and then provides a quick review of the modeling techniques for the determination of the void fraction.

3.3.1 Effect of Pipe Orientation

The effect of pipe orientation on the void fraction is essentially due to the change in flow patterns and influence of buoyancy force acting on the gas phase. As shown in Figure 3.10, the effect of pipe orientation on void fraction is significant (up to 100%) for low gas and liquid flow rates. These flow rates correspond to slug/intermittent flow in upward pipe inclinations and stratified flow in downward pipe inclinations. At these flow rates, buoyancy acting on the gas phase aids the two-phase flow motion in upward pipe inclinations while resists its flow in downward pipe inclinations increasing its residence time in the pipe and hence the void fraction. For a fixed flow pattern (slug/intermittent) in upward inclined flow, it is seen that the void fraction initially decreases up to $+30° < \theta < +45°$ and then increases again with increase in the pipe orientation. This trend of change in void fraction with change in pipe orientation is due to the similar trend of the translational velocity of the gas slug (as a function of pipe orientation) that decides the residence time of the gas phase in the pipe and hence the void fraction. The effect of pipe orientation on void fraction is found to vanish for the inertia-driven region of intermittent (wavy annular) and annular two-phase flow. Moreover, the void fraction in stratified flow is apparently insensitive to the change in pipe orientation. At moderate

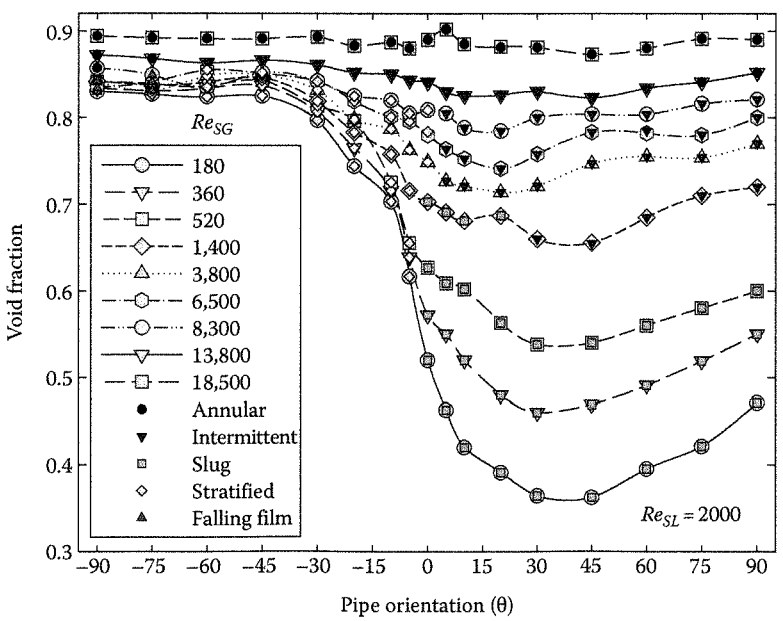

Figure 3.10

Effect of pipe orientation on void fraction at low liquid flow rates. (Data from the Two-Phase Flow Lab, OSU, Stillwater, OK.)

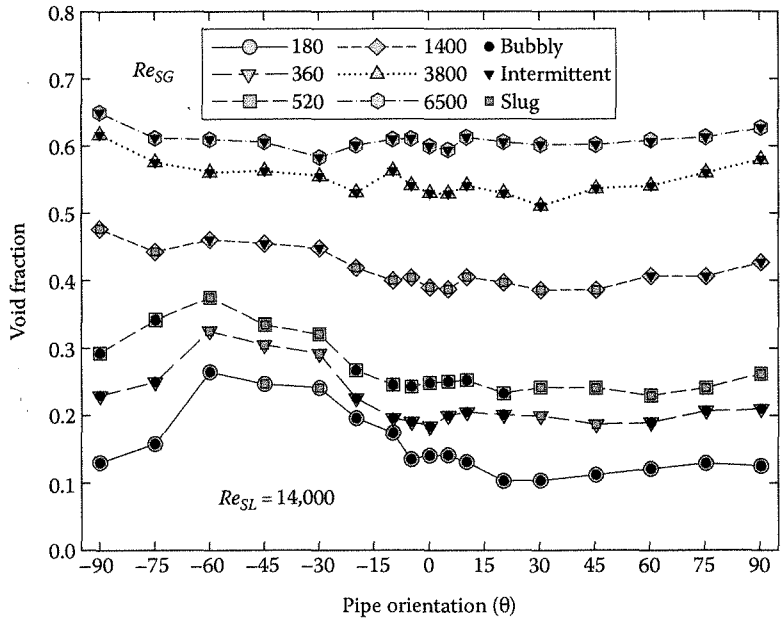

Figure 3.11

Effect of pipe orientation on void fraction at high liquid flow rates. (Data from the Two-Phase Flow Lab, OSU, Stillwater, OK.)

gas and liquid flow rates, void fraction in pipe orientations steeper than −45° drops downs due to the change in flow pattern from stratified to slug/intermittent at similar phase flow rates. As shown in Figure 3.11, at high liquid flow rates, the effect of pipe orientation on void fraction gradually fades away; however, a similar type of flip in void fraction trend as mentioned earlier occurs after −60° of pipe orientations. This change in trend of void fraction is again due to dissimilar flow patterns that may exist for similar phase flow rates but different pipe orientations. It is also clear from these trends that the void fraction in downward pipe inclinations is always greater than that in upward pipe inclinations essentially due to the resistance offered by the buoyancy force to the gas phase.

Considering the overall effect of the pipe orientation on the void fraction, three different relationships between α_G and λ can be deduced such that for buoyancy-driven flows $\alpha_G > \lambda$ and for inertia-driven flows $\alpha_G < \lambda$ hold true. The third relationship would be $\alpha_G = \lambda$ when the change in buoyancy to inertia-driven flow takes place. The relationship $\alpha_G > \lambda$ implies that for buoyancy-driven two-phase flow in downward pipe inclinations, the gas phase travels at a lower velocity than the liquid phase and hence results into higher void fraction values. Note that for all upward pipe inclinations, gas phase moves faster than the liquid phase giving a positive slippage at the gas–liquid interface and hence $\alpha_G < \lambda$ holds true. These three different cases of $\alpha_G - \lambda$ relationship that may exist in downward pipe inclinations are illustrated in Figure 3.12. In general, the flow patterns/pipe orientations that may correspond to these different cases of $\alpha_G - \lambda$ are summarized in Table 3.3.

3.3.2 Effect of Phase Flow Rates and Fluid Properties

The effect of phase flow rate on void fraction is indirectly through the change in flow pattern with change in phase flow rates. Figure 3.13 shows the effect of change in gas and liquid flow rate on void fraction. The void fraction data are plotted against a nondimensional phase velocity ratio (U_{SG}/U_{SL}) to reduce the scatter of the data. Broadly, the void fraction as a function of phase flow rates can be divided into three regions shown in Figure 3.13. In region I occupied by bubbly and slug flow patterns, for a fixed liquid flow rate, void fraction increases rapidly with a small increase in the gas flow rate, whereas in region III occupied by intermittent, stratified, and annular flow patterns, void fraction remains virtually independent of change in gas- and liquid-phase flow rates. Region II is a mixed bag of slug, intermittent, and stratified flow patterns, and its slope merges smoothly with that in regions I and III. Compared to other flow patterns, the void fraction corresponding to stratified flow shows a different behavior in region II. Void fraction in stratified flow regime remains relatively insensitive to the change in phase flow rates for

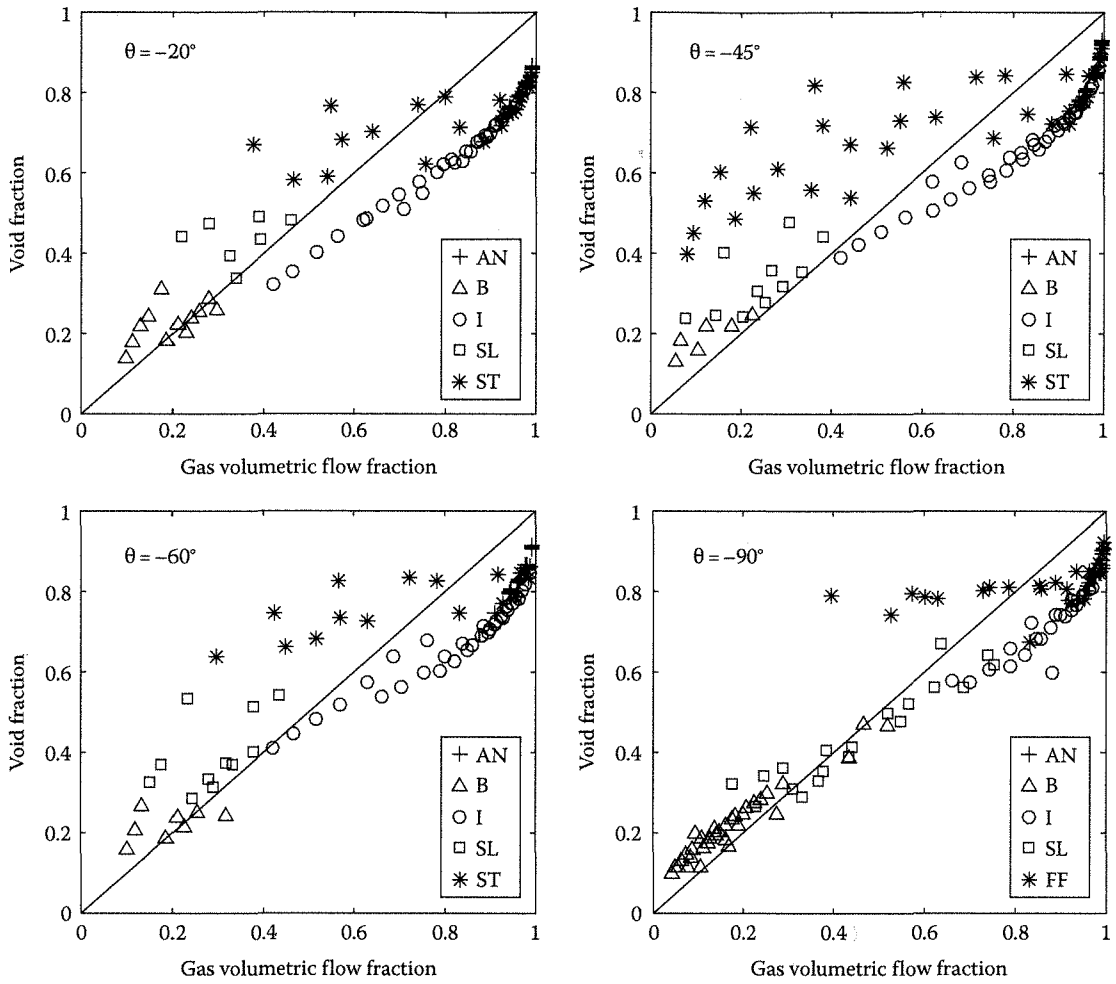

Figure 3.12

Void fraction and gas volumetric flow fraction relationship in downward pipe inclinations. (AN, annular; B, bubbly; FF, falling film; I, intermittent; SL, slug; ST, stratified.)

Table 3.3 Summary of Two-Phase Flow Situations Corresponding to $\alpha_G - \lambda$ Relationships

Condition	Flow Patterns/Pipe Orientation
$\alpha_G < \lambda$ ($U_G > U_L$, $S > 1$)	All flow patterns in upward pipe inclination
$\alpha_G = \lambda$ ($U_G \approx U_L$, $S \approx 1$)	Homogeneous flow (dispersed bubbly, annular mist)
$\alpha_G > \lambda$ ($U_G < U_L$, $S < 1$)	Stratified, slug flow $Fr_{SG} < 0.1$ and $\theta < 0°$

both regions II and III. Similar conclusions could be drawn by plotting the void fraction against two-phase flow quality, a well-adopted presentation style in high system pressure two-phase flows.

The variation of void fraction with change in two-phase flow quality is depicted in Figure 3.14 for (a) constant system pressure and varying slip ratios and (b) constant slip ratio and varying system pressure. For fixed two-phase flow conditions such as system pressure and quality, an increase in slip ratio reduces the void fraction. For these fixed conditions, the maximum void fraction is essentially the homogeneous void fraction obtained for no-slip condition ($S = 1$). In case of fixed slip ratio, an increase in system pressure decreases the specific volume occupied by the gas phase (due to increase in gas-phase density) and hence reduces the void fraction. Intuitively, it can be said that for a limiting case of critical system pressure or ($\rho_G \approx \rho_L$), void fraction varies linearly with change in two-phase flow quality ($\alpha_G = x$). Considering the definition of gas volumetric flow fraction (see Table 3.1), the relationship $\alpha_G = \lambda$ is also true for $\rho_G \approx \rho_L$. In addition to the gas-phase density, void fraction is also known to be affected by the

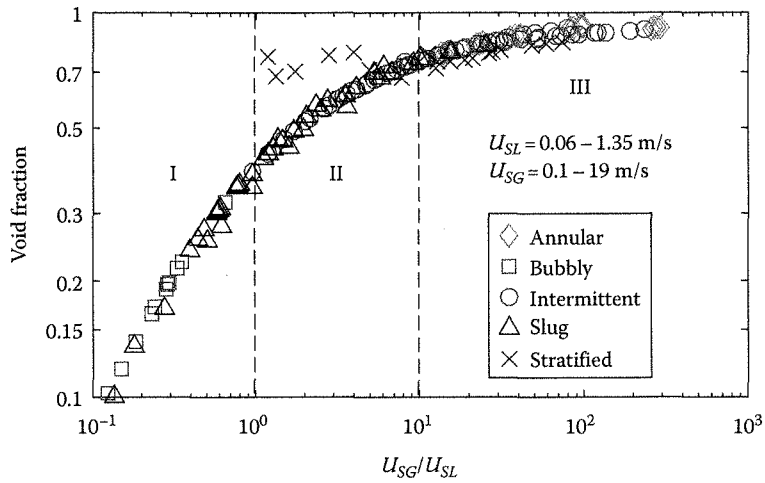

Figure 3.13

Variation of void fraction with change in gas and liquid flow rates.

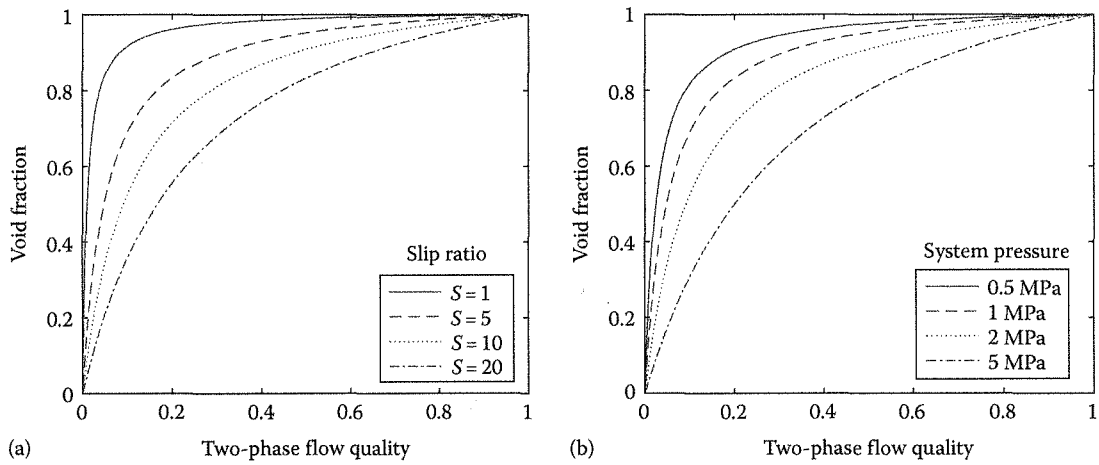

Figure 3.14

Variation of void fraction with change in two-phase flow quality. (a) System pressure = 1 MPa. (b) Slip ratio = 2.

change in liquid dynamic viscosity. Experiments of Oshinowo (1971), Mukherjee (1979), and Gokcal (2008) reveal that the void fraction is inversely proportional to the liquid dynamic viscosity. These studies report that the increase in liquid viscosity increases the viscous drag on liquid phase and reduces its velocity causing it to accumulate in the pipe and hence results in decrease in void fraction due to increase in liquid holdup.

3.3.3 Effect of Pipe Diameter

The effect of pipe diameter on void fraction is reflected in the form of pipe wall–induced drag exerted on the gas phase. In comparison to large pipes, small-diameter pipes offer more resistance to the motion of gas phase increasing its residence time and hence the local and averaged void fraction in pipes. Experimental data of Bowers and Hrnjak (2010) in Figure 3.15 show about 20%–80% increase in measured void fraction for a decrease in pipe diameter from 15 to 7 mm. The void fraction as a function of pipe diameter also depends upon phase flow rates (flow patterns/mass flux/quality) such that the effect of change in pipe diameter on void fraction is most prominent for bubbly/slug/intermittent flows, while it is fairly insensitive to the annular flow regime. Kaji and Azzopardi (2010) have reported negligible effect of change in pipe diameter (5–50 mm) on the void fraction in annular flow regime for similar gas and liquid superficial velocities. This relationship between void fraction and pipe diameter may not be applicable to microscale two-phase flow.

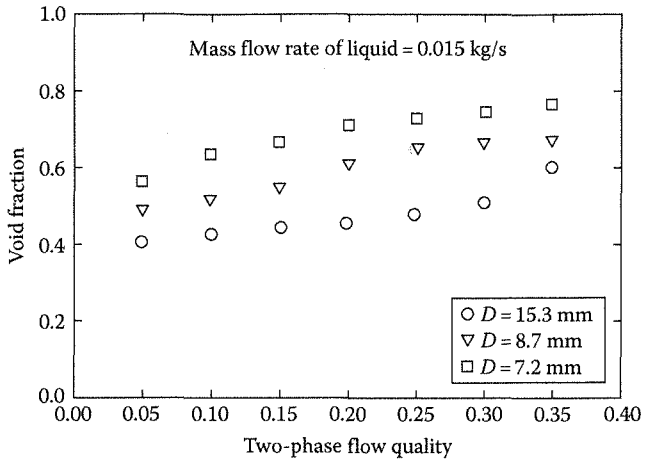

Figure 3.15

Effect of pipe diameter on void fraction. (Adapted from Bowers, C.D. and Hrnjak, P.S., Determination of void fraction in separated two phase flows using optical techniques, *International Refrigeration and Air-Conditioning Conference*, Purdue University, West Lafayette, IN, 2010, pp. 2293–2302.)

The parametric analysis of void fraction reveals that the void fraction must be modeled to consider the effect of flow patterns, pipe orientation, pipe diameters, and fluid properties. What follows is a brief review of some of the void fraction modeling methods available in the two-phase flow literature and recommendation of well-scrutinized void fraction correlations applicable for a wide range of two-phase flow conditions.

3.3.4 Modeling of Void Fraction

The two-phase flow literature reports a plethora of void fraction models/correlations; however, most of these models are confined to certain flow patterns, pipe orientation, and fluid properties. Based on the general physical form of these correlations, they can be broadly classified as those based on separated flow models (SFMs), drift flux model (DFM), $k - \lambda$ models, and empirical models. A comprehensive review of these different types of models is presented by Woldesemayat and Ghajar (2007), Godbole et al. (2011), and Ghajar and Bhagwat (2014b). Among all these models, correlations based on SFM and DFM are more versatile and flexible and are also preferred in several industrial applications. The following is a brief summary of the physical structure of SFM- and DFM-based void fraction correlations.

3.3.4.1 Separated Flow Model

The SFM considers the two phases to flow separately in the form of two streams: each phase is constant but with different velocities sharing a definite interface. The flow patterns such as stratified and annular flow behave as a separated flow and can be effectively modeled using these types of correlations. The SFM-based correlations are mostly preferred in refrigeration industry due to the stratified and annular flow pattern–dominated two-phase flow in evaporators and condensers. The general form of SFM-based void fraction correlations is presented in Equation 3.28. Some of the well-known SFM model-based void fraction correlations are listed in Table 3.4. The multiplying factor "S" is essentially the slip ratio, that is, the ratio of actual gas velocity (U_G) to actual liquid velocity (U_L) (see Table 3.1). The slip ratio (S) for homogeneous flow that assumes no slippage at

Table 3.4 Parameters Used in SFM by Different Correlations

Correlation	S	q	r	s
Homogeneous	1	1	1	0
Lockhart and Martinelli (1949)	0.28	0.64	0.36	0.07
Zivi (1964)	1	1	0.67	0
Chen (1986)	0.18	0.6	0.33	0.07
Smith (1969)	Equation 3.30	1	1	0
Xu and Fang (2014)	Equation 3.31	1	1	0

the gas–liquid interface is equal to unity ($S = U_G/U_L = 1$). Thus, for such a case, the void fraction expressed by Equation 3.28 is essentially equal to the gas volumetric flow fraction (λ) as shown in Equation 3.29:

$$\alpha_G = \left[1 + S\left(\frac{1-x}{x}\right)^q \left(\frac{\rho_G}{\rho_L}\right)^r \left(\frac{\mu_L}{\mu_G}\right)^s\right]^{-1} \tag{3.28}$$

$$\alpha_G = \left[1 + \left(\frac{1-x}{x}\right)\left(\frac{\rho_G}{\rho_L}\right)\right]^{-1} = \frac{U_{SG}}{U_{SG} + U_{SL}} = \lambda \tag{3.29}$$

$$S = 0.4 + 0.6\sqrt{\frac{\rho_L/\rho_G + 0.4(1/x - 1)}{1 + 0.4(1/x - 1)}} \quad \left.\begin{array}{l} 6 < D < 38\,\text{mm} \\ 0.1 \le p_{sys} \le 14.5\,\text{MPa} \\ 50 \le G \le 2050\,\text{kg/m}^2\,\text{s} \end{array}\right. \tag{3.30}$$

Equation 3.30 gives the expression for slip ratio used by Smith (1969). The constant of 0.4 used in Smith (1969) correlation is applicable only for circular pipes and may not guarantee accurate results for other pipe geometries. The correlation of Smith (1969) is valid for all flow patterns and the entire range of two-phase flow quality; however, it is observed that this correlation does not predict void fraction accurately in stratified flow regime. A recent work of Xu and Fang (2014) also provides an expression shown in Equation 3.31 to determine slip ratio to be used in SFM. Their model for slip ratio is mostly based on two-phase flow of refrigerants in small-size pipe ($D < 10$ mm) and is a function of mass flux, gas volumetric flow fraction, pipe diameter, and the liquid-phase density:

$$S = 1 + 2\lambda^{3.5}\left(\frac{G^2}{gD\rho_L^2}\right)^{-0.2} \quad \left.\begin{array}{l} 0.5 \le D \le 10\,\text{mm} \\ 40 \le G \le 1000\,\text{kg/m}^2\,\text{s} \\ 6 \le \rho_L/\rho_G \le 250 \end{array}\right. \tag{3.31}$$

Recently, Cioncolini and Thome (2012a) have developed a void fraction model for annular flow regime consisting of data for both circular and noncircular channels and applicable for both adiabatic and evaporating two-phase flows:

$$\alpha_G = \frac{hx^n}{1 + (h-1)x^n} \quad \left.\begin{array}{l} \text{(annular flow)} \\ 1 < D < 45.5\,\text{mm} \\ 0.1 < p_{sys} < 20\,\text{MPa} \\ 20 \le G \le 3400\,\text{kg/m}^2\,\text{s} \end{array}\right. \tag{3.32}$$

$$h = -2.129 + 3.129\left(\frac{\rho_G}{\rho_L}\right)^{-0.2186} \tag{3.33}$$

$$n = 0.3487 + 0.6513\left(\frac{\rho_G}{\rho_L}\right)^{0.515} \tag{3.34}$$

Figure 3.16 shows the discrepancy between predictions of void fraction by different SFMs typically for $\alpha_G < 0.7$. This difference between the outcomes of different correlations is probably because these correlations

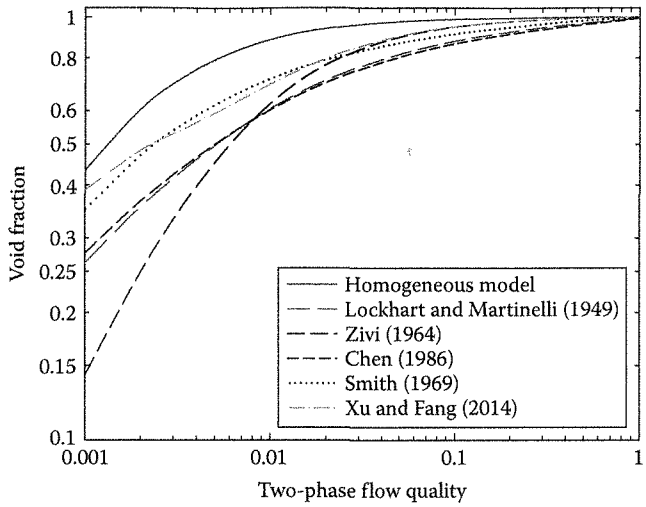

Figure 3.16

Void fraction prediction of separated flow models.

are based on the assumptions and flow physics of annular (separated) flow and are supposed to be used for higher values of void fraction. It is also evident that the homogeneous void fraction (under no-slip assumption) is the highest and sets the theoretical limit of the maximum possible void fraction in two-phase flow systems. This statement is true for all two-phase flow situations with the exception of buoyancy-driven region in downward pipe inclinations identified by $Fr_{SG} < 0.1$. Note that since these correlations based on SFM are essentially developed or valid for annular flow regime and since annular flow is relatively insensitive to the change in pipe orientation, these models can be used independent of pipe orientations provided annular flow pattern exists.

3.3.4.2 Drift Flux Model

The DFM assumes one phase dispersed in other continuous phase and requires the determination of distribution parameter (C_o) and drift velocity (U_{GM}) as variables to calculate the void fraction. The DFM is best applicable for 1D flows and is usually not recommended for flow patterns involving significant interfacial slippage such as stratified and annular flow patterns. The flow patterns such as bubbly flow, slug flow, and mist flow are the preferred flow patterns to be modeled using the concept of drift flux. However, with appropriate formulations that consider the two-phase flow physics, the application of DFM can also be extended to other flow patterns such as annular flow. The general form of DFM to calculate void fraction is presented by

$$\langle \alpha_G \rangle = \frac{\langle U_{SG} \rangle}{C_o \langle U_M \rangle + \langle \langle U_{GM} \rangle \rangle} \tag{3.35}$$

where $U_M = U_{SL} + U_{SG}$.

The terms involving $\langle\rangle$ represent cross-sectional averaged properties, while those involving $\langle\langle\rangle\rangle$ indicate cross-sectional and void fraction weighted averaged properties. The distribution parameter C_o is a representation to account for the distribution of the gas phase across the pipe cross section (concentration profile). It also serves as a correction factor to the homogeneous flow theory (which assumes no local slip between the two phases) to acknowledge the fact that the concentration profile and the two-phase flow velocity profile can vary independently of each other across the pipe cross section. Whereas the physical interpretation of drift velocity (U_{GM}) is the cross-sectional void fraction weighted average of the local relative velocity of the gas phase with respect to the two-phase mixture velocity at the pipe volume center. The local relative motion between the gas- and the two-phase mixtures is considerable and uniform across the pipe cross section when there is a strong coupling between the two phases as in case of the flow of dispersed bubbles in continuous liquid medium, that is, dispersed bubbly flow. As the two-phase flow transits to annular flow regime, the local relative velocity of the gas phase with

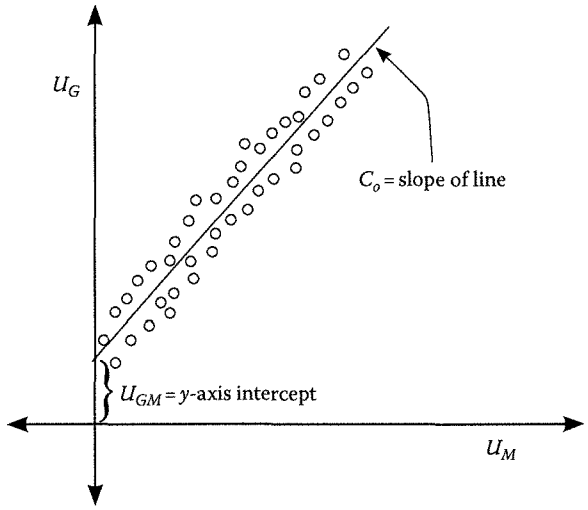

Figure 3.17

Graphical representation of drift flux model.

respect to the two-phase mixture at the pipe volume center becomes negligible and so does the drift velocity. Although the 1D DFM is used in the context of cross-sectional averaged void fraction, there are several DFM-based correlations available in the literature that can be practically implemented for void fraction calculations based on volumetric void fraction experimental data instead of the cross-sectional void fraction. The parity between the cross-sectional and volumetric void fraction holds true in case of nonboiling two-phase flow (two-component two-phase flow) where the cross-sectional distribution of the gas phase with respect to the liquid phase remains virtually unaltered over a short length of pipe. Henceforth, without making any distinction between the cross-sectional and volumetric void fractions, the void fraction is simply expressed as $\langle\alpha_G\rangle = \alpha_G$. Similar justification is applicable for all the cross-sectional averaged quantities involved in Equation 3.35. The physical form of Equation 3.35 resembles the equation of a straight line ($y = mx + c$) shown in Figure 3.17 such that the distribution parameter C_o is analogous to the slope "m" and the drift velocity is analogous to the y-intercept "c." Thus, the distribution parameter and the drift velocity could be obtained by plotting the data with $U_G = U_{SG}/\alpha_G$ and U_M coordinates and then by finding the slope and intercept of the best-fitting line. However, this method is highly impractical since the slope and intercept of line would depend on the scatter of data and cannot be used in case of real-time applications where void fraction information is not known beforehand. Obviously, another approach to determine C_o and U_{GM} is to use empirical correlations (as a function of two-phase flow variables) available in the two-phase flow literature. The following text presents some of the well-scrutinized and validated flow pattern–specific and flow pattern–independent correlations to determine C_o and U_{GM}.

The distribution parameter and drift velocity equations given by Hibiki and Ishii (2003) for vertical upward bubbly flow are given in Equation 3.36. To use these equations, the existence of bubbly flow could be determined by first using flow pattern transition equation given by Equation 3.7.

$$\left.\begin{aligned} C_o &= \left(1.2-0.2\sqrt{\frac{\rho_G}{\rho_L}}\right)\left(1-\exp(-18\alpha_G)\right) \\ U_{GM} &= \sqrt{2}\left(\frac{\sigma g(\rho_L-\rho_G)}{\rho_L^2}\right)^{0.25}(1-\alpha_G)^{1.75} \end{aligned}\right\} \quad \begin{matrix}\text{(bubbly flow)} \\ \theta = +90^\circ\end{matrix} \tag{3.36}$$

Another most referred void fraction model for bubbly flow is that of Gomez et al. (2000) given by Equation 3.37. This model is essentially developed for upward pipe inclinations, and it may not reproduce correct results if used for horizontal two-phase flow since Equation 3.37 would give $U_{GM} = 0$. Moreover, Gomez et al. (2000) have recommended the use of a constant to represent distribution parameter that does not account for the effect of fluid properties, flow properties, and pipe orientation on the

distribution parameter. Although the void fraction model of Gomez et al. (2000) is developed for bubbly flow, our experience shows that this correlation also works well for the slug flow regime. Note that to use Equation 3.37, the existence of bubbly flow can be confirmed by using bubbly–slug flow transition model given by Equation 3.4:

$$\left.\begin{aligned} C_o &= 1.15 \\ U_{GM} &= 1.53\left(\frac{g\sigma(\rho_L-\rho_G)}{\rho_L^2}\right)^{0.25}\sqrt{1-\alpha_G}\sin\theta \end{aligned}\right\} \quad \begin{matrix}\text{(bubbly, slug flow)} \\ 0° < \theta \le +90°\end{matrix} \tag{3.37}$$

For slug flow regime, Hibiki and Ishii (2003) proposed expressions for distribution parameter and drift velocity given by Equation 3.38. The drift velocity used in their equations is essentially the modified form of proportionality (between pipe diameter and slug translational velocity) proposed by Nicklin et al. (1962). These correlations given by Equations 3.36 and 3.38 are valid for small-diameter pipes ($10 < D_h < 50$ mm). For large-diameter pipes, Kataoka and Ishii (1987) have proposed sets of equations given by Equation 3.39 to account for the effect of pipe diameter and fluid properties on the drift velocity. The nondimensional hydraulic pipe diameter (D_h^+), nondimensional drift velocity (U_{GM}^+), and viscosity number (N_μ) are defined by Equations 3.40 through 3.42, respectively. Their equation is developed based on data of air–water and steam–water vertical upward two-phase flow consisting of data with $20 < D_h < 240$ mm and $0.1 \le p_{sys} \le 18$ MPa. The distribution parameter of Kataoka and Ishii (1987) correlation is the same as that of Equation 3.38. In case of two-phase flow through rectangular ducts, the constants "1.2" and "0.2" in Equation 3.38 are replaced by "1.35" and "0.35," respectively:

$$\left.\begin{aligned} C_o &= \left(1.2-0.2\sqrt{\frac{\rho_G}{\rho_L}}\right) \\ U_{GM} &= 0.35\sqrt{\frac{gD(\rho_L-\rho_G)}{\rho_L}} \end{aligned}\right\} \quad \begin{matrix}\text{(slug flow)} \\ \theta = +90°\end{matrix} \tag{3.38}$$

$$U_{GM}^+ = \begin{cases} 0.00019(D_h^+)^{0.809}\left(\dfrac{\rho_G}{\rho_L}\right)^{-0.157} N_\mu^{-0.562} & : N_\mu \le 2.25\times10^{-3}, D_h^+ > 30 \\ 0.030\left(\dfrac{\rho_G}{\rho_L}\right)^{-0.157} N_\mu^{-0.562} & : N_\mu \le 2.25\times10^{-3}, D_h^+ \le 30 \\ 0.92\left(\dfrac{\rho_G}{\rho_L}\right)^{-0.157} & : N_\mu > 2.25\times10^{-3} \end{cases} \tag{3.39}$$

$$D_h^+ = \frac{D_h}{\sqrt{\sigma/(g\Delta\rho)}} \tag{3.40}$$

$$U_{GM}^+ = \frac{U_{GM}}{((\sigma g\Delta\rho)/\rho_L^2)^{0.25}} \tag{3.41}$$

$$N_\mu = \frac{\mu_L}{(\rho_L\sigma\sqrt{\sigma/(g\Delta\rho)})^{0.5}} \tag{3.42}$$

The DFM-based void fraction correlation of Rouhani and Axelsson (1970) given by Equations 3.43 and 3.44 is one of the most preferred correlations used in refrigeration industry to estimate void fraction in

evaporators and condensers. The term $(1 - x)$ ensures decrease in distribution parameter with increase in two-phase flow quality or alternatively shift of flow pattern from bubbly/slug to annular flow.

$$C_o = \begin{cases} 1+0.2(1-x)\left(\dfrac{gD\rho_L^2}{G^2}\right)^{0.25} & : \theta = +90°, 0.1 \le p_{sys} \le 14\,\text{MPa} \\ 1+0.12(1-x) & : \theta = 0°, 0.1 \le p_{sys} \le 14\,\text{MPa} \end{cases} \tag{3.43}$$

$$U_{GM} = 1.18\left[\frac{g\sigma(\rho_L - \rho_G)}{\rho_L^2}\right]^{0.25} \tag{3.44}$$

To get rid of the flow pattern dependency, Woldesemayat and Ghajar (2007) proposed equations for distribution parameter and drift velocity as a function of fluid properties, pipe diameter, and pipe orientation shown in Equations 3.45 and 3.46. Woldesemayat and Ghajar (2007) correlation is a modification of Dix (1971) correlation for two-phase flow over rod bundles and is independent of flow patterns. The correlation of Woldesemayat and Ghajar (2007) is verified against data for horizontal and the entire range of upward pipe inclinations and pipe diameters in the range of 12–80 mm. In case of unknown flow pattern in horizontal and upward pipe inclinations, Woldesemayat and Ghajar (2007) correlation can be used with a reasonable accuracy (except for stratified flow). Note that the multiplying factor of 2.9 has units of $m^{-0.25}$.

$$C_o = \lambda\left(1+\left[\frac{U_{SL}}{U_{SG}}\right]^{(\rho_G/\rho_L)^{0.1}}\right) \tag{3.45}$$

$$U_{GM} = 2.9\left[\frac{gD\sigma(1+\cos\theta)(\rho_L - \rho_G)}{\rho_L^2}\right]^{0.25}(1.22+1.22\sin\theta)^{p_{atm}/p_{sys}} \tag{3.46}$$

A recent modeling work of Bhagwat and Ghajar (2014) considers the effect of flow patterns (in the form of phase flow rates), pipe orientation, pipe diameter, and fluid properties on the distribution parameter and drift velocity as shown in Equations 3.47 and 3.50, respectively. The void fraction correlation of Bhagwat and Ghajar (2014) is based on the most comprehensive data bank and is the most robust correlation applicable for a wide range of two-phase flow conditions listed in Table 3.5. The variable $C_{o,1}$ in Equation 3.48 is modeled as a variable such that it may vary between 0.2 and 0 to ensure the variation of distribution parameter for bubbly flow $C_o \approx 1.2$ to annular flow where $C_o \to 1.0$. Note that the two-phase friction factor (f_M) is based on two-phase mixture Reynolds number (Re_M) given by Equation 3.49 and could be calculated using appropriate single-phase friction factor equation for laminar and turbulent flows.

$$C_o = \frac{2-(\rho_G/\rho_L)^2}{1+(Re_M/1000)^2} + \frac{\left[\sqrt{(1+(\rho_G/\rho_L)^2\cos\theta)/(1+\cos\theta)}^{(1-\alpha_G)}\right]^{2/5} + C_{o,1}}{1+(1000/Re_M)^2} \tag{3.47}$$

Table 3.5 Application Range of Two-Phase Flow Parameters for Bhagwat and Ghajar (2014) Void Fraction Correlation

Parameter	Range
Pipe diameter (mm)	0.5–305
Pipe orientation (θ)	$-90° \le \theta \le +90°$
Density ratio (ρ_L/ρ_G)	6–875
Liquid dynamic viscosity (Pa s)	0.0005–0.6
Mixture mass flux (kg/m^2 s)	10–8450
Two-phase quality (x)	0–1
Two-phase Reynolds number (Re_M)	$10 - 5 \times 10^6$
Pipe geometry	Circular, rectangular, annular
Flow patterns	All (except stratified flow with $Fr_{SG} \le 0.1$ in $\theta < 0°$)

$$C_{o,1} = \left(c_1 - c_1\sqrt{\rho_G/\rho_L}\right)\left[(2.6-\lambda)^{0.15} - \sqrt{f_M}\right](1-x)^{1.5} \tag{3.48}$$

The constant c_1 is 0.2 for circular pipes and 0.4 for rectangular and annular ducts.

$$Re_M = \frac{(U_{SL}+U_{SG})\rho_L D_h}{\mu_L} \tag{3.49}$$

The expression for drift velocity used by Bhagwat and Ghajar (2014) is essentially based on the translational velocity of the gas slug in different pipe inclinations suggested by Bendiksen (1984). However, instead of using the constant of 0.54 as originally proposed by Bendiksen (1984), a proportionality constant of 0.45 is used since it gave a better accuracy in overall prediction of the void fraction. The correction factors c_2 and c_3 used in Equation 3.50 account for the effect of increase in liquid viscosity and pipe diameter on the reduction in drift velocity. These correction factors are expressed by Equations 3.51 and 3.52. More details and justification about the effect of these parameters on drift velocity and hence the use of these correction factors could be obtained from Gokcal et al. (2009), Kataoka and Ishii (1987), and Bhagwat and Ghajar (2014). The pipe diameter beyond which the correction to drift velocity in the form of c_3 is deemed necessary is identified using Laplace number (nondimensional pipe diameter) defined by Equation 3.53:

$$U_{GM} = (0.35\sin\theta + 0.45\cos\theta)\sqrt{\frac{gD_h(\rho_L-\rho_G)}{\rho_L}}(1-\alpha_G)^{0.5}c_2c_3 \tag{3.50}$$

$$c_2 = \begin{cases} \left(\dfrac{0.434}{\log_{10}(\mu_L/0.001)}\right)^{0.15} & :(\mu_L/0.001) > 10 \\ 1 & :(\mu_L/0.001) \le 10 \end{cases} \tag{3.51}$$

$$c_3 = \begin{cases} (La/0.025)^{0.9} & :La < 0.025 \\ 1 & :La \ge 0.025 \end{cases} \tag{3.52}$$

$$La = \sqrt{\frac{\sigma}{g(\rho_L-\rho_G)}}\frac{1}{D_h} \tag{3.53}$$

Note that the correlation of Bhagwat and Ghajar (2014) is not validated against data for microchannels with pipe diameters less than 0.5 mm. For gas–liquid two-phase flow in small-size pipes less than 0.5 mm, the correlation of Xiong and Chung (2006) could be used. Their correlation is based on the experimental data for pipe diameters in the range of 0.1–0.6 mm and consists of bubbly, slug, annular flow, and entire range of gas volumetric flow fraction (λ). The correlation of Xiong and Chung (2006) accounts for the nonlinear relationship between void fraction and gas volumetric flow fraction as a function of hydraulic pipe diameter (D_h) measured in mm:

$$\left.\begin{aligned} \alpha_G &= \frac{a_1\lambda^{0.5}}{1-(1-a_1)\lambda^{0.5}} \\ 0.1 \le D_h &\le 0.6\,\text{mm} \\ 4 \le Re_{SL} &\le 1670, 4 \le Re_{SG} \le 1725 \end{aligned}\right\} \tag{3.54}$$

$$a_1 = \frac{0.266}{1+13.8\exp(-6.88D_h)} \tag{3.55}$$

It must be noted that DFM-based void fraction correlations are not suitable to model stratified type of flow. Compared to DFMs, SFMs listed in Table 3.4 work better for stratified flow. However, these models too cannot provide accurate prediction of the void fraction with desired accuracy. In particular for stratified flows, flow pattern–specific models are required, which will be discussed later in Section 3.5.

3.4 Pressure Drop

Similar to single-phase flow, pressure drop in gas–liquid two-phase flow comprises hydrostatic, accelerational, and frictional components as shown in Equation 3.56. However, unlike the single-phase flow, these components of two-phase pressure drop in gas–liquid flows may depend upon several parameters such as void fraction, pipe orientation, flow patterns, and liquid entertainment fraction. The hydrostatic or gravitational component of two-phase pressure drop due to the pipe inclination depends on the two-phase mixture density, which in turn is a function of flow patterns and void fraction. Accelerational pressure drop is due to the change in momentum of the two-phase mixture and can be neglected for adiabatic two-phase flows within a short pipe length. However, for two-phase flow undergoing phase change process or even for adiabatic two-phase flow in long and inclined pipes, depending upon the flow pattern, the accelerational pressure drop can contribute up to 20% of the total two-phase pressure drop. Finally, the frictional component of two-phase pressure drop is a result of the interfacial friction between the two phases and wall friction with both or either phase and depends upon the flow pattern structure, pipe diameter, and fluid properties:

$$-\left(\frac{dp}{dz}\right)_{TP} = -\left(\frac{dp}{dz}\right)_{h} - \left(\frac{dp}{dz}\right)_{f} - \left(\frac{dp}{dz}\right)_{a} \tag{3.56}$$

Before discussing different two-phase pressure drop modeling methods, it is interest to know about the effect of different two-phase flow variables on the two-phase pressure drop. Following text describes the effect of pipe orientation on the total two-phase pressure drop and the effects of phase flow rates and pipe surface roughness on the frictional component of two-phase pressure drop. Following this discussion, different modeling approaches to determine hydrostatic, accelerational, and frictional components of two-phase pressure drop are presented.

3.4.1 Effect of Pipe Orientation

The effect of pipe orientation on two-phase pressure drop is primarily due to the effect of pipe orientation on the hydrostatic component of the two-phase pressure drop. The two-phase literature reports that very few studies focused on the measurement of two-phase pressure drop over the entire range of pipe orientations. Some of these studies include the works of Beggs (1972), Mukherjee (1979), Spedding et al. (1982), and Lips and Meyer (2012). The experimental measurements carried out at the Two-Phase Flow Lab, OSU and that reported in the literature are presented in Figures 3.18 and 3.19.

A comparison between Figures 3.18 and 3.19 shows that the variation of two-phase pressure drop as a function of pipe orientation is similar for both nonboiling and condensing two-phase flows. It is evident that at low gas and liquid flow rates, two-phase pressure drop is relatively insensitive to the change in downward pipe inclination. This is due to the fact that at these flow rates, stratified flow exists and its physical structure and associated void fraction is relatively insensitive to the change in pipe orientation. In upward pipe inclinations, two-phase pressure drop increases rapidly with increase in the pipe orientation, and it is fascinating to see that two-phase pressure drop at lower gas flow rates is greater than that at higher gas flow rates. This is because of the reversal of liquid film that induces decreasing trend of pressure gradient with increase in gas flow rates. Please refer to Section 3.4.6 for more details on this phenomenon. At higher liquid flow rates, negative values of the total two-phase pressure drop in downward pipe inclinations represent partial pressure recovery due to gain in hydrostatic component of two-phase pressure drop.

3.4.2 Effect of Phase Flow Rates

The effect of change in phase flow rates on the two-phase pressure drop is essentially due to the change in physical structure of the flow patterns and is of different nature for the hydrostatic and frictional components of two-phase pressure drop. Since the hydrostatic component of two-phase pressure drop depends only on the void fraction, for a fixed liquid flow rate, increase in gas flow rate decreases the contribution of hydrostatic pressure drop (due to decrease in mixture density), whereas it increases the frictional pressure drop component. The relation between change in phase flow rates and the frictional pressure drop could be construed in a better way by presenting their relationship in different coordinate systems. As shown in Figure 3.20, for low liquid and low gas flow rates, the two-phase frictional pressure drop remains virtually constant and increases drastically only for moderate to high gas flow rates (intermittent and annular flow regimes). For intermittent type of flow, sharp increase in the frictional pressure drop is essentially due to the turbulent and chaotic nature of the two-phase mixture. For annular flow, the pressure gradient increases

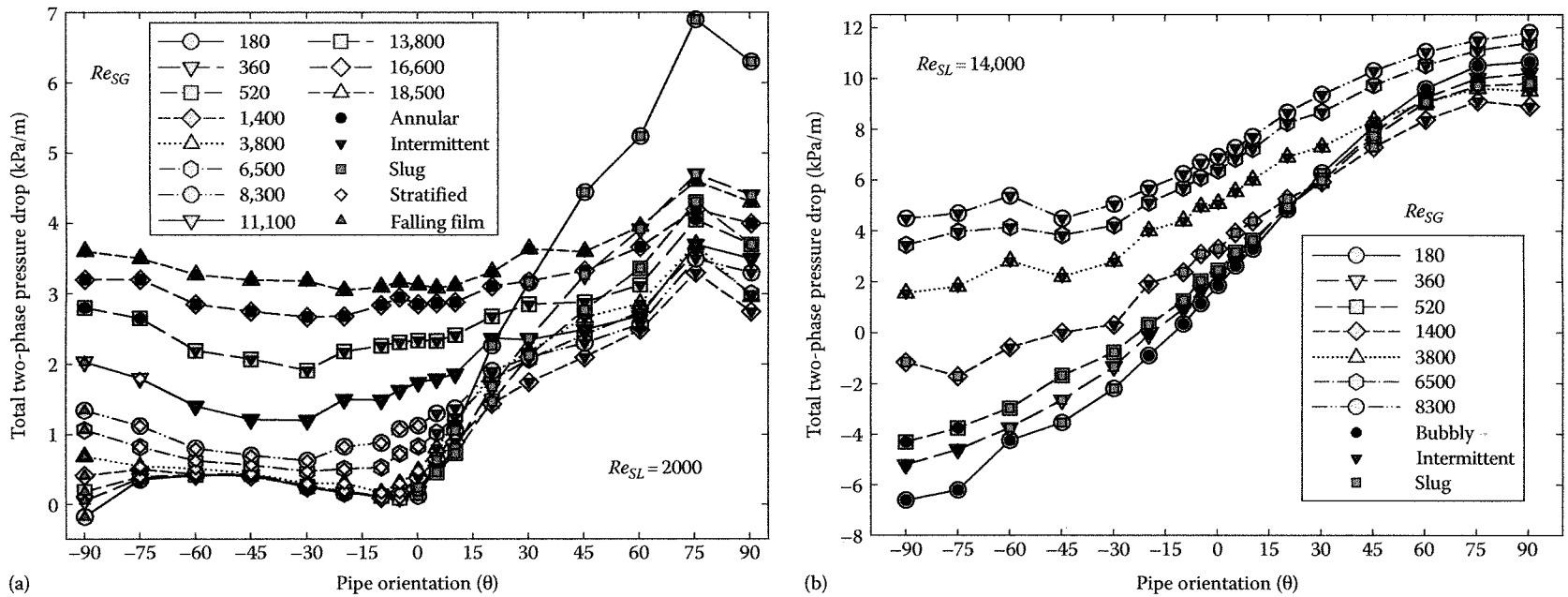

Figure 3.18

Effect of pipe orientation on total two-phase pressure drop. (a) Re_{SL} = 2,000 and Re_{SG} = 180-18,500. (b) Re_{SL} = 14,000 and Re_{SG} = 180-8,300. (Data measured at the Two-Phase Flow Lab, OSU, Stillwater, OK.)

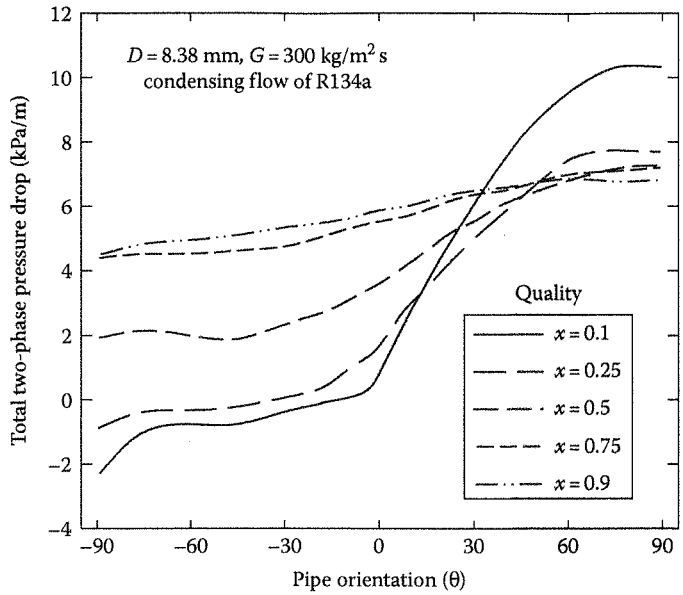

Figure 3.19

Effect of pipe orientation on two-phase pressure drop. (Data of Lips, S. and Meyer, J.P., *Int. J. Heat Mass Transfer*, 55, 405, 2012.)

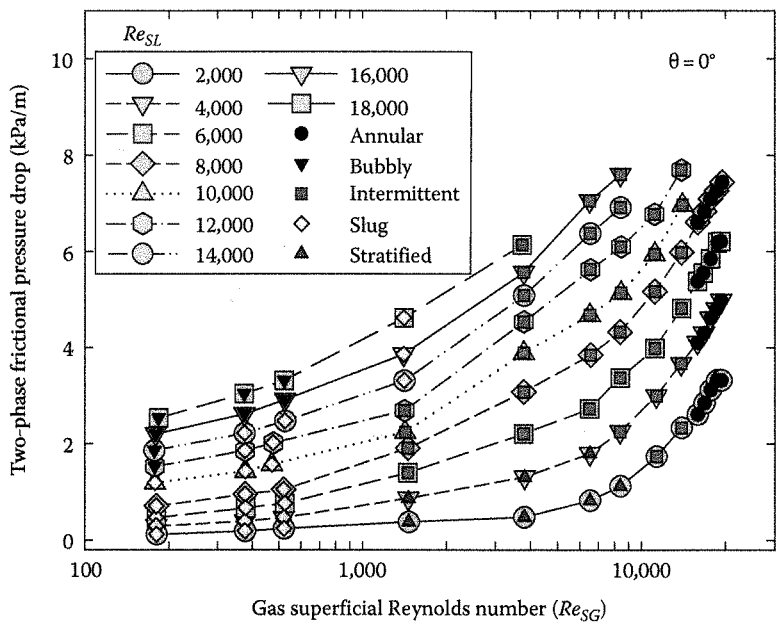

Figure 3.20

Two-phase frictional pressure drop for varying gas and liquid flow rates. (Data measured at the Two-Phase Flow Lab, OSU, Stillwater, OK.)

sharply with increase in the gas and liquid flow rates. At a fixed gas flow rate, increase in the liquid flow rate increases the liquid film thickness and thus reduces the cross-sectional area available for the gas phase. This increases the actual gas velocity and exerts higher shear on the gas–liquid interface to increase the two-phase frictional pressure drop. Additionally, the gas–liquid interface offers a rough surface to the gas flow, and the interface gets roughened progressively with the increase in the liquid film thickness or alternatively the liquid flow rate that augments the frictional pressure drop.

Variation of two-phase pressure drop with change in two-phase flow rates could also be presented in an another perspective using two-phase flow quality. This type of presentation shown in Figure 3.21 is usually

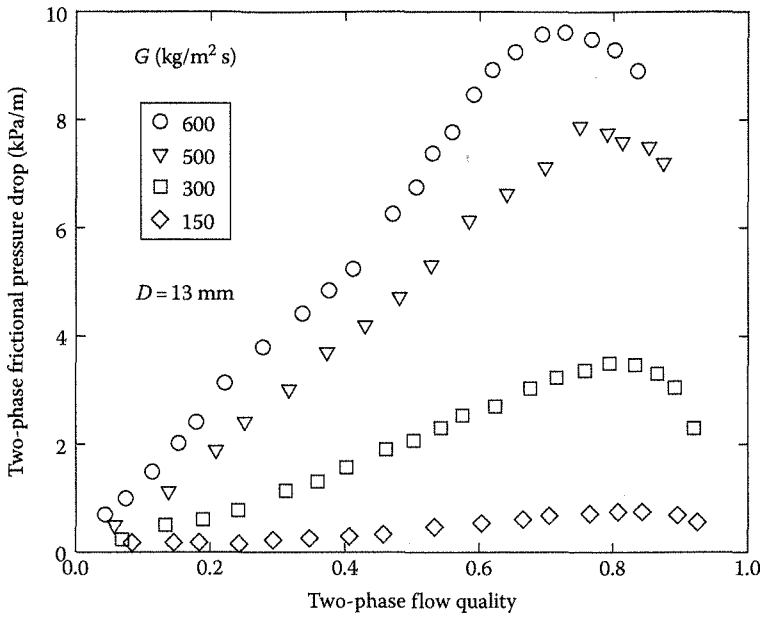

Figure 3.21

Two-phase pressure drop as a function of phase flow rates. (Data of Quiben, J.M. and Thome, J.R., *Int. J. Heat Fluid Flow*, 28, 1049, 2007.)

adopted for high-pressure systems (often encountered in refrigeration and nuclear applications) that tend to occupy the entire range of two-phase flow quality ($0 < x < 1$). It is evident that the two-phase pressure drop increases systematically with increase in the mass flux and quality. An inflection point that flips the trend of increase in two-phase pressure drop with increase in quality is quite noticeable. This change in the trend of two-phase pressure drop could be explained based on the change in structure of the two-phase flow pattern at the inflection point. By the time the two-phase flow system reaches the point of maximum pressure drop (inflection point), the flow pattern attains annular flow structure; however, beyond that point due to severe entrainment process, the liquid phase in contact with the pipe wall is gradually moved to the central gas core reducing the liquid film thickness and consequently reducing the effective viscosity in the near-wall region. This ultimately results into a reduced frictional pressure drop. This type of trend is not evident in Figure 3.20 since the data presented there do not contain two-phase flow with significant entrainment. It is also evident from Figure 3.21 that the quality at the point of maximum pressure drop shifts toward lower qualities with increase in the two-phase mixture mass flux. Additionally, Ducoulombier et al. (2011) reported that the quality associated with maximum frictional pressure drop also depends upon the fluid properties. The combined effect of mass flux and fluid thermophysical properties on the quality at maximum pressure drop is reported in Figure 3.22. It is clear that the two-phase flow quality corresponding to the point of maximum pressure drop may vary approximately between 0.65 and 0.95.

3.4.3 Effect of Pipe Diameter

Similar to the single-phase pressure drop, the effect of decrease in pipe diameter is to increase the two-phase frictional pressure drop. However, this effect of pipe diameter is usually in conjunction with two-phase flow patterns. The two-phase frictional pressure drop in the annular flow regime depends on the pipe diameter to a great extent, whereas it is relatively less sensitive to the pipe diameter in the bubbly flow regime. It is evident from Figure 3.23a that for a fixed mass flux of R134a, the two-phase frictional pressure drop for different pipe diameters deviates significantly for higher values of two-phase flow quality (annular flow pattern), whereas for low values of two-phase flow quality (bubbly flow), the effect of pipe diameter on two-phase frictional pressure drop gradually diminishes. Similar conclusions could be drawn for air–water two-phase flow system from the work of Kaji and Azzopardi (2010) who studied the effect of pipe diameters in the range of 10–50 mm on two-phase pressure drop in the annular flow regime. As shown in Figure 3.23b, for a fixed liquid flow rate, the effect of change in pipe diameter is most significant at higher gas flow rates (i.e., higher two-phase flow qualities). The two-phase frictional pressure

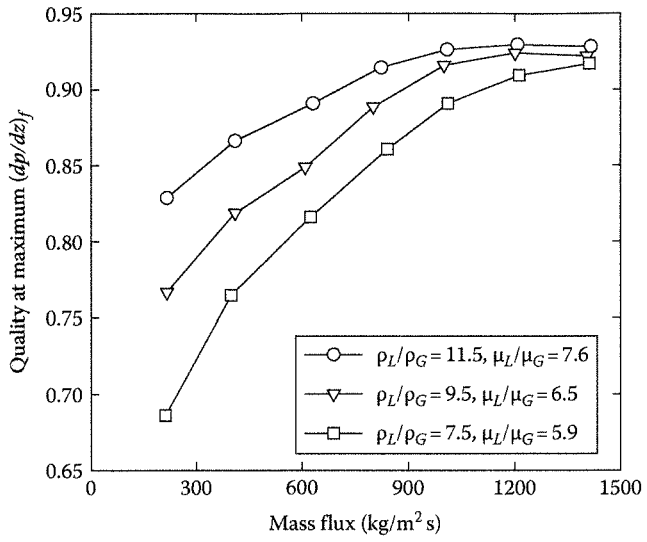

Figure 3.22

Influence of mass flux and fluid properties on quality corresponding to maximum pressure drop. (Adapted from Ducoulombier, M. et al., *Exp. Therm. Fluid Sci.*, 35, 581, 2011.)

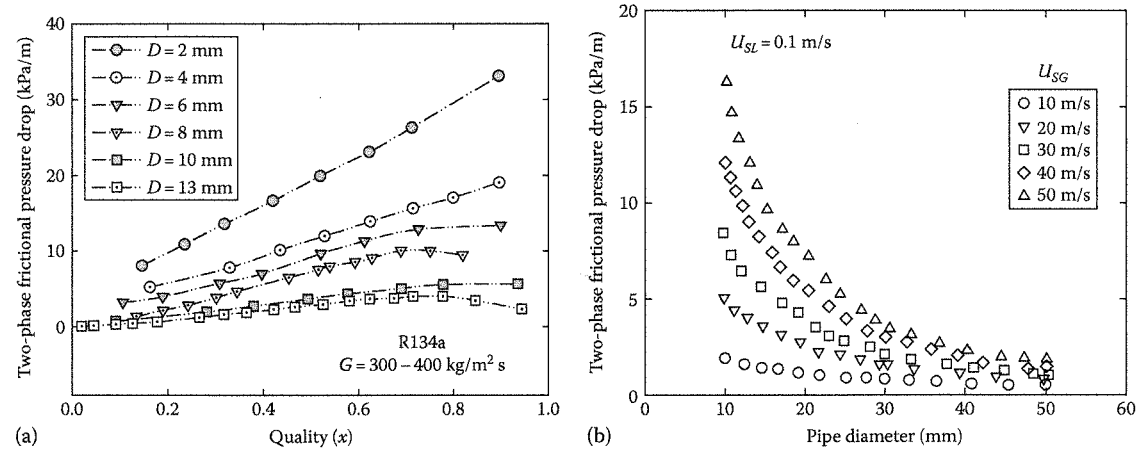

Figure 3.23

Effect of pipe diameter on two-phase frictional pressure drop. (a) Two-phase flow of R134a refrigerant. (b) Two-phase flow of air-water. (Adapted from Kaji, M. and Azzopardi, B.J., *Int. J. Multiphase Flow*, 36, 303, 2010.)

drop is due to the friction at the pipe wall as well as the gas–liquid interface and the gas–liquid interfacial area increases with increase in the pipe diameter, and hence, the nondimensional two-phase pressure drop (Φ^2) may be greater than that for the relatively smaller-diameter pipes. Thus, it is evident that any two-phase frictional pressure drop correlation must definitely account for the pipe diameter effect in the annular flow regime.

3.4.4 Effect of Fluid Properties

The important fluid properties that show a noticeable effect on two-phase frictional pressure drop are the gas-phase density and liquid-phase dynamic viscosity. The increase in gas-phase density decreases the slippage at the gas–liquid interface and hence decreases the frictional component of two-phase pressure drop, whereas the increase in liquid dynamic viscosity increases the shear in the liquid phase in contact with the pipe wall and also the shear at the gas–liquid interface resulting in increase in frictional pressure drop. Intuitively, it can be said that the effect of fluid properties on two-phase frictional pressure drop is more prominent for shear-driven flows than for buoyancy-driven two-phase flow. For more details on the effect

of fluid properties on frictional pressure drop, readers are advised to refer to Oshinowo (1971), Fukano and Furukawa (1998), Abduvayat et al. (2003), Hlaing et al. (2007), and Gokcal (2008).

3.4.5 Effect of Surface Roughness

The effect of pipe surface roughness on two-phase pressure drop is crucial in applications involving two-phase flow through steel or microfinned tubes. The internally ribbed or microfinned tubes are used in air-conditioning and refrigeration applications to improve the tube side heat transfer, however, at the expense of enhanced pressure drop. Most of the two-phase flow research reported in the literature is carried out in a transparent (smooth pipe), while the effect of pipe surface roughness on the frictional two-phase pressure drop is a relatively less investigated issue. The work of Wongs-ngam et al. (2004) and Shannak (2008) reported a considerable effect (20%–60%) of wall roughness on pressure drop especially for the two-phase flow at high mass flux and quality. Figure 3.24 shows that the effect of pipe wall roughness on two-phase pressure drop is considerable at high gas velocities and increases with increase in liquid velocity. Obviously, similar to single-phase flow, the effect of wall roughness on two-phase pressure drop increases with decrease in the pipe diameter. Experiments performed at the Two-Phase Flow Lab, OSU, confirm these observations. Moreover, their work also shows that the effect of pipe roughness on two-phase pressure drop is independent of the pipe orientation. The effect of pipe surface roughness on two-phase frictional pressure drop is maximum for the annular flow (at high gas flow rates) since, in addition to the effect of pipe wall roughness acting on the liquid phase, the structure of this flow pattern also offers a continuous and rough gas–liquid interface responsible for enhanced pressure drop.

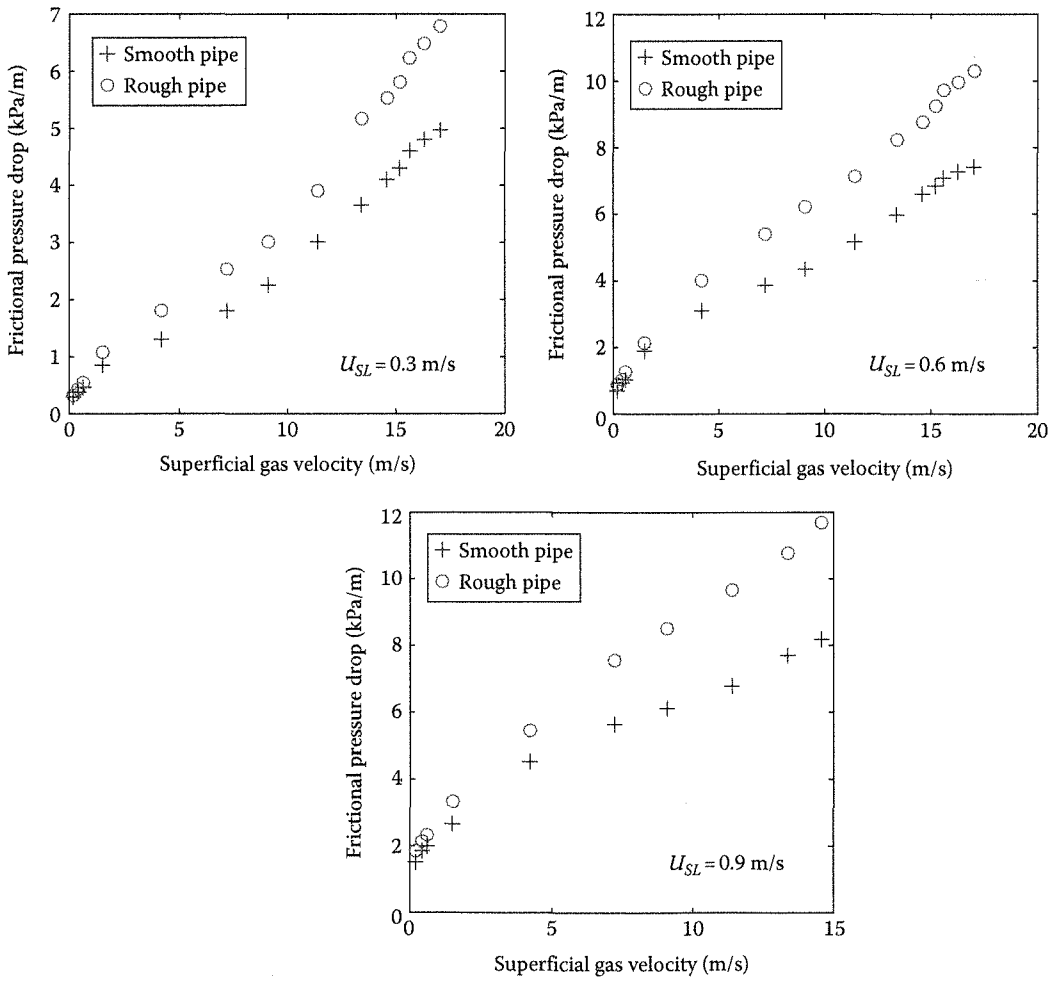

Figure 3.24

Effect of pipe surface roughness on two-phase frictional pressure drop. (Data from the Two-Phase Flow Lab, OSU, Stillwater, OK.) (D = 12.5 mm, ε = 20 μm for rough pipe).

3.4.6 Pressure Gradient Minimum and Flow Reversal in Upward Inclined Flow

In cocurrent gas–liquid upward inclined two-phase flow, at low liquid and moderate gas flow rates, although the net two-phase flow is observed in the upward direction, reversal of liquid film in contact with the pipe wall is observed under the influence of gravity forces. This phenomenon is a consequence of the interaction between the interfacial shear stress (exerted by gas phase on liquid film) and the gravitational forces acting on the liquid film. The liquid film in contact with the pipe wall may undergo a partial reversal (fluctuating wall shear stress) or complete reversal (negative wall shear stress) depending upon the gas and liquid flow rates and exhibit a decreasing trend of two-phase pressure gradient. Assuming churn/annular–annular flow regime with constant phase density, uniform circumferential film thickness, and negligible acceleration of the liquid film, the shear stress distribution in the liquid film in upward inclined flow can be given by Equation 3.57 where d is any given location on the pipe diameter (see Hewitt and Hall-Taylor (1970) and Collier and Thome (1996)):

$$\tau = \tau_i\left(\frac{D-2\delta}{d}\right)+\frac{1}{4}\left(\rho_L g\sin\theta+\frac{dp}{dz}\right)\left(\frac{(D-2\delta)^2-d^2}{d}\right) \tag{3.57}$$

Using the boundary condition of zero wall shear stress at $d = D$ for the case of stationary liquid film in contact with pipe wall, Equation 3.57 can be expressed as

$$\tau_w = \tau_i\left(\frac{D-2\delta}{D}\right)+\frac{1}{4}\left(\rho_L g\sin\theta+\frac{dp}{dz}\right)\left(\frac{(D-2\delta)^2-D^2}{D}\right)=0 \tag{3.58}$$

Assuming negligible acceleration in the gas core and negligible entrainment of liquid drops to the gas core, the interfacial shear stress exerted by the gas phase on the liquid film can be expressed as

$$\tau_i = \frac{D-2\delta}{4}\left(\frac{dp}{dz}+\rho_G g\sin\theta\right) \tag{3.59}$$

After combining Equations 3.58 and 3.59 and considering that $\delta \ll D$, the following relationship given by Equation 3.60 is obtained. Following our assumption of negligible liquid entrainment and uniform film thickness distribution, the void fraction can simply be expressed as that given by Equation 3.61. Using this definition of void fraction, it is evident that the right-hand side of Equation 3.60 is indeed the hydrostatic component of two-phase pressure drop:

$$\left(\frac{dp}{dz}\right)_{\tau_w=0} = \left[\rho_G\left(\frac{(D-2\delta)^2}{D^2}\right)+\rho_L\left(1-\frac{(D-2\delta)^2}{D^2}\right)\right]g\sin\theta \tag{3.60}$$

$$\alpha_G = \frac{A_G}{A} = \frac{(D-2\delta)^2}{D^2} = 1-\frac{4\delta}{D}\Bigg\}(\delta \ll D) \tag{3.61}$$

The physical implication of Equation 3.60 is that as long as there is a balance between interfacial shear stress and hydrostatic pressure drop, the liquid film in contact with the pipe wall will either remain stationary or oscillate giving a net zero wall shear stress. Thus, when the interfacial shear stress is large enough to supersede the gravity forces (in the form of hydrostatic pressure drop), the net flow of two-phase mixture will be in upward direction without any reversal of liquid film.

Experimentally, this condition could be determined by analyzing the pressure drop signal as a function of gas and liquid flow rates. At a fixed liquid flow rate and with an increase in the gas flow rate, a point is reached where the gas phase does not have enough potential to carry liquid phase along with it in the downstream direction. At this point, the liquid phase in contact with the pipe wall appears to oscillate or move in the downward direction. The point corresponding to the inception of decreasing pressure gradient trend (in spite of increase in gas flow rate) is regarded as the flow reversal point, while the condition at which the pressure

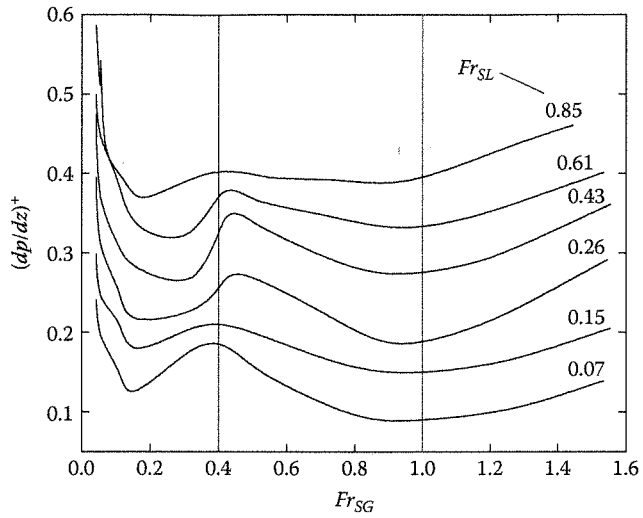

Figure 3.25

Nondimensional pressure drop for varying nondimensional gas and liquid flow rates. (Data measured at the Two-Phase Flow Lab, OSU, Stillwater, OK.)

gradient commence to increase again with increase in gas flow rate is identified as pressure gradient minimum point. The two-phase literature provides several instances of decreasing pressure gradient trends in context to churn–annular transition in vertical upward two-phase flow. As a matter of fact, the decreasing trend of pressure gradient minimum also exists at lower gas flow rates during slug–churn transition in upward inclined pipes. Nevertheless, the flow physics governing these two separate regions of pressure gradient minimum is significantly different. A typical example of decreasing trends of pressure gradient minimum in vertical upward pipe inclination is illustrated in Figure 3.25. The measured two-phase pressure drop and corresponding gas and liquid flow rates are made nondimensional as shown in Equations 3.62 through 3.64, respectively:

$$\left(\frac{dp}{dz}\right)^{+}_{t} = \frac{(dp/dz)_t}{(\rho_L - \rho_G)g} \tag{3.62}$$

$$Fr_{SG} = \frac{U_{SG}}{\sqrt{gD}}\sqrt{\frac{\rho_G}{(\rho_L - \rho_G)}} \tag{3.63}$$

$$Fr_{SL} = \frac{U_{SL}}{\sqrt{gD}}\sqrt{\frac{\rho_L}{(\rho_L - \rho_G)}} \tag{3.64}$$

It is seen that for a fixed liquid flow rate, when the gas flow rate is increased, the two-phase pressure gradient exhibits first a minimum at $Fr_{SG} \approx 0.2 - 0.3$ and a maximum at $Fr_{SG} \approx 0.4$. The first instance of decreasing pressure drop is due to falling film surrounding the gas slug. As the gas slug rises in downstream direction it sheds liquid phase surrounding it to maintain the continuity. The sudden increase in pressure drop between $Fr_{SG} \approx 0.2 - 0.4$ is due to the high level of turbulence caused by disintegration of gas slug during slug to churn/intermittent flow transition. Further this point of maximum pressure gradient at $Fr_{SG} \approx 0.4$, churn/intermittent flow is known to commence and again a decreasing trend of pressure gradient followed by a pressure gradient minimum is observed at $Fr_{SG} \approx 0.9 - 1$. Beyond this point, the annular flow is known to exist. Note that this value of the nondimensional gas flow rate is essentially the criteria given by Equation 3.26.

The second trend of decreasing pressure drop could be explained using Figure 3.26. During churn–annular flow transition, large interfacial disturbance waves are generated that travel in downstream direction (Figure 3.26-sketch b). During the swiping action of disturbance wave, the liquid film travels in downstream direction under the influence of interfacial drag. However, once the disturbance wave passes by a certain pipe cross section, there is no driving potential for the liquid film and it tends to fall back under the influence

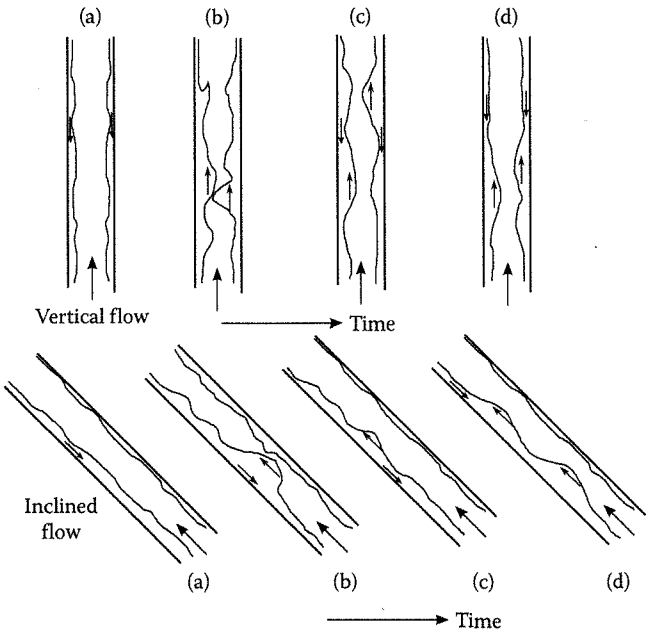

Figure 3.26

Schematics of mechanism governing pressure gradient minimum phenomenon.

of gravity (Figure 3.26 sketch c and d). The direction of travel of liquid film for different cases is depicted by small arrows inside the film. During and just after the encounter of liquid film with the disturbance wave, the portion of liquid film near interface may travel in upward direction, while that away from interface (or near pipe wall) may travel in downward direction leading to severe fluctuations in shear stress and velocity distributions in liquid film. The falling liquid film is again lifted up by upcoming disturbance wave, and the process continues until the frequency of disturbance waves is high enough to prevent the reversal of liquid film. More details about this phenomenon and its dependency on disturbance waves could be found in Hewitt et al. (1965, 1985), Hewitt and Lacey (1965), and Owen (1986).

When it is desirable to operate a two-phase flow system in the region *not affected* by the reversal of liquid film, it is crucial to identify the gas and liquid flow rates that belong to the region *affected* by flow reversal. Compared to first trend of decreasing pressure gradient, its second instance is more important since this region is marked by severe turbulence and instability of the liquid film. The two-phase flow literature reports that the point of second pressure gradient minimum occurs at $Fr_{SG} \approx 1$. However, this criterion does not provide any idea on the range of liquid flow rates for which this trend would exist. Experiments carried out at the Two-Phase Flow Lab, OSU, reveal that the liquid flow rates at which this trend of second pressure gradient minimum would exist depend upon the pipe orientation such that the relationship between nondimensional liquid flow rates and pipe orientation corresponding to second pressure gradient minimum is given by Equation 3.65. Note that this relationship need not be used for pipe orientations less than +10° from horizontal since the effect of pipe orientation on pressure gradient is negligibly small. For a fixed pipe orientation, Equation 3.65 gives a threshold value of nondimensional liquid flow rate (Fr_{SL}) above which decreasing pressure gradient trends or alternatively reversal of liquid film will no longer exist. Independent of pipe orientation and liquid flow rates, the nondimensional gas flow rates (Fr_{SG}) corresponding to this point are in the range of 0.9–1:

$$Fr_{SL} = 0.6575(\sin\theta)^{1.1175}\Big\} + 10° \le \theta \le +90° \tag{3.65}$$

3.4.7 Two-Phase Pressure Drop Modeling

The two-phase flow literature provides different methods for the calculation of two-phase pressure drop that can be broadly classified as methods based on (1) homogeneous flow model, (2) SFM, (3) phenomenological models, and (4) empirical models. The following text provides a brief description of these models and presents some of the top-performing pressure drop correlations.

3.4.7.1 Homogeneous Flow Model

As mentioned earlier, the correlations based on homogeneous flow model assume the two phases to remain well mixed and move with identical velocities (no slippage at the gas–liquid interface). The homogeneous flow model thus considers the two-phase mixture as a pseudo single-phase mixture having two-phase physical properties. Under the consideration of homogeneous flow model, the hydrostatic two-phase pressure drop is calculated using homogeneous two-phase mixture density (ρ_M) as shown in Equation 3.66. The two-phase mixture density can be expressed either in terms of two-phase flow quality (x) or the gas volumetric flow fraction (λ_G). See Table 3.1 for interchangeability between λ and x:

$$-\left(\frac{dp}{dz}\right)_h = \rho_M g \sin\theta \tag{3.66}$$

$$\rho_M = \left(\frac{x}{\rho_G} + \frac{1-x}{\rho_L}\right)^{-1} = \lambda_G \rho_G + (1-\lambda_G)\rho_L \tag{3.67}$$

The pressure drop due to acceleration of the two-phase mixture is calculated from Equation 3.68. For the case of two-component two-phase flow (nonboiling, noncondensing), the two-phase flow quality remains constant for a relatively short length of pipe and the magnitude of pressure drop due to change in specific volume of two-phase mixture is negligible and hence is ignored:

$$-\left(\frac{dp}{dz}\right)_a = G^2 \frac{dv_M}{dz} = G^2\left(v_{LG}\frac{dx}{dz} + x\frac{dv_G}{dp}\frac{dp}{dz}\right) \tag{3.68}$$

Finally, the frictional component of two-phase pressure drop is expressed in terms of the two-phase friction factor. The two-phase friction factor (f_M) is calculated based on two-phase Reynolds number (Re_M), which in turn is the function of two-phase mixture dynamic viscosity (μ_M). The two-phase flow literature provides several models to calculate two-phase dynamic viscosity as a function of two-phase flow quality. Some of these models are listed in Table 3.6:

$$-\left(\frac{dp}{dz}\right)_f = \frac{2f_M G^2}{D\rho_M} \tag{3.69}$$

$$Re_M = \frac{GD}{\mu_M} \tag{3.70}$$

Table 3.6 Two-Phase Dynamic Viscosity Models

Source	Correlation
McAdams et al. (1942)	$\mu_M = \left(\frac{x}{\mu_G} + \frac{1-x}{\mu_L}\right)^{-1}$
Ciccihitti et al. (1960)	$\mu_M = x\mu_G + (1-x)\mu_L$
Dukler et al. (1964)	$\mu_M = \lambda_G\mu_G + (1-\lambda_G)\mu_L$
Beattie and Whalley (1982)[a]	$\mu_M = \mu_L(1-\lambda_G)(1+2.5\lambda_G) + \lambda_G\mu_G$
Awad and Muzychka (2008) Model 1[b]	$\mu_M = \mu_L\left[\frac{2\mu_L+\mu_G-2(\mu_L-\mu_G)x}{2\mu_L+\mu_G+2(\mu_L-\mu_G)x}\right]$
Awad and Muzychka (2008) Model 2[b]	$\mu_M = \mu_G\left[\frac{2\mu_G+\mu_L-2(\mu_G-\mu_L)(1-x)}{2\mu_G+\mu_L+2(\mu_G-\mu_L)(1-x)}\right]$
Awad and Muzychka (2008) Model 3[b]	Arithmetic mean of Model 1 and Model 2
Awad and Muzychka (2008) Model 4[b]	$\mu_M = 0.25[(3x-1)\mu_G + [3(1-x)-1]\mu_L] + \sqrt{[(3x-1)\mu_G + [3(1-x)-1]\mu_L]^2 + 8\mu_L\mu_G}$

[a] Use the correlation of Colebrook (1939) to calculate two-phase friction factor.

[b] Use the correlation of Churchill (1977) to calculate two-phase friction factor.

The two-phase friction factor (f_M) is calculated using single-phase fanning friction factor correlations such as Blasius (1913) and Churchill (1977) shown in Equations 3.71 and 3.72, respectively. The Reynolds number (Re_j) is expressed for jth phase that can be gas-, liquid-, or two-phase mixture:

$$f_j = \begin{cases} 16/Re_j & : Re_j \le 2300 \\ 0.079/Re_j^{0.25} & : Re_j > 2300 \end{cases} \tag{3.71}$$

$$f_j = 2\left[\left(\frac{8}{Re_j}\right)^{12} + \frac{1}{(a+b)^{3/2}}\right]^{1/12} \tag{3.72}$$

In Equation 3.72, parameters a and b are expressed as follows:

$$a = \left[2.457 \ln\left(\frac{1}{(7/Re_j)^{0.9} + (0.27\varepsilon/D)}\right)\right]^{16} \quad \text{and} \quad b = \left(\frac{37530}{Re_j}\right)^{16}$$

Thus, the total two-phase pressure drop assuming negligible contribution of the accelerational component is calculated from Equation 3.73. Note that the frictional component of two-phase pressure drop can also be expressed in terms of wall shear stress calculated as $\tau_w = (f_M G^2)/2\rho_M$:

$$-\left(\frac{dp}{dz}\right)_t = \frac{2f_M G^2}{D\rho_M} + (\lambda_G \rho_G + (1-\lambda_G)\rho_L) g \sin\theta \tag{3.73}$$

$$= \tau_w \frac{P}{A} + \rho_M g \sin\theta \tag{3.74}$$

It is interesting to see that the two-phase frictional pressure drop calculation method based on homogeneous flow model can also be expressed in terms of two-phase frictional multiplier (Φ^2) (see Equations 3.85 through 3.88). Consider the two-phase frictional pressure drop equation of homogeneous flow model and divide it with the pressure drop equation for single-phase gas or liquid phase. The resultant equation would be the two-phase frictional multiplier. Assuming turbulent flow of each phase and using the Blasius (1913) correlation for friction factor, this two-phase frictional multiplier using homogeneous flow model approach can be casted as

$$\Phi_{LO}^2 = \frac{(dp/dz)_f}{(dp/dz)_{LO}} = \frac{2f_M G^2/(D\rho_M)}{2f_{LO} G^2/(D\rho_L)} = \frac{\rho_L}{\rho_M}\left(\frac{\mu_L}{\mu_M}\right)^{-0.25} \tag{3.75}$$

Using the definition of homogeneous two-phase mixture density given by Equation 3.67 and two-phase mixture viscosity definition of McAdams et al. (1942) (Table 3.6), Equation 3.75 would become Equation 3.76. Similarly, using the definitions for single-phase pressure drop due to flow of liquid and gas (see Equations 3.86 through 3.88), two-phase frictional multipliers Φ_L^2, Φ_{GO}^2, and Φ_G^2 using homogeneous flow models can be expressed as Equations 3.77 through 3.79, respectively:

$$\Phi_{LO}^2 = \left[(1-x) + x\frac{\mu_L}{\mu_G}\right]^{-0.25}\left[1 + x\left(\frac{\rho_L}{\rho_G} - 1\right)\right] \tag{3.76}$$

$$\Phi_L^2 = (1-x)^{-1.75}\Phi_{LO}^2 \tag{3.77}$$

$$\Phi_{GO}^2 = \left[x + (1-x)\frac{\mu_G}{\mu_L}\right]^{-0.25}\left[x + (1-x)\frac{\rho_G}{\rho_L}\right] \tag{3.78}$$

$$\Phi_G^2 = x^{-1.75}\Phi_{GO}^2 \tag{3.79}$$

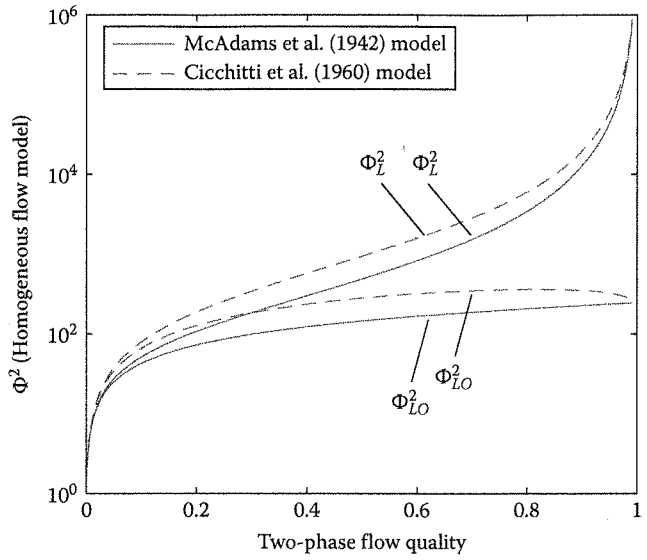

Figure 3.27

Two-phase frictional multiplier based on homogeneous flow model.

It must be mentioned here that the physical form of homogeneous flow model-based two-phase frictional multiplier derived in the aforementioned equations depends on the selection of friction factor and two-phase dynamic viscosity model. For instance, the use of the two-phase dynamic viscosity model of Ciccihitti et al. (1960) would render a different form of two-phase frictional multiplier. The comparison between Φ_{LO}^2 and Φ_L^2 using the dynamic viscosity models of McAdams et al. (1942) and Ciccihitti et al. (1960) is presented in Figure 3.27. Based on the trends of Φ_{LO}^2 and Φ_L^2 using homogeneous flow model, some discrepancies between these theoretical trends and reality can be highlighted. The trend of Φ_{LO}^2 shows a rapid increase with increase in two-phase flow quality up to $x \approx 0.1$ and thereafter increases slowly with increase in quality. Comparatively, Φ_L^2 increases rapidly for both lower and higher values of two-phase flow quality. In reality, Φ_{LO}^2 or Φ_L^2 may not exhibit a continuous increasing trend but rather show an inflection point close to higher values of $x \approx 0.7 - 0.9$ (see Figure 3.21). It must be noted that the two-phase pressure drop calculation based on homogeneous flow model is appropriate for bubbly and annular mist region that to a good extent exhibits homogeneous flow characteristics. The use of these models for intermittent, stratified, and annular flow regimes may result into significant deviations from the actual two-phase flow conditions.

3.4.7.2 Separated Flow Model

As mentioned earlier, SFM assumes two phases to flow separately and share a definite and continuous interface between them, and unlike homogeneous flow model, it considers the slippage at the gas–liquid interface. Thus, using two-phase SFM, the two-phase mixture density and hence the two-phase hydrostatic pressure drop calculation are based on the void fraction as given by Equation 3.80 where the two-phase mixture density is $\rho_M = \alpha_G\rho_G + (1 - \alpha_G)\rho_L$:

$$-\left(\frac{dp}{dz}\right)_h = \rho_M g \sin\theta = (\alpha_G\rho_G + (1-\alpha_G)\rho_L)g\sin\theta \tag{3.80}$$

It is of interest to check the agreement between the calculated values of two-phase mixture density considering the interfacial slippage (SFM approach) and assuming no slip at the gas–liquid interface (HFM approach). It is clear from Figure 3.28 that the agreement between the two methods is valid only for $\lambda < 0.2$ and $\lambda \to 1$. These two conditions approximately correspond to the bubbly and annular mist types of the flow where to some extent two-phase flow may exhibit homogeneous flow characteristics.

The accelerational component of two-phase pressure drop is expressed by Equation 3.81. This expression is valid for all but annular flow pattern with considerable liquid entrainment. In particular, for annular flow,

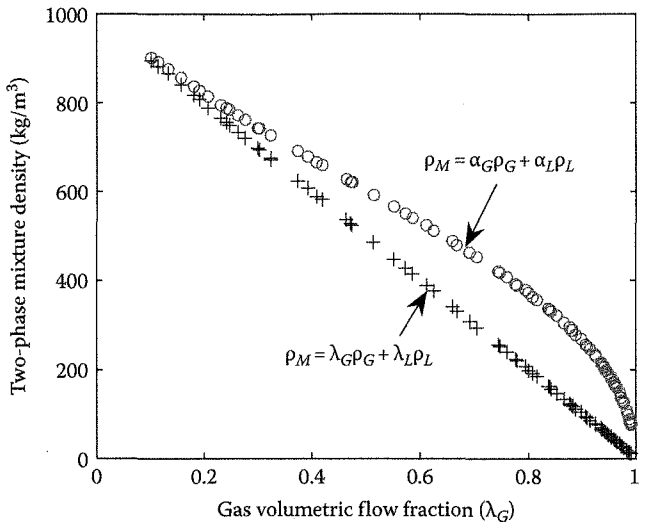

Figure 3.28

Two-phase mixture density calculation using a homogeneous and separated flow model.

when the entrainment of liquid droplets into the central gas core is significant, the error associated with the assumption of negligible accelerational pressure drop can be severe. In case of annular flow with liquid entrainment, the process of entrainment also contributes to the two-phase pressure drop and hence cannot be ignored. For such a specific case (annular flow with liquid entrainment), Equation 3.81 can be expressed in the form of Equation 3.82:

$$-\left(\frac{dp}{dz}\right)_a = G^2 \frac{d}{dz}\left[\frac{x^2}{\alpha_G \rho_G} + \frac{(1-x)^2}{(1-\alpha_G)\rho_L}\right] \tag{3.81}$$

$$-\left(\frac{dp}{dz}\right)_a = G^2 \frac{d}{dz}\left[\frac{x^2}{\alpha_G \rho_G} + \frac{(1-E)^2(1-x)^2}{\beta \rho_L} + \frac{E^2(1-x)^2}{(1-\alpha_G-\beta)\rho_L}\right] \tag{3.82}$$

The volume fraction occupied by the liquid film (β) defined by Equation 3.83 does not consider the fraction of liquid droplets entrained in the gas core and hence may not be confused with liquid holdup (α_L). However, it is evident that under the condition of $E \approx 0$, the volume fraction of liquid film is equal to the liquid holdup, that is, $\beta = \alpha_L$. Equation 3.83 is based on a valid assumption that entrained liquid droplets travel at a velocity same as that of the gas:

$$\beta = 1 - \alpha_G - \frac{\alpha_G E(1-x)}{x(\rho_L/\rho_G)} \tag{3.83}$$

It must be reiterated that this is required only in case of annular flow with considerable liquid entrainment. For the case of annular flow at low system pressures ($E \approx 0$) and at flow patterns other than annular flow ($E = 0$), it is simplified back to Equation 3.81 such that the accelerational pressure drop at a given location can be determined based on void fraction and mass flux of each phase. For the case of adiabatic two-phase flow over a short pipe length, two-phase flow quality and void fraction can be assumed to remain constant and hence $(dp/dz)_a \approx 0$.

Finally, the frictional component of two-phase pressure drop is calculated as

$$\left(\frac{dp}{dz}\right)_f = \Phi_j^2 \left(\frac{dp}{dz}\right)_j \tag{3.84}$$

The two-phase frictional multiplier Φ^2 can be expressed in several different forms depending upon the assumption of flow of either single phase through the pipe. Broadly, four different cases of two-phase

frictional multiplier can be defined as shown in Equations 3.85 through 3.88. In these equations, single-phase pressure drop is the single-phase frictional drop unless otherwise specified and $(dp/dz)_f$ would always represent the frictional component of the two-phase pressure drop:

$$\left(\frac{dp}{dz}\right)_f = \Phi_{LO}^2 \left(\frac{dp}{dz}\right)_{LO} \quad \text{where} \left(\frac{dp}{dz}\right)_{LO} = \frac{2f_L G^2}{D\rho_L} \tag{3.85}$$

$$\left(\frac{dp}{dz}\right)_f = \Phi_L^2 \left(\frac{dp}{dz}\right)_L \quad \text{where} \left(\frac{dp}{dz}\right)_L = \frac{2f_L G^2(1-x)^2}{D\rho_L} \tag{3.86}$$

$$\left(\frac{dp}{dz}\right)_f = \Phi_{GO}^2 \left(\frac{dp}{dz}\right)_{GO} \quad \text{where} \left(\frac{dp}{dz}\right)_{GO} = \frac{2f_G G^2}{D\rho_G} \tag{3.87}$$

$$\left(\frac{dp}{dz}\right)_f = \Phi_G^2 \left(\frac{dp}{dz}\right)_G \quad \text{where} \left(\frac{dp}{dz}\right)_G = \frac{2f_G G^2 x^2}{D\rho_G} \tag{3.88}$$

The two-phase literature provides several frictional pressure drop correlations based on these different two-phase frictional multipliers. One of the first such correlations is proposed by Lockhart and Martinelli (1949). Their correlation expresses two-phase frictional multipliers Φ_L^2 and Φ_G^2 as a function of X parameter and is expressed by Equation 3.89. The parameter (X) of Lockhart and Martinelli (1949) is given by Equation 3.90 where the single-phase friction factors (f_L and f_G) are found using appropriate single-phase friction factors such as Equations 3.71 and 3.72. In these equations, $Re_j = Re_{SG}$ and $Re_j = Re_{SL}$ for gas and liquid phase, respectively:

$$\Phi_L^2 = 1 + C/X + 1/X^2 \quad \text{or} \quad \Phi_G^2 = 1 + CX + X^2 \tag{3.89}$$

$$X = \left[\frac{(dp/dz)_{f,L}}{(dp/dz)_{f,G}}\right]^{0.5} = \frac{1-x}{x}\left[\frac{f_L}{f_G}\frac{\rho_G}{\rho_L}\right]^{0.5} = \frac{U_{SL}}{U_{SG}}\left[\frac{f_L}{f_G}\frac{\rho_L}{\rho_G}\right]^{0.5} \tag{3.90}$$

The value of C used in Equation 3.89 given by Chisholm (1967) is given in Table 3.7, and it depends on the laminar or turbulent nature of the gas and liquid phase, respectively. The graphical form of Equation 3.89 for laminar and turbulent regimes of single-phase flow of gas and liquid phase is illustrated in Figure 3.29. Apart from the correlation of Lockhart and Martinelli (1949), there are several other correlations for two-phase frictional multiplier that could be used to determine the frictional component of the two-phase pressure drop. Some of these correlations valid for a wide range of two-phase flow conditions are listed as follows.

Chisholm (1973) proposed a method to calculate two-phase frictional pressure drop in adiabatic and evaporating flow conditions based on the concept of SFM and applicable for vapor qualities $0 \leq x \leq 1$. The two-phase friction multiplier is expressed as shown in Equation 3.91, where Y is defined by Equation 3.92:

$$\Phi_{LO}^2 = 1 + (Y^2 - 1)\left(B_s x^{0.875}(1-x)^{0.875} + x^{1.75}\right) \tag{3.91}$$

$$Y = \sqrt{\frac{(dp/dz)_{GO}}{(dp/dz)_{LO}}} \tag{3.92}$$

Table 3.7 Values of Constant C to Be Used in the Correlation of Lockhart and Martinelli (1949) for Different Single-Phase Flow Regimes

Liquid Phase	Gas Phase	C
Turbulent (t)	Turbulent (t)	20
Laminar (l)	Turbulent (t)	12
Turbulent (t)	Laminar (l)	10
Laminar (l)	Laminar (l)	5

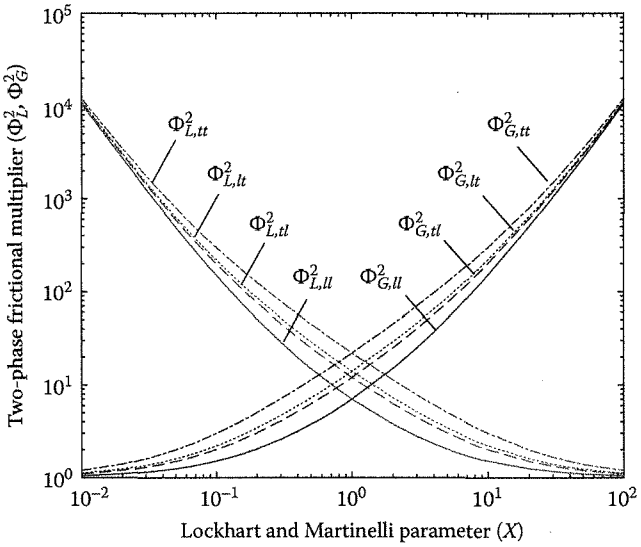

Figure 3.29

Graphical representation of different forms of two-phase frictional multiplier given by Lockhart and Martinelli (1949).

The frictional pressure gradients for single-phase liquid and gas phase are calculated using Equations 3.85 and 3.87, respectively. His correlation is essentially a transformation of graphical solution of Barcozy (1966) to predict the two-phase frictional pressure drop. The correlation is claimed to be applicable for a pressure range of 0.6–4 MPa. Chisholm (1973) proposed a set of different conditional equations to predict parameter B_s for different values of Y and mixture mass flux (G) as shown in Table 3.8.

Muller-Steinhagen and Heck (1986) developed a correlation to extrapolate between single-phase liquid and single-phase gas flow. This correlation can be used for both adiabatic and evaporating two-phase flow conditions (provided the two-phase flow quality distribution across the pipe length is known). The physical form of the correlation is as shown in Equation 3.93. The parameter Y is the same as that defined by Chisholm (1973) in Equation 3.92. The correlation is verified against 9300 measurements including data of air–oil, air–water, and steam–water fluid combinations and pipe diameters ranging from 4 to 39 mm I.D. The application of Equation 3.93 is restricted to $Re_{LO} > 100$ and $Y^2 > 1$. Note that for the determination of single-phase friction factor f_j, their correlation separates single-phase laminar and turbulent regions using a threshold value of $Re_j = 1187$ where "j" can be gas or liquid phase:

$$\Phi_{LO}^2 = Y^2 x^3 + (1-x)^{0.33}(1+2x(Y^2-1)) \tag{3.93}$$

Recently, Xu and Fang (2012) have proposed a two-phase frictional pressure drop correlation for evaporating two-phase flow of refrigerants in horizontal pipe. Their correlation is based on 2622 data points

Table 3.8 Values of Parameter B_s Used in the Correlation of Chisholm (1973)

Y	G (kg/m²s)	Equation for B_s
$0 < Y < 9.5$	$G \geq 1900$	$B_s = 55/\sqrt{G}$
	$500 < G < 1900$	$B_s = 2400/G$
	$500 > G$	$B_s = 4.8$
$9.5 < Y < 28$	$G \leq 600$	$B_s = 520/(Y\sqrt{G})$
	$G \geq 600$	$B_s = 21/Y$
$Y > 28$		$B_s = 15{,}000/(Y^2\sqrt{G})$

of 14 refrigerants (R11, R12, R22, R134a, R32, R407C, R507, R507A, R410A, CO_2, R404A, R32/R125, R123, and ammonia) for $1 < D_h < 19$ mm (circular and rectangular pipe geometries) and $25 < G < 1150$ kg/m^2 s. They found that the pipe hydraulic diameter and gas–liquid interface surface tension affect the two-phase frictional pressure drop significantly than any other two-phase flow parameter, and hence, their correlation accounts for these two variables through the inclusion of nondimensional Laplace number. The physical form of their correlation is as expressed in

$$\Phi_{LO}^2 = \left[Y^2x^3 + (1-x)^{0.33}\left(1+2x(Y^2-1)\right)\right]\left(1+1.54(1-x)^{0.5}La\right) \tag{3.94}$$

In this equation, Y is calculated from Equation 3.92, while La is the Laplace number defined by Equation 3.53. Their correlation is claimed to predict the two-phase frictional pressure drop data with a mean absolute relative deviation of 25.2%. It should be noted that Xu and Fang (2012) recommend the use of the correlation of Fang et al. (2011) to calculate single-phase Darcy friction factor (4× fanning friction factor), and hence, the single-phase liquid pressure drop required in Equation 3.85 must be changed to $(dp/dz)_f = f_L G^2/(2D\rho_L)$. The correlation of Fang et al. (2011) for single-phase Darcy friction factor is reported in

$$f_{LO} = 0.25\left[\log\left(\frac{150.39}{Re_{LO}^{0.98865}} - \frac{152.66}{Re_{LO}}\right)\right]^{-2} \tag{3.95}$$

For mini-/microchannels having pipe diameters in the range of 0.1–6 mm, Zhang et al. (2010) proposed a two-phase frictional pressure drop correlation (for adiabatic two-phase flow) based on the experimental data of two-phase flow of refrigerants, air–water and air–ethanol. Their correlation for two-phase frictional multiplier is the same as that of Lockhart and Martinelli (1949) (see Equation 3.89), however with the parameter C as a variable given by

$$C = \begin{cases} 21[1-\exp(-0.674/La)] \text{(two-component two-phase flow)} \\ 21[1-\exp(-0.142/La)] \text{(one-component two-phase flow)} \end{cases} \tag{3.96}$$

3.4.7.3 Two-Phase Friction Factor Models

In addition to homogeneous and SFMs, the two-phase literature also reports two-phase friction factor models of empirical nature. Although these models provide two-phase friction factor, they are different from two-phase friction factors used in homogeneous flow models. Some of the recent correlations developed for determining two-phase friction factors are that of Shannak (2008) and Cioncolini et al. (2009). The two-phase Darcy friction factor correlation (4× fanning friction factor) of Shannak (2008) is developed based on data for both boiling and nonboiling two-phase flow and accounts for the pipe wall surface roughness. His correlation requires the determination of modified two-phase flow Reynolds number (Re_M) given by Equation 3.97. Based on this two-phase mixture Reynolds number, the two-phase friction factor (f_M) is defined using the correlation of Chen (1979) given by Equation 3.98. The two-phase frictional pressure drop is calculated using the modified form of Equation 3.69 expressed as $(dp/dz)_f = f_M G^2/(2D\rho_M)$ where ρ_M is the homogeneous mixture density defined by Equation 3.67. Equation 3.98 is verified against 16,000 data consisting of the entire range of two-phase flow quality, pipe diameters in the range of 3–150 mm, system pressure in the range of 0.1–17 MPa, and two-phase mixture mass flux in the range of 15–8200 kg/m^2 s:

$$Re_M = \frac{GD\left(x^2 + (1-x)^2\rho_G/\rho_L\right)}{\mu_G x + \mu_L(1-x)\rho_G/\rho_L} \tag{3.97}$$

$$\frac{1}{\sqrt{f_M}} = -2\log\left[\frac{\varepsilon}{3.7065D} - \frac{5.0452}{Re_M}\log\left(\frac{1}{2.2857}\left(\frac{\varepsilon}{D}\right)^{1.1098} + \frac{5.8506}{Re_M^{0.8981}}\right)\right] \tag{3.98}$$

Since Shannak (2008) correlation is based on two-phase mixture Reynolds number and uses Equation 3.67 to find two-phase mixture density, Equation 3.66 based on homogeneous flow model should be used to determine the hydrostatic component of the two-phase pressure drop.

Another two-phase friction factor correlation developed exclusively for the annular flow is given by Cioncolini et al. (2009). The two-phase friction factor (f_M) given by Equation 3.99 is modeled as a function of core Weber number (We_c) and liquid film Reynolds number (Re_{LF}) given by Equations 3.100 and 3.101, respectively. The core mass flux (G_c), core density (ρ_c), and core diameter (D_c) are defined using Equations 3.102 through 3.104, respectively. Appropriate void fraction (see Section 3.3.4) and liquid entrainment fraction E (see Section 3.6.1) correlation developed for the annular flow must be used in the calculation of parameters G_c, ρ_c, and D_c. Note that the expression recommended by Cioncolini et al. (2009) for two-phase frictional pressure drop in the form of Equation 3.105 is based on gas core mass flux (G_c) and core density (ρ_c). Unlike Shannak (2008) correlation, Cioncolini et al. (2009) recommend the use of Equations 3.80 and 3.82 based on SFM to determine the total two-phase pressure drop:

$$f_M = \begin{cases} 0.172 We_c^{-0.372} & : D > 3\,\text{mm} \\ 0.0196 We_c^{-0.372} Re_{LF}^{0.318} & : D \le 3\,\text{mm} \end{cases} \tag{3.99}$$

$$We_c = \frac{G_c^2 D_c}{\rho_c \sigma} \tag{3.100}$$

$$Re_{LF} = \frac{(1-E)(1-x)GD}{\mu_L} \tag{3.101}$$

$$G_c = \frac{4\dot{m}[x + E(1-x)]}{\pi D_c^2} \tag{3.102}$$

$$\rho_c = \frac{x + E(1-x)}{(x/\rho_G) + (E(1-x)/\rho_L)} \tag{3.103}$$

$$D_c = D\alpha_G^2 \sqrt{1 + E\left(\frac{1-x}{x}\right)\frac{\rho_G}{\rho_L}} \tag{3.104}$$

$$-\left(\frac{dp}{dz}\right)_f = \frac{2 f_M G_c^2}{\rho_c D} \tag{3.105}$$

The two-phase pressure drop models listed in this section are some of the relatively good performing correlations validated over a fairly comprehensive range of two-phase flow conditions. The accuracy of these correlations could be up to ±50% compared to actual operating conditions. Considering the difficulty in modeling two-phase pressure drop as a function of several two-phase flow variables, this range of accuracy has received acceptance in the two-phase flow community. All the correlations presented in this section are found to work well for all but stratified flow pattern. In the following section, we will present stratified flow pattern–specific mechanistic and semimechanistic models to estimate void fraction and two-phase pressure drop.

3.5 Modeling of Stratified Flow

As mentioned earlier, stratified flow pattern in horizontal and downward pipe inclinations has a peculiar flow structure, and it is practically difficult to accurately model it with existing flow pattern–independent two-phase flow models. Apparently, the stratified flow pattern needs to be modeled using mechanistic

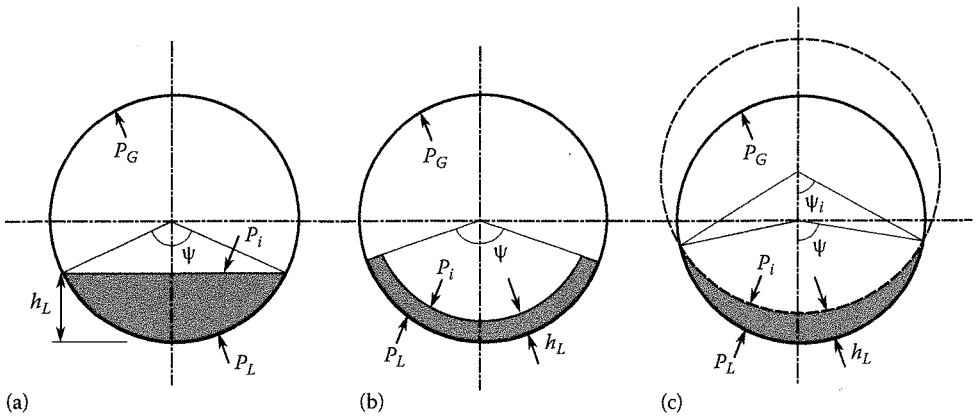

Figure 3.30

Geometry considerations in different types of stratified flow models. (a) Flat surface model. (From Taitel, Y. and Dukler, A.E., *AIChE J.*, 22, 47, 1976.) (b) Apparent rough surface model. (From Hart, J. et al., *Int. J. Multiphase Flow*, 15, 947, 1989.) (c) Double circle model. (From Chen, X.T. et al., *J. Energy Resour. Technol.*, 119, 209, 1997.)

flow model approach introduced by Taitel and Dukler (1976) and its derivatives. In addition to Taitel and Dukler (1976) model, the two-phase literature also reports semimechanistic models such as apparent rough surface (*ARS*) model and "double circle model" to calculate void fraction and two-phase pressure drop in stratified two-phase flow. It must be mentioned that the ARS and double circle models are developed only for stratified flow in horizontal pipe orientation and needs to be scrutinized against stratified flow data in downward pipe inclinations. This section describes step-by-step procedure involved in solving the stratified flow model using these three different methods. The schematics of the type (shape) of gas–liquid interface associated with each of these methods are illustrated in Figure 3.30.

3.5.1 Taitel and Dukler (1976) Model

The Taitel and Dukler (1976) model also known as "flat surface model" is developed for stratified flow at equilibrium, and as its name suggests, it assumes a flat interface between the gas and the liquid phase. It also assumes that the gas–liquid interface is smooth and that the interfacial friction factor is equal to the gas-phase friction factor. Their model considers the stratified flow of the pattern shown in Figure 3.31. The momentum balance equations for each phase (gas and liquid) could be written as shown in Equations 3.106 and 3.107. These equations also show the simplified forms of these momentum balance equations under the assumption of negligible acceleration of each phase and constant liquid level (height) along the pipe length. Considering that the pressure drop in the gas phase is equal to the pressure drop in the liquid phase, the momentum balance equations written for individual phases can be combined together to form Equation 3.108. The individual phase and interfacial shear stress required in Equation 3.108 are calculated using Equation 3.109 where the single-phase friction factor for individual phase ($j = G, L$) is calculated from Equation 3.110:

$$-A_G\left(\frac{dp}{dz}\right) = \tau_{wG}P_G + \tau_i P_i + A_G\rho_G g\left(\sin\theta - \cos\theta\frac{d}{dz}(1-h_L)\right) - A\frac{d}{dz}(GxU_G)$$

$$= \tau_{wG}P_G + \tau_i P_i + A_G\rho_G g\sin\theta \qquad (3.106)$$

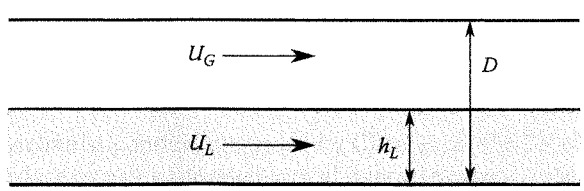

Figure 3.31

Schematic of horizontal stratified flow at equilibrium.

$$-A_L\left(\frac{dp}{dz}\right)=\tau_{wL}P_L-\tau_iP_i+A_L\rho_Lg\left(\sin\theta-\cos\theta\frac{dh_L}{dz}\right)-A\frac{d}{dz}(G(1-x)U_L)$$

$$=\tau_{wL}P_L-\tau_iP_i+A_L\rho_Lg\sin\theta \tag{3.107}$$

$$\tau_{wL}\frac{P_L}{A_L}-\tau_{wG}\frac{P_G}{A_G}-\tau_iP_i\left(\frac{1}{A_L}+\frac{1}{A_G}\right)+(\rho_L-\rho_G)g\sin\theta=0 \tag{3.108}$$

The interfacial friction factor (f_i) is assumed to be equal to the gas-phase friction factor (f_G). The gas- and liquid-phase Reynolds number are based on the actual phase velocity and the hydraulic pipe diameters (based on the area occupied by each phase) expressed as $Re_G = (\rho_G D_G U_G)/\mu_G$ and $Re_L = (\rho_L D_L U_L)/\mu_L$, respectively. The hydraulic diameters are calculated from Equation 3.111 where the area occupied by gas (A_G) and liquid (A_L) phase is defined by Equation 3.112. Considering the flat gas–liquid interface geometry of the Taitel and Dukler (1976) model, the wetted perimeter of pipe occupied by the gas (P_G) and liquid (P_L) phase and the interface (P_i) is expressed by Equation 3.113:

$$\tau_{wG}=\frac{f_G\rho_GU_G^2}{2},\quad \tau_{wL}=\frac{f_L\rho_LU_L^2}{2},\quad \tau_i=\frac{f_i\rho_G(U_G-U_L)^2}{2} \tag{3.109}$$

$$f_j=\begin{cases}16/Re_j & :(Re_j\le 2300)\\ 0.046Re_j^{-0.2} & :(Re_j>2300)\end{cases} \tag{3.110}$$

$$D_G=\frac{4A_G}{P_G+P_i},\quad D_L=\frac{4A_L}{P_L} \tag{3.111}$$

$$A_G=\alpha_G\frac{\pi D^2}{4},\quad A_L=(1-\alpha_G)\frac{\pi D^2}{4} \tag{3.112}$$

$$P_L=\frac{\Psi D}{2},\quad P_G=\pi D-P_L,\quad P_i=\sin\left(\frac{\Psi}{2}\right)D \tag{3.113}$$

$$\alpha_G=1-\frac{\Psi-\sin\Psi}{2\pi} \tag{3.114}$$

$$\Psi=2\arccos\left(1-\frac{2h_L}{D}\right) \tag{3.115}$$

The void fraction, liquid height, and the angle subtended by the flat interface with the pipe centerline are correlated with each other in the form of Equations 3.114 and 3.115. The liquid height (h_L) required in calculation of Ψ can be obtained using graphical solution presented in Figure 3.8. Alternatively, Equations 3.106 through 3.114 are to be solved iteratively until Equation 3.108 is satisfied. The void fraction value that satisfies Equation 3.108 is then used to calculate actual phase velocities, hydraulic diameters, Reynolds number, friction factors, and subsequently the shear stress values. Finally, Equation 3.106 or 3.107 is solved to obtain the frictional pressure gradient.

3.5.2 Apparent Rough Surface Model

The concept of ARS model was first introduced by Hamersma and Hart (1987) and Hart et al. (1989) for wavy stratified two-phase flow in horizontal pipes and is in the form of gas pressure drop equation using

two-phase friction factor. This two-phase friction factor (f_{TP}) is based on the gas (f_G) and interfacial (f_i) friction factors weighted by the fraction of pipe circumference (ϕ) wetted by the liquid phase. The following step-by-step approach needs to be followed to determine the values of α_G, f_G, f_i, ϕ, and f_{TP} and finally the two-phase frictional pressure drop using the ARS model:

1. First, calculate the void fraction using

$$\frac{1-\alpha_G}{\alpha_G} = \frac{U_{SL}}{U_{SG}}\left[1+\left(108 Re_{SL}^{-0.726}\frac{\rho_L}{\rho_G}\right)^{0.5}\right] \tag{3.116}$$

2. Calculate fraction of the pipe circumference (ϕ) wetted by the liquid phase using Equation 3.117. It must be noted that ϕ is the fraction of circumference and not the angle formed by the pipe centerline with the gas–liquid interface (Ψ). The relation between ϕ and Ψ can be expressed as, $\phi = \Psi/2\pi$:

$$\phi = 0.52(1-\alpha_G)^{0.374} + 0.26\left(\frac{\rho_L U_L^2}{(\rho_L-\rho_G)gD}\right)^{0.58} \tag{3.117}$$

3. Calculate interfacial friction factor (f_i) using Equation 3.118, where ε is the interfacial roughness:

$$f_i = \left.\frac{0.0625}{\left[\log\left(\frac{15}{Re_G}+\frac{\varepsilon}{3.715D}\right)\right]^2}\right\} \quad \text{where } \varepsilon = \frac{2.3D(1-\alpha_G)}{4\phi} \tag{3.118}$$

4. From Equation 3.119, calculate the gas-phase friction factor (f_G) based on gas-phase Reynolds number as a function of actual gas velocity ($Re_G = (\rho_G U_G D)/\mu_G$):

$$f_G = \left.\frac{0.07725}{(\log(Re_G/7))^2}\right\} \quad 2100 < Re_G < 10^8 \tag{3.119}$$

5. The two-phase friction factor is then calculated using

$$f_{TP} = f_G(1-\phi) + f_i\phi \tag{3.120}$$

6. Finally, the two-phase pressure drop based on two-phase friction factor is calculated from Equation 3.121. Note that Equation 3.121 uses actual gas-phase velocity (U_G) and not the superficial gas velocity (U_{SG}):

$$-\left(\frac{dp}{dz}\right)_f = \frac{2f_{TP}\rho_G U_G^2}{D} \tag{3.121}$$

3.5.3 Double Circle Model

Double circle model is a mechanistic model proposed by Chen et al. (1997), which considers the concave shape of the gas–liquid interface by using the geometrical intersection of a hypothetical circle with the pipe centerline (see Figure 3.30). Compared to the ARS model, the shape of gas–liquid interface used by double circle model is more realistic and the overall model is based on the mechanistic model of Taitel and Dukler (1976). To begin with, the use of Chen et al. (1997) model requires the determination of Ψ and Ψ_i in radians.

Note that the subtended angle (Ψ) used by Chen et al. (1997) is half of that used by Taitel and Dukler (1976) and ARS models. The following step-by-step procedure is required to solve for void fraction and frictional pressure drop using double circle model:

1. Calculate the angle subtended by the liquid phase with the pipe centerline using the relationship $\Psi = \pi\phi$ where the fraction of pipe circumference wetted by the liquid phase is obtained by Equation 3.117 (same as the ARS model).
2. Once the angle Ψ is known, the angle Ψ_i is calculated from Equation 3.122 using iterative technique. The value of void fraction required in this equation is a guess value obtained by solving for the Taitel and Dukler (1976) flat surface model:

$$\Psi_i = \left(\frac{\sin\Psi_i}{\sin\Psi}\right)^2\left(\Psi + \frac{\sin^2\Psi}{\tan\Psi_i} - \frac{\sin 2\Psi}{2} - \pi(1-\alpha_G)\right) \tag{3.122}$$

3. Next, the diameter of offset circle (D_i) is determined from

$$D_i = D\frac{\sin\Psi}{\sin\Psi_i} \tag{3.123}$$

4. The perimeter of pipe occupied by the gas and liquid phase and the gas–liquid interface is determined from Equation 3.124. The calculation of the hydraulic diameters (D_G and D_L) and the area occupied by each phase (A_G and A_L) is the same as that given by Equations 3.111 and 3.112:

$$P_G = (\pi - \Psi)D, \quad P_L = \Psi D, \quad P_i = \Psi_i D_i \tag{3.124}$$

5. Interfacial friction factor is calculated using Equation 3.125 where the superficial gas velocity during smooth to wavy stratified flow transition is defined by Equation 3.126. Friction factors for gas (f_G) and liquid (f_L) phase are obtained using the procedure similar to Taitel and Dukler (1976) model, that is, Equation 3.110.

$$\frac{f_i}{f_G} = 1 + 3.75\left(\frac{1-\alpha_G}{\phi}\right)^{0.2}\left(\frac{U_{SG}}{U_{SG,t}} - 1\right)^{0.08} \tag{3.125}$$

$$U_{SG,t} = \sqrt{\frac{4\nu_L(\rho_L - \rho_G)g}{0.06\rho_G U_L}} \tag{3.126}$$

6. Solve for Equation 3.108 by updating the values of void fraction until convergence is obtained.
7. Use converged value of void fraction obtained from step 6 to calculate for two-phase pressure drop using Equation 3.106 or 3.107.

Note that for a quick convergence, the initial guess of void fraction required to calculate actual phase velocities, hydraulic diameters, and Ψ_i is calculated from the Taitel and Dukler (1976) model. It must be mentioned that the double circle method is more complex than the Taitel and Dukler (1976) and ARS models since it involves two iterative solutions for α_G and Ψ_i. The following example problem provides an overview of the procedure required to solve for void fraction and pressure drop in two-phase stratified flow.

Example Problem 3.1

Consider the horizontal two-phase flow of air and water in a 78 mm I.D. smooth polycarbonate pipe. The gas- and liquid-phase superficial velocities are 20 and 0.04 m/s, respectively. Assuming the stratified flow pattern to exist, determine the void fraction and two-phase frictional pressure drop using

(a) Taitel and Dukler (1976) (flat surface), (b) ARS, and (c) double circle models. The physical properties of gas and liquid phase can be taken as follows:

Property	Air	Water
Density	1.2 kg/m^3	998 kg/m^3
Dynamic viscosity	18.5 × 10^{-6} Pa s	0.001 Pa s

Solution

(a) Calculation of void fraction and pressure drop using Taitel and Dukler (1976) method: First, calculate the Reynolds number based on superficial velocity of gas and liquid phase. The single-phase friction factors for smooth pipe are found using appropriate friction factor correlation such as that of Blasius (1913) (see Equation 3.71):

$$Re_{SG} = \frac{\rho_G U_{SG} D}{\mu_G} = \frac{1.2 \times 20 \times 0.078}{18.5 \times 10^{-6}} = 1.012 \times 10^5 \Rightarrow f_G = 0.00448$$

$$Re_{SL} = \frac{\rho_L U_{SL} D}{\mu_L} = \frac{998 \times 0.04 \times 0.078}{0.001} = 3113.7 \Rightarrow f_L = 0.0107$$

Now calculate single-phase pressure drop (based on superficial phase velocity) for each phase and hence X parameter from Equation 3.90. The single-phase pressure drop calculation for each phase using Equations 3.88 and 3.86 is shown as follows:

$$-\left(\frac{dp}{dz}\right)_G = \frac{2 f_G \rho_G U_{SG}^2}{D} = \frac{2 \times 0.00448 \times 1.2 \times 20^2}{0.078} = 55.14 \text{ Pa/m}$$

$$-\left(\frac{dp}{dz}\right)_L = \frac{2 f_L \rho_L U_{SL}^2}{D} = \frac{2 \times 0.0107 \times 998 \times 0.04^2}{0.078} = 0.438 \text{ Pa/m}$$

$$\therefore X = \sqrt{\frac{(dp/dz)_L}{(dp/dz)_G}} = \sqrt{\frac{0.438}{55.14}} = 0.09$$

For horizontal two-phase flow, Equation 3.14 gives $Y = 0$, and using the graphical solution in Figure 3.8, the nondimensional liquid height is $h_L/D \approx 0.1$. Using this ratio of equilibrium liquid height and pipe diameter, the angle subtended by the liquid phase with pipe centerline and hence the void fraction in stratified flow is calculated using Equations 3.115 and 3.114:

$$\Psi = 2\arccos(1 - 0.2) = 73.74°(1.287^r) \Rightarrow \alpha_G = 1 - \frac{\Psi - \sin\Psi}{2\pi} = 0.948$$

This value of void fraction of 0.948 is an initial estimate of the void fraction obtained using the graphical solution. This void fraction may be further updated to satisfy Equation 3.108. Once the void fraction is determined, the actual phase velocities (see Table 3.1 for U_G and U_L), hydraulic diameters (Equation 3.111), the cross-sectional area occupied by each phase (Equation 3.112), and the wetted perimeter of each phase (Equation 3.113) are calculated as follows:

$$U_G = \frac{U_{SG}}{\alpha_G} = \frac{20}{0.948} = 21.1 \text{ m/s}, \quad U_L = \frac{U_{SL}}{1 - \alpha_G} = \frac{0.04}{1 - 0.948} = 0.77 \text{ m/s}$$

$$A_G = \alpha_G \frac{\pi D^2}{4} = 0.00453 \text{ m}^2, \quad A_L = (1 - \alpha_G)\frac{\pi D^2}{4} = 0.000248 \text{ m}^2$$

$$P_L = 0.0502 \text{ m}, \quad P_G = 0.195 \text{ m}, \quad P_i = 0.0468 \text{ m}, \quad D_G = 0.0749 \text{ m}, \quad D_L = 0.0197 \text{ m}$$

The Reynolds numbers based on actual gas and liquid-phase velocities are found to be

$$Re_G = \frac{1.2\times(20/0.948)\times 0.0749}{18.5\times 10^{-6}} = 1.025\times 10^5$$

$$Re_L = \frac{998\times(0.04/(1-0.948))\times 0.0197}{0.001} = 15139$$

The single-phase friction factors for each phase are found using Equation 3.110:

$$f_G = 0.046(1.025\times 10^5)^{-0.2} = 0.00457$$

$$f_L = 0.046\times(15139)^{-0.2} = 0.00671$$

Now, the wall and interfacial shear stresses using $f_i = f_G$ are calculated using Equation 3.109:

$$\tau_{wG} = \frac{0.00457\times 1.2\times 21.1^2}{2} = 1.232\ \text{N/m}^2$$

$$\tau_{wL} = \frac{0.00671\times 998\times 0.77^2}{2} = 1.985\ \text{N/m}^2$$

$$\tau_i = \frac{0.00457\times 1.2\times(21.1-0.77)^2}{2} = 1.133\ \text{N/m}^2$$

Now solve Equation 3.108 using the known values of shear stress, wetted perimeter, and cross-sectional area occupied by each phase. For these values, Equation 3.108 is not satisfied (residual = −121.1), and hence, the value of h_L/D is updated to find a new value of void fraction and the remaining steps are repeated. Iterate through these calculations until the residual of Equation 3.108 is approximately zero. After a few iterations, it is found that Equation 3.108 is satisfied (residual = 0.008) for $h_L/D \approx 0.1117$ and $\alpha_G = 0.938$ ($\Psi = 78.1° = 1.363^r$). Finally, after the convergence of Equation 3.108, two-phase frictional pressure drop is obtained by solving either Equation 3.106 or Equation 3.107. It should be noted that the use of Equation 3.106 or 3.107 requires calculation of updated values of shear stresses (τ_{wL}, τ_{wG}, τ_i) based on updated friction factors (f_G, f_L, f_i), the cross-sectional area occupied by each phase (A_G, A_L), and wetted perimeters of each phase and the gas–liquid interface (P_G, P_L, P_i). Two-phase pressure drop calculation using Equation 3.107 is shown as follows:

$$-\left(\frac{dp}{dz}\right)_f = \tau_{wL}\frac{P_L}{A_L} - \tau_i\frac{P_i}{A_L} = 1.445\frac{0.0531}{0.000296} - 1.17\frac{0.0491}{0.000296} = 66.1\ \text{Pa/m}$$

(b) *ARS model*: Calculate void fraction using Equation 3.116 where $Re_{SL} = \rho_L U_{SL} D/\mu_L = 3113.7$:

$$\frac{1-\alpha_G}{\alpha_G} = \frac{0.04}{20}\left[1+\left(108\times 3113.7^{-0.726}\times\frac{998}{1.2}\right)^{0.5}\right] \Rightarrow \alpha_G = 0.966$$

Now, calculate the actual gas and liquid-phase velocities (see Table 3.1), U_G = 20.7 m/s and U_L = 1.176 m/s. The fractional wetted perimeter is calculated from Equation 3.117:

$$\phi = 0.52(1-0.966)^{0.374} + 0.26\left(\frac{998\times 1.176^2}{(998-1.2)\times 9.81\times 0.078}\right)^{0.58} = 0.523$$

Calculate gas Reynolds number based on the actual gas velocity:

$$Re_G = \frac{\rho_G U_G D}{\mu_G} = \frac{1.2 \times 20.7 \times 0.078}{18.5 \times 10^{-6}} = 1.046 \times 10^5$$

Using Equation 3.119, the friction factor for single-phase gas flow (f_G) is calculated as follows:

$$f_G = \frac{0.07725}{(\log(Re_G/7))^2} = \frac{0.07725}{(\log(1.046 \times 10^5)/7)^2} = 0.0044$$

The interfacial friction factor is calculated using Equation 3.118 where the interfacial roughness is $\varepsilon = 2.3D(1-\alpha_G)/4\phi = 0.00291$:

$$f_i = \frac{0.0625}{\left[\log\left(\frac{15}{Re_G} + \frac{\varepsilon}{3.715D}\right)\right]^2} = \frac{0.0625}{\left[\log\left(\frac{15}{1.046 \times 10^5} + \frac{0.00291}{3.715 \times 0.078}\right)\right]^2} = 0.0156$$

Now, from Equation 3.120, the two-phase friction factor is calculated as

$$f_{TP} = (1-\phi) f_G + \phi f_i = (1-0.523) \times 0.0044 + 0.523 \times 0.0156 = 0.01025$$

The two-phase frictional pressure drop is calculated using Equation 3.121:

$$-\left(\frac{dp}{dz}\right)_f = \frac{2 f_{TP} \rho_G U_G^2}{D} = \frac{2 \times 0.01025 \times 1.2 \times 20.7^2}{0.078} = 135.1 \text{ Pa/m}$$

(c) *Double circle model*: Initially, the angle subtended by the liquid layer with the pipe centerline is calculated using the relationship $\Psi = \pi\phi = 1.153^r$ where $\phi = 0.367$ is calculated at a void fraction of $\alpha_G = 0.938$ (converged solution of Taitel and Dukler (1976) model) using Equation 3.117. Next, the angle Ψ_i is calculated using Equation 3.122. It should be noted that the angles (Ψ and Ψ_i) used in Equation 3.122 are expressed in radians:

$$\Psi_i = \left(\frac{\sin\Psi_i}{\sin(1.153)}\right)^2 \left(1.153 + \frac{\sin^2(1.153)}{\tan\Psi_i} - \frac{\sin(2 \times 1.153)}{2} - \pi(1-0.938)\right)$$

The solution to this equation, $\Psi_i = 0.931^r$, is obtained iteratively. Now, the diameter D_i of eccentric circle is found using Equation 3.123:

$$D_i = D\frac{\sin\Psi}{\sin\Psi_i} = 0.078 \times \frac{\sin(1.153)}{\sin(0.931)} = 0.088 \text{ m}$$

The wetted perimeter of gas and liquid phase based on Ψ and that of gas–liquid interface based on Ψ_i is calculated from Equation 3.124. The calculation of hydraulic diameters is similar to that of Taitel and Dukler (1976) given by Equation 3.111:

$$P_L = 0.0899 \text{ m}, \quad P_G = 0.155 \text{ m}, \quad P_i = 0.0827 \text{ m}, \quad D_G = 0.0753 \text{ m}, \quad D_L = 0.0132 \text{ m}$$

The Reynolds number of each phase is based on actual phase velocity and hydraulic pipe diameter, and the single-phase friction factors for each phase using Equation 3.110 are calculated as follows:

$$Re_G = \frac{\rho_G U_G D_G}{\mu_G} = \frac{1.2 \times 21.3 \times 0.0753}{18.5 \times 10^{-6}} = 104{,}036$$

$$Re_L = \frac{\rho_L U_L D_L}{\mu_L} = \frac{998 \times 0.645 \times 0.0132}{0.001} = 8497$$

$$f_G = 0.046(Re_G)^{-0.2} = 0.046(104{,}036)^{-0.2} = 0.00456$$

$$f_L = 0.046(Re_L)^{-0.2} = 0.046 \times (8497)^{-0.2} = 0.00753$$

To find f_i from Equation 3.125, first, determine the superficial gas velocity corresponding to the smooth to wavy stratified flow transition ($U_{SG,t}$) from Equation 3.126:

$$U_{SG,t} = \sqrt{\frac{4 \times (0.001/998)(998 - 1.2) \times 9.81}{0.06 \times 1.2 \times 0.465}} = 0.918$$

$$f_i = 0.00456\left[1 + 3.75\left(\frac{1 - 0.938}{0.367}\right)^{0.2}\left(\frac{20}{0.918} - 1\right)^{0.08}\right] = 0.0198$$

Now, the wall and interfacial shear stresses are calculated using Equation 3.109:

$$\tau_{wG} = \frac{0.00456 \times 1.2 \times 21.3^2}{2} = 1.244 \text{ N/m}^2$$

$$\tau_{wL} = \frac{0.00753 \times 998 \times 0.645^2}{2} = 1.563 \text{ N/m}^2$$

$$\tau_i = \frac{0.0198 \times 1.2 \times (21.3 - 0.645)^2}{2} = 5.087 \text{ N/m}^2$$

Equation 3.108 is not satisfied (residual = 1083), and hence, the void fraction value is updated and all other subsequent steps are repeated. At convergence (residual = 0.002), α_G = 0.961, Ψ = 1.48^r, and Ψ_i = 1.407^r. For the converged value of void fraction, recalculate the gas, liquid, and interfacial shear stress from Equation 3.109 and then calculate two-phase pressure drop using Equation 3.106 or 3.107. Note that these equations require updated values of shear stresses based on the converged values of void fraction. Pressure drop from Equation 3.107 is calculated as follows:

$$-\left(\frac{dp}{dz}\right)_f = \tau_{wL}\frac{P_L}{A_L} - \tau_i\frac{P_i}{A_L} = 4.277\frac{0.1156}{0.0001834} - 4.234\frac{0.1109}{0.0001834} = 135.6 \text{ Pa/m}$$

Discussion: For similar flow conditions, Badie et al. (2000) measured α_G = 0.956 and $(dp/dz)_f$ = 115 Pa/m. Note that the void fraction and frictional pressure drop obtained by solving for ARS model and double circle model are comparable to the measurements of Badie et al. (2000). The prediction of void fraction using Taitel and Dukler (1976) model is within ±2% of the measured void fraction by Badie et al. (2000). However, the frictional pressure drop calculated using Taitel and Dukler (1976) is significantly less than the experimental value. This is possibly because of the use of f_i/f_G = 1 in their model. The use of suitable and more realistic model for f_i/f_G in Taitel and Dukler

(1976) may yield better results. For example, the use of $f_i/f_G = 10$ recommended by Crowley et al. (1992) would give a better prediction of frictional pressure drop as 126.5 Pa/m. Conclusively, the success of these three methods in the prediction of void fraction and pressure drop in stratified two-phase flow is subject to the validity and accuracy of the closure relationships used in these models. Different forms of models for the calculation of f_i/f_G could be obtained from Ottens et al. (2001).

3.6 Modeling of Annular Flow

The annular flow structure exhibits separated flow characteristics and hence could be appropriately modeled using SFM approach. The two-phase flow literature reports several annular flow pattern–specific models to determine two-phase flow parameters such as void fraction, pressure drop, and heat transfer. Section 3.3.4 gives some of the existing correlations in the two-phase flow literature that can satisfactorily predict void fraction in annular flow. This section specifically focuses on some salient features of annular flow such as liquid entrainment fraction, film thickness, film flow rates, interfacial friction, and their interrelationships.

3.6.1 Entrainment

A peculiar phenomenon known as entrainment is observed in the annular flow due to the relative motion between the gas and the liquid phase. The entrainment process is characterized by the flow of tiny liquid droplets into the central fast-moving gas core. The liquid entrainment is a consequence of the significant shear at the gas–liquid interface that causes tearing of the liquid waves crests in the form of ligaments and depends on the phase flow rates, pipe diameter, and orientation and the surface tension at the gas–liquid interface. The liquid entrainment fraction (E) is defined as the ratio of mass flow rate/flux of liquid drops entering into the gas core to the total mass flow rate/flux of the liquid phase. Correct knowledge of the rate of liquid entrainment or alternatively the fraction of liquid entrainment is crucial in analyzing heat and mass transfer processes in annular flows. In case of boiling two-phase flows, accurate estimation of the liquid entrainment fraction is necessary in the determination of critical heat flux and dryout conditions. Ishii and Grolmes (1975) studied the different possible mechanisms responsible for liquid entrainment process. They found that liquid entrainment can happen due to any or all of the wave undercut, wave rolling, wave coalescence, and ripple shearing mechanisms. Additionally, the phenomenon of "bubble burst" due to rupture of liquid-phase crests and "droplet impingement" due to rolling waves may also contribute to the entrainment process.

The different entrainment mechanisms suggested by Ishii and Grolmes (1975) are illustrated in Figure 3.32. As shown in Figure 3.33, critical values of gas and liquid flow rates are associated with the entrainment process and below which no liquid entrainment is expected to occur. Based on the experimental data, two-phase flow literature offers several correlations to determine the nondimensional critical gas

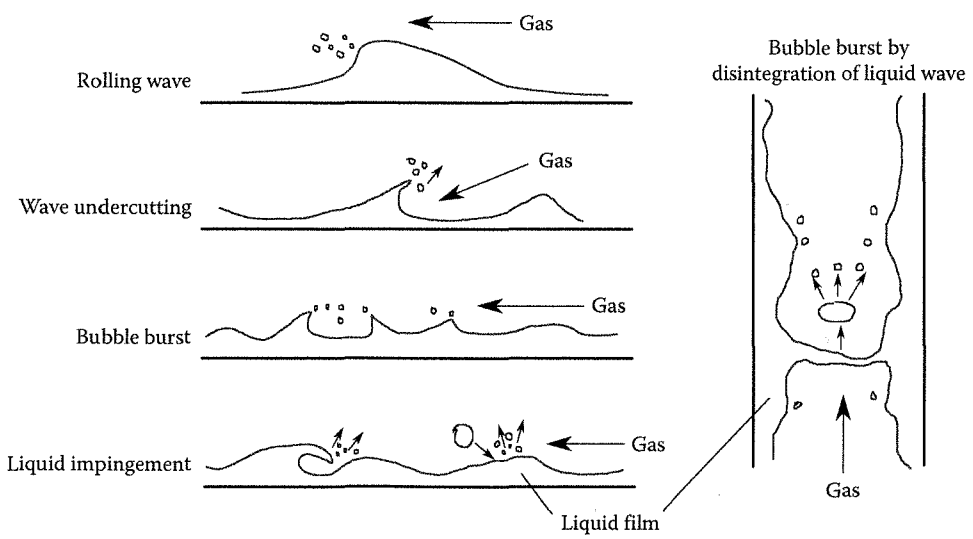

Figure 3.32

Entrainment mechanisms suggested by Ishii and Grolmes (1975).

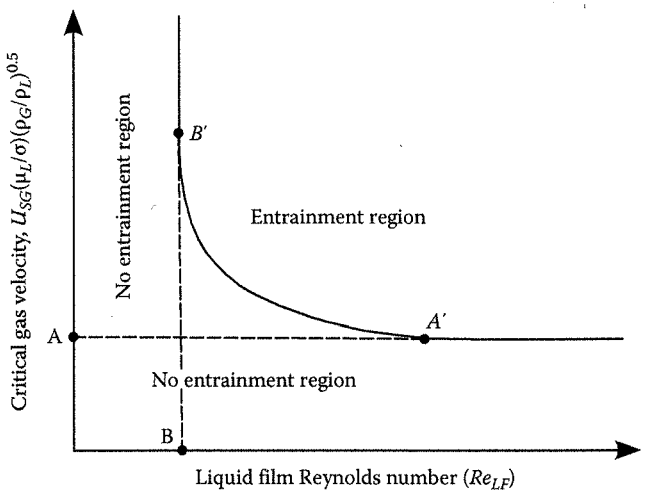

Figure 3.33

Inception criteria for entrainment. (Adapted from Ishii, M. and Grolmes, M.A., *AIChE J.*, 21, 308, 1975.)

velocity and the liquid film Reynolds (Re_{LF}) number below which the entrainment phenomenon is negligible or alternatively above which the amount of liquid entrainment is significant. Note that the Reynolds number based on liquid flowing in the form of film is defined by Ishii and Grolmes (1975) as $Re_{LF} = (4\delta U_L \rho_L)/\mu_L$ and using the concept of equivalent diameter it follows that $Re_{SL} = (\rho_L U_{SL} D)/\mu_L$. Refer to Section 3.6.2, Equation 3.138, for this identity between two forms of Reynolds number ($Re_{LF} = Re_{SL}$).

One such criterion in terms of liquid film Reynolds number proposed by Ishii and Grolmes (1975) is represented by Equation 3.127. Equation 3.127 sets the absolute limit for the inception of entrainment process and represents point B in Figure 3.33 below which entrainment cannot take place. Ishii and Grolmes (1975) found that at point A', $Re_{LF} = 1635$ and beyond which the entrainment affected region is insensitive to the increase in liquid flow rates. The critical gas velocity for Re_{LF} greater than that by Equation 3.127 is obtained from Equation 3.128. The critical gas velocity to the left-hand side of this equation is essentially a nondimensional superficial gas velocity normalized using liquid-phase dynamic viscosity and the surface tension. Note that for Re_{LF} greater than $Re_{LF,C}$ but less than 160, critical gas velocity is independent of liquid viscosity number given by Equation 3.129:

$$Re_{LF,C} = 154.7\left(\frac{\rho_L}{\rho_G}\right)^{0.75}\left(\frac{\mu_G}{\mu_L}\right)^{1.5} \tag{3.127}$$

$$\frac{U_{SG}\mu_L}{\sigma}\sqrt{\frac{\rho_G}{\rho_L}} \geq \begin{cases} 1.5Re_{LF}^{-0.5} & : Re_{LF,C} < Re_{LF} < 160 \\ 11.78N_{\mu}^{0.8}Re_{LF}^{-0.33} & : N_{\mu} \leq 0.066, 160 \leq Re_{LF} \leq 1635 \\ 1.35Re_{LF}^{-0.33} & : N_{\mu} > 0.066, 160 \leq Re_{LF} \leq 1635 \\ N_{\mu}^{0.8} & : N_{\mu} \leq 0.066, Re_{LF} > 1635 \\ 0.1146 & : N_{\mu} > 0.066, Re_{LF} > 1635 \end{cases} \tag{3.128}$$

$$N_{\mu} = \frac{\mu_L}{(\rho_L \sigma\sqrt{\sigma/(g\Delta\rho)})^{0.5}} \tag{3.129}$$

Note that Equations 3.127 and 3.128 predict the onset of entrainment and not the magnitude of entrainment fraction. To predict the liquid entrainment fraction, Ishii and Mishima (1989) proposed a correlation applicable to air–water equilibrium annular flow. As shown in Equation 3.130, their correlation is a function of modified Weber number given by Equation 3.131. Although the correlation of Ishii and Mishima (1989) consists of nondimensional numbers as a function of fluid physical

properties, their correlation is primarily based on air–water data and its validity for other fluid combinations must be scrutinized before use:

$$E = \tanh\left(7.25\times10^{-7} We^{1.25} Re_{SL}^{0.25}\right) \left\{ \begin{array}{l} 0.1 \le p_{sys} \le 0.4\,\text{MPa} \\ 9.5 \le D \le 32\,\text{mm} \\ 370 \le Re_{SL} \le 6400 \end{array} \right. \tag{3.130}$$

$$We = \frac{\rho_G U_{SG}^2 D}{\sigma}\left(\frac{\rho_L - \rho_G}{\rho_G}\right)^{0.33} \tag{3.131}$$

Cioncolini and Thome (2012b) proposed a method to predict liquid entrainment fraction in gas–liquid annular flows. In comparison to Ishii and Mishima (1989), their correlation is based on a more comprehensive data set and is claimed to be valid for $5 \le D \le 95$ mm, $0.1 \le p_{sys} \le 20$ MPa, and for both adiabatic and evaporating flows in vertical upward flow. Recently, Bhagwat and Ghajar (2015b) have introduced a correction factor ($\xi + 120\cos^2\theta$) to the Cioncolini and Thome (2012b) correlation to improve its accuracy at high system pressures and horizontal and inclined pipe orientations. This correction factor embedded into the original correlation of Cioncolini and Thome (2012b) is expressed by Equation 3.132 where ξ is calculated from Equation 3.133. The need of a correction factor for the effect of high system pressure on liquid entrainment fraction is explained in the work by Bhagwat and Ghajar (2015b). Note that the use of Equation 3.133 requires system pressure (p_{sys}) with units of MPa. The gas core Weber number and the gas core density are calculated using Equations 3.134 and 3.135, respectively:

$$E = \left(1 + \left(\xi + 120\cos^2\theta\right) We_c^{-0.8395}\right)^{-2.209} \left\{ \begin{array}{l} 0.1 \le p_{sys} \le 20\,\text{MPa} \\ 5 \le D \le 95\,\text{mm} \\ 10 \le We_c \le 10^5 \end{array} \right. \tag{3.132}$$

$$\xi = \begin{cases} 280 & : 0.1 \le p_{sys} < 10\,\text{MPa} \\ 4637.8 \times p_{sys}^{-1.6} & : p_{sys} \ge 10\,\text{MPa} \end{cases} \tag{3.133}$$

$$We_c = \frac{\rho_c U_{SG}^2 D}{\sigma} \tag{3.134}$$

$$\rho_c = \frac{x + E(1-x)}{(x/\rho_G) + (E(1-x)/\rho_L)} \tag{3.135}$$

Equation 3.132 needs to be solved using iterative technique since the core density required in the calculation of the core Weber number depends upon the liquid entrainment fraction. Cioncolini and Thome (2012b) suggested a two-step predictor and corrector method such that the predictor method predicts the liquid entrainment fraction for an initial guess of core density approximately equal to the gas-phase density (i.e., $\rho_c \approx \rho_G$). In the corrector step, the E value from predictor step is used to calculate new value of gas core density and hence the liquid entrainment fraction. The variation of liquid entrainment fraction as a function of system pressure using the proposed modification by Bhagwat and Ghajar (2015b) to the original Cioncolini and Thome (2012b) correlation is illustrated in Figure 3.34. It is evident that at low ($We_c \le 10$) and high ($We_c \ge 10^5$) gas core Weber numbers, the effect of system pressure on liquid entrainment fraction is small. Figure 3.34 is plotted for vertical two-phase flow and can be used as a graphical solution to determine liquid entrainment fraction.

3.6.2 Triangular Relationship in Annular Flow

Triangular relationship in the annular flow in essence is a relationship between three principle dependent system parameters, that is, pressure gradient, liquid film thickness (δ), and the liquid film flow rate ($\dot{m}_{LF}$), such that if any of these two variables are known, the third unknown variable may be calculated. Although the triangular relationship forms a basis for different correlations developed for annular flow, these dependent

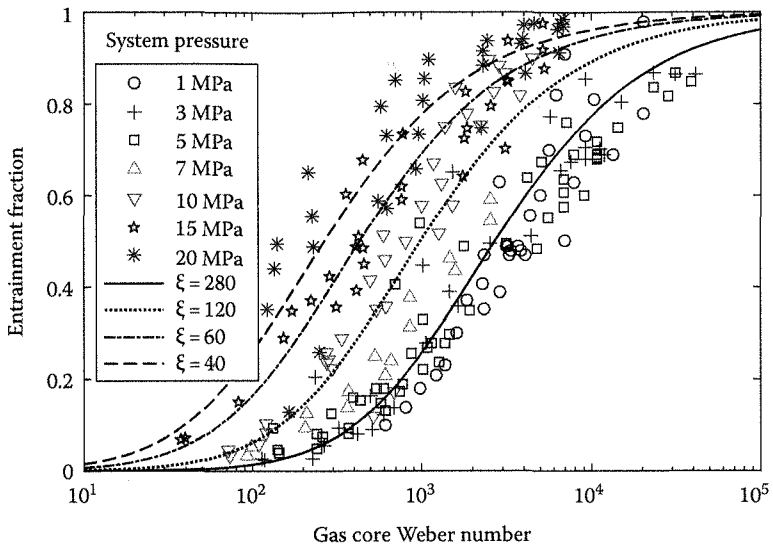

Figure 3.34

Variation of liquid entrainment fraction as a function of system pressure (trends predicted by Equation 3.132).

variables that form a triangular relationship cannot be practically calculated from the independent system parameters such as phase flow rates, fluid properties, and pipe geometry and thus further require closed-form solutions. The closed-form solutions required to form triangular relationship for the annular flow are usually in the form of equations for liquid entrainment fraction (E) and two-phase frictional multiplier (Φ^2) involving two-phase (f_{TP}) or interfacial (f_i) friction factors. This section briefly introduces the concept of triangular relationship and illustrates a step-by-step approach to calculate the system parameters in the annular flow. For more details, refer to works of Hewitt and Hall-Taylor (1970) and Collier and Thome (1996).

In order to solve for the triangular relationship, Hewitt and Hall-Taylor (1970) recommend the use of the following simplifying assumptions:

1. Film thickness is very small with respect to pipe diameter, that is, $\delta \ll D$.
2. Shear stress in liquid film is constant and equal to the wall shear stress.
3. Hydrostatic and accelerational effects on the gas core and liquid film are negligible (compared to frictional pressure drop).

Assuming axis symmetric flow, uniform film thickness, and negligible contribution of hydrostatic and accelerational pressure drops (in comparison to frictional pressure drop), the momentum balance on the liquid film in the annular flow leads to Equation 3.136 for two-phase frictional pressure drop. This two-phase frictional pressure drop is expressed in terms of actual velocity of the liquid flowing in the form of film (in contact with pipe wall) and that the liquid entrainment is negligible. Using the definition of Φ_L^2, Equation 3.86 could also be expressed as Equation 3.137:

$$-\left(\frac{dp}{dz}\right)_f = \frac{4\tau_{wL}}{D} = \frac{2f_{TP}\rho_L U_L^2}{D} \tag{3.136}$$

$$\Phi_L^2 = \frac{(dp/dz)_f}{(dp/dz)_L} = \frac{1}{(1-\alpha_G)^2}\left(\frac{f_{TP}}{f_L}\right) \tag{3.137}$$

Hewitt and Hall-Taylor (1970) have reported that using the concept of equivalent diameter and definition of void fraction under no entrainment, the Reynolds number of liquid flowing in the form of film is identical to the Reynolds number of liquid phase flowing alone through the pipe. This implies that based on identical Reynolds number defined by Equation 3.138, the friction factors of liquid flowing in the form of film and that alone through the pipe must be identical, that is, $f_{TP} = f_L$. Using this relationship,

Equation 3.137 reduces to Equation 3.139. This relationship however does not acknowledge the existence of liquid entrainment fraction that in certain practical cases may not be ignored. To account for the liquid entrainment fraction, Turner and Wallis (1965) have proposed the use of a similar relationship in which the single-phase pressure drop for the total liquid flow is replaced by the single-phase pressure drop for that part of the liquid flow that is in the form of film. The two-phase frictional multiplier suggested by Turner and Wallis (1965) is expressed by Equation 3.140 where the single-phase pressure drop of the liquid film flow is obtained from Equation 3.141:

$$\frac{\rho_L U_L 4\delta}{\mu_L} = \frac{\rho_L U_{SL} D}{\mu_L} \tag{3.138}$$

$$\Phi_L^2 = \frac{1}{(1-\alpha_G)^2} \tag{3.139}$$

$$\Phi_{LF}^2 = \frac{(dp/dz)_f}{(dp/dz)_{LF}} = \frac{1}{(1-\alpha_G)_{LF}^2} \tag{3.140}$$

$$-\left(\frac{dp}{dz}\right)_{LF} = \frac{2f_{LF}\rho_L(U_{SL}(1-E))^2}{D} = \frac{2f_{LF}(G(1-x)(1-E))^2}{D\rho_L} \tag{3.141}$$

Equation 3.140 can be considered as an empirical correlation for the determination of void fraction in the presence of liquid entrainment process; however, its implementation also requires the knowledge of two-phase frictional pressure drop. For a known or measured value of void fraction and liquid entrainment fraction, Equation 3.140 may not predict the correct magnitude of two-phase frictional pressure drop due to lack of information on the interfacial roughness and hence the interfacial shear stress. To address this issue, one more closure relationship is required that links the interfacial friction/roughness to the liquid flow rate or any other previously calculated variables such as void fraction or liquid entrainment fraction. This relationship could be obtained by considering yet another form of two-phase frictional multiplier in the form of Φ_G^2. Using similar assumptions that are used to obtain Equation 3.136, a momentum balance for gas core is used to obtain Equation 3.142. Using Equation 3.142, the two-phase frictional multiplier (Φ_G^2) assuming only gas phase flowing through pipe can be written as Equation 3.143 where the interfacial and gas shear stress are expressed by Equations 3.144 and 3.145, respectively. Thus, Φ_G^2 could be expressed as a function of void fraction, interfacial friction factor, core density, actual gas velocity, and liquid film velocity as expressed by Equation 3.146:

$$-\left(\frac{dp}{dz}\right)_f = \frac{4\tau_i}{(D-2\delta)} \tag{3.142}$$

$$\Phi_G^2 = \frac{(dp/dz)_f}{(dp/dz)_G} = \frac{4\tau_i/(D-2\delta)}{4\tau_G/D} \tag{3.143}$$

$$\tau_i = f_i\left(\frac{\rho_c(U_G - U_{LF})^2}{2}\right) \tag{3.144}$$

$$\tau_G = f_G\left(\frac{\rho_G U_{SG}^2}{2}\right) \tag{3.145}$$

$$\Phi_G^2 = \frac{1}{\sqrt{\alpha_G}}\frac{f_i}{f_G}\frac{\rho_c}{\rho_G}\frac{(U_G - U_{LF})^2}{U_{SG}^2} = \frac{1}{\sqrt{\alpha_G}}\frac{f_i}{f_G}\frac{\rho_c}{\rho_G}\left[\frac{1}{\alpha_G} - \frac{U_L(1-E)}{U_{SG}}\right]^2 \tag{3.146}$$

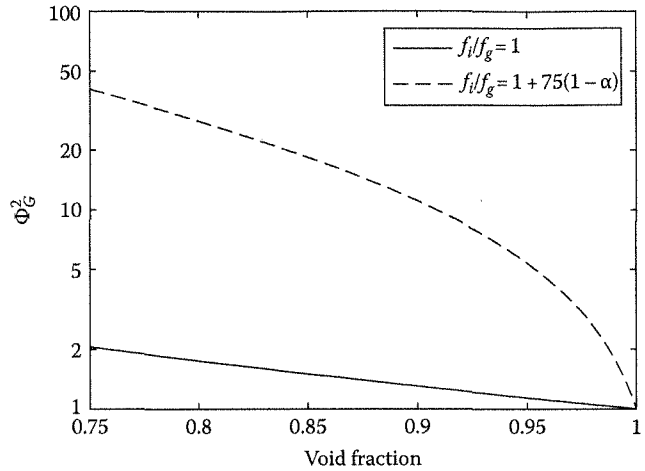

Figure 3.35

Effect of f_i/f_G on two-phase frictional multiplier (Φ_G^2).

Note that for low liquid flow rates, the velocity of liquid flowing in the form of film may be small compared to the fast-moving gas core such that $U_{LF} \ll U_G$. Also for low liquid flow rates, the liquid entrainment fraction may be negligible leading to $\rho_c/\rho_G \approx 1$. Thus, for such a simplified two-phase flow situation, Equation 3.146 reduces to Equation 3.147. Furthermore, for a more simplified assumption of smooth gas–liquid interface, ($f_i \approx f_G$) and Φ_G^2 can be expressed as Equation 3.148:

$$\Phi_G^2 = \frac{1}{\alpha_G^{5/2}} \frac{f_i}{f_G} \tag{3.147}$$

$$\Phi_G^2 = \frac{1}{\alpha_G^{5/2}} \tag{3.148}$$

It must be mentioned that the assumption of smooth gas–liquid interface (f_i/f_G) is an unrealistic assumption for the annular flow and the calculation of two-phase frictional multiplier, and, the two-phase frictional pressure drop may deviate significantly from actual conditions. It is evident from Figure 3.35 that by accounting for the interfacial roughness, the predicted values of Φ_G^2 could be significantly greater than that for the ideal conditions. Going back to Equation 3.146, the ratio f_i/f_G could be replaced with the empirical correlation in the form of Equation 3.149 proposed by Wallis (1962). Note that the two-phase flow literature reports several empirical relationships to model the ratio of f_i/f_G. Some of these correlations are listed in Table 3.9:

$$\frac{f_i}{f_G} = 1 + 300\frac{\delta}{D} = 1 + 75(1-\alpha_G) \tag{3.149}$$

The mass flow rate of liquid phase in the form of film, the actual velocity of the liquid film, and the Reynolds number of the liquid film are defined by Equations 3.150 through 3.152, respectively:

$$\dot{m}_{LF} = \dot{m}_L(1-E) \tag{3.150}$$

$$U_{LF} = U_L(1-E) \tag{3.151}$$

$$Re_{LF} = Re_{SL}(1-E) \tag{3.152}$$

The density of the gas core (ρ_c) is obtained using Equation 3.135 based on liquid entrainment fraction. Note that only for negligible liquid entrainment fraction $\rho_c \approx \rho_G$. Figure 3.36 shows the algorithm to use in

Table 3.9 List of Correlations for Interfacial Friction Factors

Source	Correlation
Moeck (1970)	$f_i = 0.005\left(1+1458\left(\frac{\delta}{D}\right)^{1.42}\right)$
Laurinat et al. (1984)	$f_i = f_G\left(2+2.5\times10^{-5}\frac{Re_{LF}}{D}\right)\alpha_G^{5/2}$
Wallis (1962)	$f_i = 0.005(1+75(1-\alpha_G))$
Wongwises and Kongkiatwanitch (2001)	$f_i = 17.172Re_{SG}^{-0.768}\left(\frac{\delta}{D}\right)^{-0.253}$
Fore et al. (2000)	$f_i = 0.005\left(1+300\left[\left(1+\frac{17{,}500}{Re_G}\right)\frac{\delta}{D}-0.0015\right]\right)$

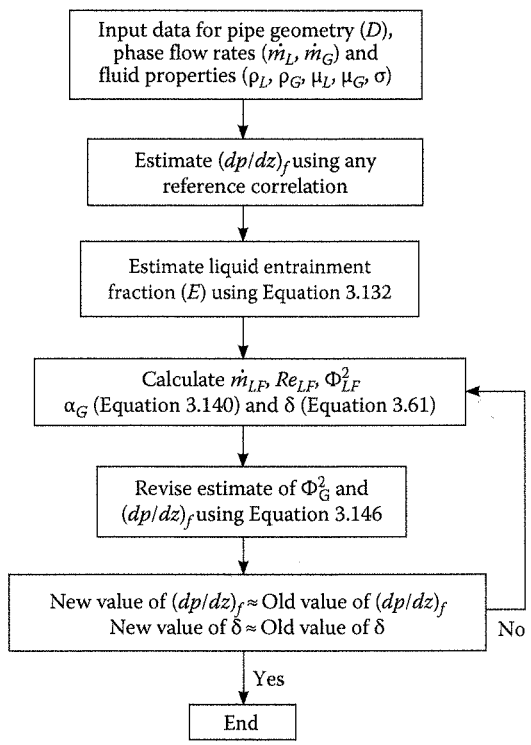

Figure 3.36

Algorithm to solve triangular relationship in annular flow.

triangular relationship for the determination of frictional pressure drop, liquid film thickness, and flow rate of liquid in the form of film.

Example Problem 3.2

Consider the vertical upward two-phase flow of air–water mixture in a 45 mm I.D. smooth pipe. At near atmospheric system pressure, the two-phase mixture flows with a quality (x) and mass flux (G) of 0.25 and 210 kg/m^2, respectively. The physical properties of air and water are as follows: $\rho_G = 1.5$ kg/m^3, $\rho_L = 998$ kg/m^3, $\mu_G = 18.5 \times 10^{-6}$ Pa s, $\mu_L = 0.001$ Pa s, and $\sigma = 0.072$ N/m. Using triangular relationship for annular flow, determine the film thickness (δ), film flow rate ($\dot{m}_{LF}$), and pressure drop $(dp/dz)_f$. Assume that adiabatic annular flow at equilibrium exists in the pipe.

Solution

The solution to this problem follows the calculation algorithm illustrated in Figure 3.36.

(1) *Make initial estimate of two-phase pressure drop*: Calculate gas- and liquid-phase Reynolds numbers (see Table 3.1) and single-phase friction factors from Equation 3.71:

$$Re_{SG} = \frac{GxD}{\mu_G} = \frac{210 \times 0.25 \times 0.045}{18.5 \times 10^{-6}} = 127703 \Rightarrow f_G = 0.00418$$

$$Re_{SL} = \frac{G(1-x)D}{\mu_L} = \frac{210 \times (1-0.25) \times 0.045}{0.001} = 7088 \Rightarrow f_L = 0.0086$$

Calculate the frictional pressure drop for gas and liquid phase assuming each phase flowing alone through the pipe:

$$-\left(\frac{dp}{dz}\right)_G = \frac{2f_G(Gx)^2}{D\rho_G} = \frac{2 \times 0.00418(210 \times 0.25)^2}{0.045 \times 1.5} = 341.3\,(\text{Pa/m})$$

$$-\left(\frac{dp}{dz}\right)_L = \frac{2f_L(G(1-x))^2}{D\rho_G} = \frac{2 \times 0.0086(210 \times 0.75)^2}{0.045 \times 998} = 9.5\,(\text{Pa/m})$$

The parameter (X) of Lockhart and Martinelli (1949) and the two-phase frictional multiplier $\left(\Phi_G^2\right)$ are now obtained from Equations 3.90 and 3.89, respectively. For turbulent–turbulent region of gas and liquid flow $C = 20$ from Table 3.7:

$$X = \sqrt{\frac{(dp/dz)_L}{(dp/dz)_G}} = \sqrt{\frac{9.5}{341.3}} = 0.167$$

$$\Phi_G^2 = 1 + CX + X^2 = 1 + 20 \times 0.167 + 0.167^2 = 4.37$$

Now, the two-phase frictional pressure drop is calculated as

$$\left(\frac{dp}{dz}\right)_f = \Phi_G^2 \times \left(\frac{dp}{dz}\right)_G = 4.37 \times 341.3 = 1491.5\,(\text{Pa/m})$$

(2) *Estimate liquid entrainment fraction* (E): Liquid entrainment fraction can be estimated using Equation 3.132. First estimate the gas core Weber number using gas-phase density and predict the initial estimate of liquid entrainment fraction. The superficial gas velocity required in the determination of We_c is calculated as $U_{SG} = Gx/\rho_G = 210 \times 0.25/1.5 = 35$ m/s. Then find the gas core density using the initial estimate of E and recalculate Weber number and liquid entrainment fraction in corrector step. For near atmospheric system pressure $\xi = 280$ from Equation 3.133.

$$We_c = \frac{\rho_G U_{SG}^2 D}{\sigma} = \frac{1.5 \times 35^2 \times 0.045}{0.072} = 1148.4$$

$$E = (1 + 280 \times We_c^{-0.8395})^{-2.209} = 0.288$$

$$\rho_c = \frac{x + E(1-x)}{(x/\rho_G) + (E(1-x)/\rho_L)} = \frac{0.25 + 0.288 \times 0.75}{(0.25/1.5) + (0.288 \times 0.75/998)} = 2.8\,(\text{kg/m}^3)$$

$$We_c = \frac{\rho_c U_{SG}^2 D}{\sigma} = \frac{2.8 \times 35^2 \times 0.045}{0.072} = 2143.7$$

$$E = (1 + 280 \times We_c^{-0.8395})^{-2.209} = 0.44$$

The updated value of core density (ρ_c) based on entrainment in corrector step is $\rho_c = 3.47$ kg/m^3. Based on the predicted entrainment value ($E = 0.44$) and using Equation 3.150, the liquid film flow rate can be calculated as follows. The liquid mass flow rate required in this equation is $\dot{m}_L = G(1-x)\times A = 210(1-0.25)\times\pi/4\times 0.045^2 = 0.25$ kg/s:

$$\dot{m}_{LF} = (1-E)\dot{m}_L = (1-0.44)\times 0.25\,(\text{kg/s}) = 0.14\,(\text{kg/s})$$

(3) *Estimate liquid film thickness* (δ): To determine the liquid film thickness, first calculate the two-phase frictional multiplier $\left(\Phi_{LF}^2\right)$ based on the liquid film flow rate given by Equation 3.140. To determine Φ_{LF}^2, first calculate the friction factor (f_{LF}) for liquid film flow. The Reynolds number of liquid film is calculated from Equation 3.152 such that $Re_{LF} = Re_{SL} \times (1 - E) = 3969$, and hence, the corresponding friction factor from Equation 3.71 is $f_{LF} = 0.00995$:

$$\left(\frac{dp}{dz}\right)_{LF} = \frac{2f_{LF}(G(1-x)(1-E))^2}{D\rho_L} = \frac{2\times 0.00995\times(210\times 0.75\times 0.56)^2}{0.045\times 998} = 3.45\,(\text{Pa/m})$$

$$\Phi_{LF}^2 = \frac{(dp/dz)_f}{(dp/dz)_{LF}} = \frac{1491.5}{3.45} = 432.3$$

$$\Phi_{LF}^2 = \frac{1}{(1-\alpha_G)^2} = 432.3 \Rightarrow (1-\alpha_G) = \frac{4\delta}{D} = 0.0481$$

$$\therefore \alpha_G = 0.952 \quad \text{and} \quad \delta = 0.541\,\text{mm}$$

(4) *Update the value of two-phase pressure drop*: Use Equation 3.146 along with Equation 3.149 to calculate the new value of two-phase frictional multiplier $\left(\Phi_G^2\right)$ and compare it with the initial calculated value of $\Phi_G^2 = 4.37$. Here, we first find $U_{SL} = G(1 - x)/\rho_L = 210 \times 0.75/998 = 0.158$ m/s and $U_L = U_{SL}/(1 - \alpha_G) = 0.158/0.0481 = 3.28$ m/s:

$$\Phi_G^2 = \frac{1}{\sqrt{\alpha_G}}\frac{f_i}{f_G}\frac{\rho_c}{\rho_G}\left[\frac{1}{\alpha_G} - \frac{U_L(1-E)}{U_{SG}}\right]^2$$

$$\Phi_G^2 = \frac{1}{\sqrt{0.952}}(1+75\times 0.0481)\times\frac{3.47}{1.5}\left(\frac{1}{0.952} - \frac{3.28\times(1-0.44)}{35}\right)^2 = 10.88$$

Now, the updated value of two-phase frictional pressure drop is calculated as

$$\left(\frac{dp}{dz}\right)_f = \Phi_G^2 \times \left(\frac{dp}{dz}\right)_G = 10.88\times 341.3 = 3713.3\,(\text{Pa/m})$$

(5) *Repeat steps (3) and (4) to get consistent values of* δ *and* $(dp/dz)_f$: Since the new value of Φ_G^2 and frictional pressure drop is greater than the initial estimate, recalculate Φ_{LF}^2 value to obtain new estimates of δ and Φ_G^2. After 12 iterations consistent values of liquid film thickness, two-phase frictional multiplier $\left(\Phi_G^2\right)$ and hence the two-phase frictional pressure drop are obtained. The final values of parameters in triangular relationship are

Liquid film thickness (δ) = 0.398 mm.
Liquid film flow rate $\left(\dot{m}_{LF}\right) = 0.14$ kg/s.
Two-phase pressure drop $(dp/dz)_f = 2745$ Pa/m.
In addition, based on the iterated value of Φ_{LF}^2, $\alpha_G = 0.965$.

Discussion: For similar experimental conditions, Nguyen (1975) measured $\alpha_G = 0.951$ and $(dp/dz)_f = 2440$ Pa/m. Note that the converged values of void fraction and pressure drop obtained by solving triangular relationship are comparable with measured data of Nguyen (1975).

Moreover, the film thickness (δ = 0.398 mm) obtained using triangular relationship is comparable to the predicted (δ = 0.431 mm) film thickness by empirical correlation of Henstock and Hanratty (1976). It must be mentioned that the final converged values obtained using triangular relationship depend upon the closure relationships for liquid entrainment fraction (E), interfacial friction factor (f_i), and hence the two-phase frictional multiplier $\left(\Phi_G^2\right)$. There is no unanimity over the use of a particular set of closure equations, and hence, the use of different set of equations may yield slightly different solutions of triangular relationship.

3.7 Nonboiling Two-Phase Heat Transfer

Knowledge about nonboiling two-phase heat transfer is important in several applications in oil and gas and chemical engineering industry. In particular, during the production of two-phase hydrocarbon fluids from oil reservoirs and its transportation to the surface processing facilities, the temperature of hydrocarbons drops drastically and is favorable for hydrates formation and wax deposition. Wax deposition can result in problems including reduction of inner tube diameter causing blockage, increase in surface roughness of tube leading to restricted flow line pressure, and decrease in production and can lead to various mechanical problems. In such situations, the correct knowledge of heat transfer coefficients in two-phase flow is of utmost importance for the purpose of flow assurance in oil and gas industry. The following text provides a brief information on the phenomenon of two-phase flow models for nonboiling two-phase heat transfer. Detailed information on the effect of fluid properties and pipe orientation on two-phase heat transfer coefficient can be obtained from Tang (2011), Ghajar and Tang (2010), and Bhagwat et al. (2012).

3.7.1 Two-Phase Heat Transfer Model

In the two-phase flow literature, majority of the documented nonboiling two-phase heat transfer modeling methods are limited to specific pipe orientations, fluid combinations, and most importantly flow patterns. The subsea and surface pipe lines carrying a mixture of oil and gas together are usually laid in undulated form having near horizontal inclinations, and the existence of a specific flow pattern is uncertain. For such a scenario, the use of flow pattern and pipe orientation-specific two-phase heat transfer correlations may predict significant deviations from the actual conditions. To address this issue, Ghajar and coworkers in a series of papers have extensively studied the phenomenon of nonboiling two-phase heat transfer in pipes at different orientations. Ghajar and Tang (2009) proposed a robust correlation for two-phase heat transfer coefficient (h_{TP}) as presented by Equation 3.153. Their correlation is based on 986 experimental data points for different pipe orientations and fluid combinations:

$$h_{TP} = h_L F_p \left[1 + 0.55 \left(\frac{x}{1-x} \right)^{0.1} \left(\frac{1-F_p}{F_p} \right)^{0.4} \left(\frac{Pr_G}{Pr_L} \right)^{0.25} \left(\frac{\mu_L}{\mu_G} \right)^{0.25} I^{0.25} \right] \tag{3.153}$$

$$F_p = (1-\alpha_G) + \alpha_G F_s^2 \tag{3.154}$$

$$F_s = \frac{2}{\pi} \arctan\left(\sqrt{\frac{\rho_G (U_G - U_L)^2}{gD(\rho_L - \rho_G)}} \right) \tag{3.155}$$

$$I = 1 + Eo\,|\sin\theta| \tag{3.156}$$

The flow pattern factor (F_p) given by Equation 3.154 makes the Ghajar and Tang (2009) correlation independent of the flow patterns and depends on shape factor F_s and void fraction (α_G). The shape factor (F_s) given by Equation 3.155 considers the effect of the shape of gas–liquid interface on two-phase heat transfer, while the void fraction needs to be calculated using the correlations of Woldesemayat and Ghajar (2007) (use Equations 3.45 and 3.46). The variable I given by Equation 3.156 is defined in terms of Eötvös number, and it accounts for the effect of pipe orientation on h_{TP}:

$$Eo = \frac{(\rho_L - \rho_G) g D^2}{\sigma} \tag{3.157}$$

The single-phase heat transfer coefficient required in Equation 3.153 is based on in situ Reynolds number. All thermophysical properties required are calculated at bulk mean temperature except for the μ_w that is calculated at the pipe wall temperature. Note that the in situ liquid phase the Reynolds number used in Equation 3.158 for h_L is defined in terms of the square root of liquid holdup as shown in Equation 3.159:

$$h_L = 0.027 Re_L^{0.8} Pr_L^{0.33} \left(\frac{k_L}{D}\right)\left(\frac{\mu_L}{\mu_w}\right)^{0.14} \tag{3.158}$$

$$Re_L = \frac{4\dot{m}_L}{\pi D \mu_L \sqrt{1-\alpha_G}} = \frac{G(1-x)D}{\mu_L \sqrt{1-\alpha_G}} \tag{3.159}$$

3.7.2 Reynolds Analogy and Two-Phase Heat Transfer

The concept of Reynolds analogy that relates the skin friction factor or the frictional pressure drop with heat transfer in single-phase flow can also be extended to the case of two-phase flow. Using the concept of Reynolds analogy, Tang and Ghajar (2011) have developed a correlation that correlates the two-phase to single-phase heat transfer coefficient ratio to the two-phase frictional multiplier (ratio of two-phase to single-phase pressure drop). The physical form of this correlation is given by Equation 3.160. The two-phase mixture density (ρ_M) is calculated using void fraction, $\rho_M = \rho_L(1 - \alpha_G) + \rho_G\alpha_G$, F_p is calculated from Equation 3.154, h_L is calculated from Equation 3.158 using the Reynolds number (Re_{SL}) based on superficial liquid velocity (see Table 3.1). Note that Φ_L is the square root of the two-phase frictional multiplier calculated using Equation 3.86. In case if the two-phase frictional pressure drop is not known/measured, then suitable correlation valid for given two-phase flow conditions may be used to determine Φ_L. The void fraction required in the calculation of two-phase mixture density (ρ_M) is calculated using Woldesemayat and Ghajar (2007) correlation (Equations 3.45 and 3.46). Tang (2011) suggested that the exponents of F_p and Φ_L could vary between 0.1 and 0.5 depending upon the pipe orientation and fluid properties; however, the general structure of Reynolds analogy–based correlation remains unaltered. In Equation 3.160, the exponent (0.3) of F_p and Φ_L is based on the overall performance of their model for various pipe inclinations and fluid combinations:

$$h_{TP} = h_L F_p^{0.3} \left(\frac{\dot{m}_L}{\dot{m}}\right)\left(\frac{\rho_L}{\rho_M}\right)^{0.5} \Phi_L^{0.3} \tag{3.160}$$

Both the correlations of Ghajar and Tang (2009) (general heat transfer correlation) and Tang and Ghajar (2011) (Reynolds analogy–based heat transfer correlation) are applicable over the following range of parameters: $750 \le Re_{SL} \le 1.27 \times 10^5$, $14 \le Re_{SG} \le 21 \times 10^5$, $0.01 \le Pr_G/Pr_L \le 0.15$, $910 \le \rho_L \le 1210$ kg/m^3, $0.0036 \le \mu_G/\mu_L \le 0.026$, and $0° \le \theta \le +90°$. Within the range of these two-phase flow variables, both correlations are known to predict more than 80% and 90% of data points within ±20% and ±30% error bands, respectively. The physical structure of these correlations is modular and robust, and hence, the application of these correlations can be potentially extended to a wider range of two-phase flow conditions by modifying the empirical multiplying factors and exponents.

Example Problem 3.3

Consider the vertical upward two-phase flow of air and silicone oil in a 12 mm I.D. stainless steel pipe having a surface roughness of 20 μm. The mass flow rates of gas and liquid phase are 0.0015 kg/s and 0.9 kg/s, respectively. The fluid thermophysical properties may be taken as follows: $\rho_G = 1.2$ kg/m^3, $\rho_L = 920$ kg/m^3, $\mu_G = 18.4 \times 10^{-6}$ Pa s, $\mu_L = 0.005$ Pa s, $\mu_w = 0.004$ Pa s, $\sigma = 0.02$ N/m, $k_L = 0.12$ W/mK, $Pr_G = 0.71$, and $Pr_L = 64$. For a measured void fraction of $\alpha_G = 0.5$, determine the two-phase heat transfer coefficient for the flow of air and silicon oil using (1) heat transfer correlation of Ghajar and Tang (2009) given by Equation 3.153 and (2) Reynolds analogy given by Equation 3.160.

Solution

(1) Calculation of h_{TP} using Ghajar and Tang (2009) correlation:
The superficial gas (U_{SG}) and liquid (U_{SL}) velocities and the two-phase flow quality (x) are first calculated as follows:

$$U_{SG} = \frac{4\dot{m}_G}{\pi D^2 \rho_G} = \frac{4 \times 0.0015}{\pi \times 0.012^2 \times 1.2} = 11.05 \text{ m/s}$$

$$U_{SL} = \frac{4\dot{m}_L}{\pi D^2 \rho_L} = \frac{4 \times 0.9}{\pi \times 0.012^2 \times 920} = 8.65 \text{ m/s}$$

$$x = \frac{\dot{m}_G}{\dot{m}_G + \dot{m}_L} = \frac{0.0015}{0.0015 + 0.9} = 0.00166$$

From the given information of void fraction, the actual velocity of each phase is calculated as follows. In case if the void fraction is not known, Woldesemayat and Ghajar (2007) correlation (Equations 3.45 and 3.46) can be used for void fraction calculation. For the given flow conditions, Woldesemayat and Ghajar (2007) correlation gives $\alpha_G = 0.52$ that is within ±5% of the given void fraction value of 0.5:

$$U_G = \frac{U_{SG}}{\alpha_G} = \frac{11.05}{0.5} = 22.1 \text{ m/s}$$

$$U_L = \frac{U_{SL}}{1 - \alpha_G} = \frac{8.65}{1 - 0.5} = 17.3 \text{ m/s}$$

Now, the shape factor is calculated from Equation 3.155:

$$F_s = \left[\frac{2}{\pi} \arctan\left(\sqrt{\frac{\rho_G (U_G - U_L)^2}{gD(\rho_L - \rho_G)}} \right) \right]$$

$$= \left[\frac{2}{\pi} \arctan\left(\sqrt{\frac{1.2 \times (22.1 - 17.3)^2}{9.81 \times 0.012 \times (920 - 1.2)}} \right) \right] = 0.298$$

The flow pattern factor is obtained from Equation 3.154:

$$F_p = (1 - \alpha_G) + \alpha_G F_S^2 = (1 - 0.5) + 0.5 \times 0.298^2 = 0.544$$

The inclination factor for the vertical flow is calculated by Equation 3.156:

$$I = 1 + \frac{(\rho_L - \rho_G) g D^2}{\sigma} |\sin\theta| = 1 + \frac{(920 - 1.2) \times 9.81 \times 0.012^2}{0.02} = 65.9$$

Next, the in situ Reynolds number based on void fraction is calculated from Equation 3.159:

$$Re_L = \frac{4\dot{m}_L}{\pi D \mu_L \sqrt{1 - \alpha_G}} = \frac{4 \times 0.9}{\pi \times 0.012 \times 0.005 \times \sqrt{1 - 0.5}} = 27{,}009.5$$

The single-phase heat transfer coefficient is then calculated using Equation 3.158:

$$h_L = 0.027 Re_L^{0.8} Pr_L^{0.33} \left(\frac{\mu_L}{\mu_w}\right)^{0.14} \left(\frac{k_L}{D}\right)$$

$$= 0.027 \times 27{,}009.5^{0.8} \times 64^{0.33} \times \left(\frac{0.005}{0.004}\right)^{0.14} \left(\frac{0.12}{0.012}\right)$$

$$= 3{,}856\ \text{W/m}^2\ \text{K}$$

Using the two-phase heat transfer correlation of Ghajar and Tang (2009) given by Equation 3.153, h_{TP} is calculated as

$$h_{TP} = h_L F_p \left[1 + 0.55 \left(\frac{x}{1-x}\right)^{0.1} \left(\frac{1-F_p}{F_p}\right)^{0.4} \left(\frac{Pr_G}{Pr_L}\right)^{0.25} \left(\frac{\mu_L}{\mu_G}\right)^{0.25} I^{0.25}\right]$$

$$= 3856 \times 0.544 \left[1 + 0.55 \left(\frac{0.00166}{1-0.00166}\right)^{0.1} \left(\frac{1-0.544}{0.544}\right)^{0.4} \left(\frac{0.71}{64}\right)^{0.25} \left(\frac{0.005}{18.4 \times 10^{-6}}\right)^{0.25} 65.9^{0.25}\right]$$

$$= 4224\ \text{W/m}^2\ \text{K}$$

(2) Calculation of h_{TP} using the concept of Reynolds analogy: To use the concept of Reynolds analogy, we first need to find the two-phase frictional pressure drop and hence the two-phase frictional multiplier $\left(\Phi_L^2\right)$. The following steps calculate the two-phase pressure drop using the method of Lockhart and Martinelli (1949).

The Reynolds number of each phase and associated friction factors are calculated as shown as follows. Since the two-phase flow is through steel pipe having a roughness of 20 μm, we need to use appropriate correlation such as Colebrook (1939) or Churchill (1977) to account for the effect of pipe wall surface roughness on friction factor. Here, we use Colebrook (1939) friction factor correlation:

$$Re_{SG} = \frac{\rho_G U_{SG} D}{\mu_G} = \frac{1.2 \times 11.05 \times 0.012}{18.4 \times 10^{-6}} = 8{,}648 \Rightarrow f_G = 0.0081$$

$$Re_{SL} = \frac{\rho_L U_{SL} D}{\mu_L} = \frac{920 \times 8.65 \times 0.012}{0.005} = 19{,}099 \Rightarrow f_L = 0.0063$$

Now the single-phase pressure drop due to flow of gas and liquid phase is calculated by

$$-\left(\frac{dp}{dz}\right)_G = \frac{2 f_G \rho_G U_{SG}^2}{D} = \frac{2 \times 0.0081 \times 1.2 \times 11.05^2}{0.012} = 197.8\ \text{Pa/m}$$

$$-\left(\frac{dp}{dz}\right)_L = \frac{2 f_L \rho_L U_{SL}^2}{D} = \frac{2 \times 0.0063 \times 920 \times 8.65^2}{0.012} = 72{,}278.5\ \text{Pa/m}$$

The parameter X of Lockhart and Martinelli (1949) is calculated using the single-phase pressure drop as shown here:

$$X = \sqrt{\frac{(dp/dz)_L}{(dp/dz)_G}} = \sqrt{\frac{72{,}278.5}{197.8}} = 19.11$$

Since the single-phase flow of both phases is in turbulent region, we use $C = 20$ from Table 3.7 and the two-phase frictional multiplier using the method of Lockhart and Martinelli (1949) is calculated from Equation 3.89 as shown here:

$$\Phi_L^2 = 1 + \frac{20}{X} + \frac{1}{X^2} = 1 + \frac{20}{19.11} + \frac{1}{19.11^2} = 2.05 \Rightarrow \Phi_L = 1.43$$

Two-phase mixture density based on void fraction is calculated as follows:

$$\rho_M = \alpha_G \rho_G + (1 - \alpha_G)\rho_L = 0.5 \times 1.2 + (1 - 0.5) \times 920 = 460.6 \text{ kg/m}^3$$

Now using Equation 3.160, the two-phase heat transfer coefficient can be found. The value of h_L based on Re_{SL} is calculated from Equation 3.158. The value of $F_p = 0.544$ is found earlier in this problem:

$$h_L = 0.027 Re_{SL}^{0.8} Pr_L^{0.33} \left(\frac{\mu_L}{\mu_w}\right)^{0.14} \left(\frac{k_L}{D}\right)$$

$$= 0.027 \times 19{,}099^{0.8} \times 64^{0.33} \times \left(\frac{0.005}{0.004}\right)^{0.14} \left(\frac{0.12}{0.012}\right) = 2{,}922.6 \text{ W/m}^2 \text{ K}$$

Finally, the two-phase heat transfer coefficient using Reynolds analogy is found using Equation 3.160:

$$h_{TP} = h_L F_p^{0.3} \left(\frac{\dot{m}_L}{\dot{m}}\right) \left(\frac{\rho_L}{\rho_M}\right)^{0.5} \Phi_L^{0.3}$$

$$= 2922.6 \times 0.544^{0.3} \left(\frac{0.9}{0.9015}\right) \left(\frac{920}{460.6}\right)^{0.5} 1.43^{0.3}$$

$$= 3824 \text{ W/m}^2 \text{ K}$$

Discussion: Rezkallah and Sims (1987) made two-phase heat transfer measurements for similar experimental conditions and found that $h_{TP} \approx 3900$ W/m² K. The value of h_{TP} predicted by Ghajar and Tang (2009) and that by Reynolds analogy of Tang and Ghajar (2011) is within ±10% and ±2% deviation from their measured values, respectively. The general heat transfer correlation and Reynolds analogy–based heat transfer correlation are sensitive to the void fraction (through F_P and ρ_M). Note that in case if the two-phase frictional pressure drop is not known, the accuracy of the Reynolds analogy concept depends on the choice of two-phase frictional multiplier correlation appropriate to the two-phase flow under consideration.

Nomenclature

Symbols	Description
a_1	Variable in the correlation of Xiong and Chung (2006)
A	Cross-sectional area (m²)
B_s	Variable in Chisholm (1973)
c_1	Variable in the correlation of Bhagwat and Ghajar (2014)
c_2	Variable in the correlation of Bhagwat and Ghajar (2014)
c_3	Variable in the correlation of Bhagwat and Ghajar (2014)
C	Constant in the parameter of Lockhart and Martinelli (1949)
C_o	Distribution parameter
$C_{o,1}$	Variable used by Bhagwat and Ghajar (2014)
C_1	Variable in the correlation of Bhagwat and Ghajar (2015a)

C_2	Variable in the correlation of Bhagwat and Ghajar (2015a)
C_3	Variable in the correlation of Bhagwat and Ghajar (2015a)
C_4	Variable in the correlation of Bhagwat and Ghajar (2015a)
d	Local distance along the pipe diameter
d_{def}	Bubble diameter above which bubble is deformed
$d_{\max}$	Maximum bubble diameter
d_{migr}	Bubble diameter below which migration of bubbles is prevented
dp/dz	Pressure gradient (Pa/m)
$(dp/dz)^+$	Nondimensional pressure gradient
D	Pipe diameter (m)
D_h	Hydraulic diameter (m)
D^+	Nondimensional pipe diameter used by Bhagwat and Ghajar (2015a)
D_h^+	Nondimensional hydraulic diameter by Kataoka and Ishii (1987)
E	Liquid entrainment fraction
Eo	Eötvös number
f	Fanning friction factor
F, Fr	Froude number
F_p	Flow pattern factor
F_s	Shape factor
g	Acceleration due to gravity (m/s^2)
G	Mass flux (kg/m^2 s)
h	Variable in Cioncolini and Thome (2012a) correlation
h_L	Liquid level in stratified flow (m), single-phase heat transfer coefficient (W/m^2 K)
h_{TP}	Two-phase heat transfer coefficient (W/m^2 K)
I	Inclination factor
k	Thermal conductivity (W/mK)
La	Laplace number
$\dot{m}$	Mass flow rate (kg/s)
n	Variable in the correlation of Cioncolini and Thome (2012a)
N_μ	Viscosity number
p	Pressure (Pa)
P	Perimeter (m)
Pr	Prandtl number
q	Exponent in SFM Equation 3.28
r	Exponent in SFM Equation 3.28
Re	Reynolds number
s	Exponent in SFM Equation 3.28
S	Slip ratio
T	Taitel and Dukler (1976) parameter
U	Phase velocity (m/s)
U_b	Bubble velocity (m/s)
U_{GM}	Drift velocity (m/s)
U_{GM}^+	Nondimensional drift velocity by Kataoka and Ishii (1987)
$U_{SG,t}$	Superficial gas velocity at smooth to wavy stratified flow transition (m/s)
v	Specific volume (m^3/kg)
V	Volume (m^3)
We	Weber number
x	Two-phase flow quality
X	The parameter of Lockhart and Martinelli (1949)
Y	The parameter of Taitel and Dukler (1976), the parameter of Chisholm (1973)

Greek Symbols

α	Void fraction
β	Volume fraction of liquid film
δ	Liquid film thickness in annular flow (m)
$\Delta\rho$	Density difference (kg/m^3)

ε	Roughness (m)
μ	Dynamic viscosity (Pa s)
ν	Kinematic viscosity (m^2/s)
σ	Surface tension (N/m)
ρ	Density (kg/m^3)
λ	Gas volumetric flow fraction
τ	Shear stress (N/m^2)
θ	Pipe orientation (°)
ϕ	Fraction of pipe circumference occupied by liquid phase
Φ^2	Two-phase frictional multiplier
Ψ	Angle subtended by liquid phase with pipe centerline (radian)
ξ	Correction factor in Equation 3.132

Subscripts

a	Accelerational
atm	Atmospheric
c	Gas core
C	Critical
f	Frictional
G	Gas
GO	Gas only
h	Hydrostatic
i	Interface
j	Phase
L	Liquid
LF	Liquid film
LO	Liquid only
max	Maximum
M	Mixture
S	Superficial
sys	System
t	Total
tt	Turbulent–turbulent
TP	Two phase
w	Wall

Superscripts

~	Nondimensional quantities in the model by Taitel and Dukler (1976)
+	Nondimensional quantities in the model by Kataoka and Ishii (1987)

References

Abduvayat, P., Manabe, R., and Arihara, N., Effects of pressure and pipe diameter on gas-liquid two-phase flow behavior in pipelines, *SPE Annual Technical Conference* SPE 84229, Denver, CO, 2003.

Awad, M.M. and Muzychka, Y.S., Effective property models for homogeneous two-phase flows, *Exp. Therm. Fluid Sci.*, 33, 106–113, 2008.

Badie, S., Hale, C.P., Lawrence, C.J., and Hewitt, G.F., Pressure gradient and holdup in horizontal two phase gas liquid flows with low liquid loading, *Int. J. Multiphase Flow*, 26, 1525–1543, 2000.

Barcozy, C.J., A systematic correlation for two phase pressure drop, *Chem. Eng. Prog.*, 62, 232–249, 1966.

Barnea, D., Transition from annular and from dispersed bubble flow—Unified models for the whole range of pipe inclinations, *Int. J. Multiphase Flow*, 12, 733–744, 1986.

Barnea, D., A unified model for predicting flow pattern transitions for the whole range of pipe inclinations, *Int. J. Multiphase Flow*, 13, 1–12, 1987.

Barnea, D., Shoham, O., and Taitel, Y., Flow pattern transition for downward inclined two phase flow: Horizontal to vertical, *Chem. Eng. Sci.*, 37, 735–740, 1982.

Beattie, D.R.H. and Whalley, P.B., A simple two-phase frictional pressure drop calculation method, *Int. J. Multiphase Flow*, 8, 83–87, 1982.

Beggs, H.D., An experimental study of two phase flow in inclined pipes, PhD thesis, University of Tulsa, Tulsa, OK, 1972.

Bendiksen, K.H., An experimental investigation of the motion of long bubbles in inclined tubes, *Int. J. Multiphase Flow*, 10, 467–483, 1984.

Bhagwat, S.M. and Ghajar, A.J., A flow pattern independent drift flux model based void fraction correlation for a wide range of gas-liquid two phase flow, *Int. J. Multiphase Flow*, 59, 186–205, 2014.

Bhagwat, S.M. and Ghajar, A.J., An empirical model to predict the transition between stratified and non-stratified gas-liquid two phase flow in horizontal and downward inclined pipes, *Heat Transfer Eng.*, 36, 1489–1498, 2015a.

Bhagwat, S.M. and Ghajar, A.J., Modified liquid entrainment fraction correlation for varying pipe orientation and system pressure, *Int. J. Multiphase Flow*, 74, 1–4, 2015b.

Bhagwat, S.M., Mollamahmutoglu, M., and Ghajar, A.J., Experimental investigation and empirical analysis of non-boiling gas-liquid two phase heat transfer in vertical downward pipe orientation, in *Proceedings of ASME 2012 Summer Heat Transfer Conference*, Vol. 2, 2012, pp. 349–359.

Blasius, H., Das Anhlichkeitsgesetz bei Reibungsvorgangen in Flussikeiten, *Gebiete Ingenieurw*, 134, 1913.

Bowers, C.D. and Hrnjak, P.S., Determination of void fraction in separated two phase flows using optical techniques, *International Refrigeration and Air-Conditioning Conference*, Purdue University, West Lafayette, IN, 2010, pp. 2293–2302.

Chen, J.J., A further examination of void fraction in annular two-phase flow, *Int. J. Heat Mass Transfer*, 29, 4269–4272, 1986.

Chen, N.H., An explicit equation for friction factor in pipes, *Ind. Eng. Chem. Fund.*, 18, 296–297, 1979.

Chen, X.T., Cai, X.D., and Brill, J.P., Gas liquid stratified wavy flow in horizontal pipelines, *J. Energy Resour. Technol.*, 119, 209–216, 1997.

Cheng, S.C., Wong, Y.L., and Groeneveld, D.C., CHF prediction for horizontal flow. *International Symposium on Phase Change Heat Transfer*, Chonqing, China, 1988, pp. 211–215.

Chisholm, D., A theoretical basis for the Lockhart-Martinelli correlation for two phase flow, *Int. J. Heat Mass Transfer*, 10, 1767–1778, 1967.

Chisholm, D., Pressure gradients due to the friction during the flow of evaporating two phase mixtures in smooth tubes and channels, *Int. J. Heat Mass Transfer*, 16, 347–358, 1973.

Churchill, S.W., Friction factor equation spans all fluid-flow regimes, *Chem. Eng.*, 7, 91–92, 1977.

Ciccihitti, A., Lombardi, C., Silvestri, M., Soldaini, R., and Zavatarelli, G., Two-phase cooling experiments: Pressure drop, heat transfer and burnout measurements, *Energ. Nucl.*, 7, 407–429, 1960.

Cioncolini, A. and Thome, J.R., Void fraction prediction in annular two phase flow, *Int. J. Multiphase Flow*, 43, 72–84, 2012a.

Cioncolini, A. and Thome, J.R., Entrained liquid fraction prediction in adiabatic and evaporating annular two phase flow, *Nucl. Eng. Des.*, 243, 200–213, 2012b.

Cioncolini, A., Thome, J.R., and Lombardi, C., Unified macro to microscale method to predict two phase frictional pressure drop of annular flows, *Int. J. Multiphase Flow*, 35, 1138–1148, 2009.

Colebrook, C.F., Turbulent flow in pipes, with particular reference to the transition between the smooth and rough pipe laws, *J. Inst. Civil Eng.*, 11, 1938–1939, 1939.

Collier, J.G. and Thome, J.R., *Convective Boiling and Condensation*, 3rd edn., Oxford Science Publications, New Jersey, 1996.

Crawford, T.J., Weinberger, C.B., and Weisman, J., Two phase flow patterns and void fractions in downward flow. Part I: Steady state flow patterns, *Int. J. Multiphase Flow*, 11, 761–782, 1985.

Crowley, C.J., Wallis, G.B., and Barry, J.J., Validation of one-dimensional wave model for the stratified to slug flow regime transition with consequences for wave growth and slug frequency, *Int. J. Multiphase Flow*, 18, 249–271, 1992.

Dix, G.E., Vapor void fractions for forced convection with subcooled boiling at low flow rates. Report NEDO-10491. General Electric Co, 1971.

Ducoulombier, M., Colasson, S., Bonjour, J., and Haberschill, P., Carbon dioxide flow boiling in a single microchannel—Part I: Pressure drops, *Exp. Therm. Fluid Sci.*, 35, 581–596, 2011.

Dukler, A.E., Wicks, M., and Cleveland, R.G., Frictional pressure drop in two phase flow: A comparison of existing correlations for pressure loss and holdup, *AIChE*, 10, 38–43, 1964.

Fang, X.D., Xu, Y., and Zhou, Z.R., New correlations of single phase friction factor for turbulent pipe flow and evaluation of existing single phase friction factor correlations, *Nucl. Eng. Des.*, 241, 897–902, 2011.

Fore, L.B., Beus, S.G., and Bauer, R.C., Interfacial friction in gas-liquid annular flow: Analogies to full and transitional roughness, *Int. J. Multiphase Flow*, 26, 1755–1769, 2000.

Fukano, T. and Furukawa, T., Prediction of the effects of liquid viscosity on interfacial shear stress and frictional pressure drop in vertical upward gas-liquid annular flow, *Int. J. Multiphase Flow*, 24, 587–603, 1998.

Ghajar, A.J. and Bhagwat, S.M., Non-boiling gas-liquid two phase flow phenomenon in near horizontal, upward and downward inclined pipe orientations, *Int. J. Mech. Aerosp. Ind. Mechatron. Eng.*, 8, 1039–1053, 2014a.

Ghajar, A.J. and Bhagwat, S.M., Flow patterns, void fraction and pressure drop in gas-liquid two phase flow at different pipe orientations, *Front. Prog. Multiphase Flow*, 157–212, 2014b (Chapter 4).

Ghajar, A.J. and Tang, C.C., Advances in void fraction, flow pattern maps and non-boiling heat transfer two phase flow in pipes with various inclinations, *Adv. Multiphase Flow Heat Transfer*, 1, 1–52, 2009.

Ghajar, A.J. and Tang, C.C., Importance of non-boiling two phase flow heat transfer in pipes for industrial applications, *Heat Transfer Eng.*, 31, 711–732, 2010.

Godbole, P.V., Tang, C.C., and Ghajar, A.J., Comparison of void fraction correlations for different flow patterns in upward vertical two phase flow, *Heat Transfer Eng.*, 32, 843–860, 2011.

Gokcal, B., An experimental and theoretical investigation of slug flow for high oil viscosity in horizontal pipes, PhD thesis, University of Tulsa, Tulsa, OK, 2008.

Gokcal, B., Al-Sarkhi, A., and Sarica, C., Effects of high oil viscosity on drift velocity for horizontal and upward inclined pipes, *SPE Proj. Fac. Const.*, 4, 32–40, 2009.

Gomez, L., Shoham, O., Schmidt, Z., Choshki, R., and Northug, T., Unified mechanistic model for steady state two phase flow: Horizontal to upward vertical flow, *Soc. Petrol. Eng.*, 5, 339–350, 2000.

Hamersma, P.J. and Hart, J., A pressure drop correlation for gas-liquid pipe flow with a small liquid holdup, *Chem. Eng. Sci.*, 42, 1187–1196, 1987.

Haramathy, T.Z., Velocity of large drops and bubbles in media of infinite or restricted extent, *AIChE J.*, 6, 281–288, 1960.

Hart, J., Hamersma, P.J., and Fortuin, J.M.H., Correlations predicting frictional pressure drop and liquid holdup during horizontal gas-liquid pipe flow with a small liquid holdup, *Int. J. Multiphase Flow*, 15, 947–964, 1989.

Henstock, W.H. and Hanratty, J., The interfacial drag and the height of the wall layer in annular flows, *AIChE J.*, 22, 990–999, 1976.

Hewitt, G., Lacey, P.M.C., and Nicholls, B., Transitions in film flow in vertical tube, in *Proceedings of Two Phase Flow Symposium*, Exeter, U.K., Paper B4 2, 1965.

Hewitt, G.F. and Hall-Taylor, N.S., *Annular Two Phase Flow*, 1st edn., Pergamon Press, Oxford, U.K., 1970.

Hewitt, G.F. and Lacey, P.M.C., The breakdown of the liquid film in annular two phase flow, *Int. J. Heat Mass Transfer*, 8, 781–791, 1965.

Hewitt, G.F., Martin, C.J., and Wilkes, N.S., Experimental and modeling studies of churn-annular flow in the region between flow reversal and the pressure drop minimum, *Physicochem. Hydrodyn.*, 6, 69–86, 1985.

Hewitt, G.F. and Roberts, D.N., Studies of two phase flow patterns by simultaneous x-ray and flash photography, Technical Report AERE-M 2159. Atomic Energy Research Establishment, Harwell, Oxfordshire, England, 1969.

Hibiki, T. and Ishii, M., One-dimensional drift flux model and constitutive equations for relative motion between phases in various two-phase flow regimes, *Int. J. Heat Mass Transfer*, 46, 4935–4948, 2003.

Hlaing, N.D., Sirivat, A., Siemanond, K., and Wilkes, J.O., Vertical two phase flow regimes and pressure gradients: Effect of viscosity, *Exp. Therm. Fluid Sci.*, 31, 567–577, 2007.

Ishii, M. and Grolmes, M.A., Inception criteria for droplet entrainment in two phase cocurrent film flow, *AIChE J.*, 21, 308–318, 1975.

Ishii, M. and Mishima, K., Droplet entrainment correlation in annular two phase flow, *Int. J. Heat Mass Transfer*, 32, 1835–1846, 1989.

Kaji, M. and Azzopardi, B.J., The effect of pipe diameter on the structure of gas-liquid flow in vertical pipes, *Int. J. Multiphase Flow*, 36, 303–313, 2010.

Kataoka, I. and Ishii, M., Drift flux model for large diameter pipe and new correlation for pool void fraction, *Int. J. Heat Mass Transfer*, 30, 1927–1939, 1987.

Laurinat, J.E., Hanratty, T.J., and Dallman, J.C., Pressure drop and film height measurements for annular gas-liquid flow, *Int. J. Multiphase Flow*, 10, 341–356, 1984.

Lips, S. and Meyer, J.P., Experimental study of convective condensation in an inclined smooth tube. Part II: Inclination effect on pressure drop and void fraction, *Int. J. Heat Mass Transfer*, 55, 405–412, 2012.
Lockhart, R.W. and Martinelli, R.C., Proposed correlation of data for isothermal two phase, two component flow in pipes, *Chem. Eng. Prog.*, 45, 39–48, 1949.
Mandhane, J.M., Gregory, G.A., and Aziz, K., A flow pattern map for gas-liquid flow in horizontal pipes, *Int. J. Multiphase Flow*, 1, 537–553, 1974.
McAdams, W.H., Woods, W.K., and Heroman, L.V., Vaporization inside horizontal tubes—II. Benzene oil mixtures, *Trans. ASME*, 64, 193–200, 1942.
Mishima, K. and Ishii, M., Theoretical prediction of onset of horizontal slug flow, *J. Fluids Eng.*, 102, 441–445, 1980.
Mishima, K. and Ishii, M., Flow regime transition criteria for upward two phase flow in vertical tubes, *Int. J. Heat Mass Transfer*, 27, 723–737, 1984.
Moeck, E.O., Annular dispersed two phase flow and critical heat flux, PhD thesis, McGill University, Montreal, Quebec, Canada, 1970.
Mukherjee, H., An experimental study of inclined two phase flow, PhD thesis, University of Tulsa, Tulsa, OK, 1979.
Muller-Steinhagen, H. and Heck, K., A simple friction pressure drop correlation for two-phase flow in pipes, *Chem. Eng. Proc.*, 20, 297–308, 1986.
Nguyen, V.T., Two phase gas-liquid cocurrent flow: An investigation of holdup, pressure drop and flow patterns in a pipe at various inclinations, PhD thesis, University of Auckland, Auckland, New Zealand, 1975.
Nicklin, D.J., Wilkes, J.O., and Davidson, J.F., Two phase flow in vertical tubes, *Inst. Chem. Eng.*, 40, 61–68, 1962.
Oshinowo, O., Two phase flow in a vertical tube coil, PhD thesis, University of Toronto, Toronto, Ontario, Canada, 1971.
Ottens, M., Hoefsloot, H.C.J., and Kamersma, P.J., Correlations predicting liquid holdup and pressure gradient in steady state nearly horizontal cocurrent gas-liquid pipe flow, *Trans. IChemE*, 79, 581–592, 2001.
Owen, D.G., An experimental and theoretical analysis of equilibrium annular flow, PhD thesis, University of Birmingham, Birmingham, U.K., 1986.
Quiben, J.M. and Thome, J.R., Flow pattern based two phase frictional pressure drop model for horizontal tubes. Part I: Diabetic and adiabatic experimental study, *Int. J. Heat Fluid Flow*, 28, 1049–1059, 2007.
Rezkallah, K.S. and Sims, G.E., An examination of correlations of mean heat transfer coefficients in two-phase and two-component flow in vertical tubes, *AIChE Symp. Ser.*, 83, 109–114, 1987.
Rouhani, S.Z. and Axelsson, E., Calculation of void volume fraction in the subcooled and quality boiling regions, *Int. J. Heat Mass Transfer*, 13, 383–393, 1970.
Shannak, B.A., Frictional pressure drop of gas liquid two-phase flow in pipes, *Nucl. Eng. Des.*, 238, 3277–3284, 2008.
Smith, S.L., Void fraction in two phase flow: A correlation based on an equal velocity head model, *Inst. Mech. Eng.*, 184, Part 1, 647–657, 1969.
Spedding, P.L., Che, J.J.J., and Nguyen, N.T., Pressure drop in two phase gas-liquid flow in inclined pipes, *Int. J. Multiphase Flow*, 8, 407–431, 1982.
Taitel, Y., Barnea, D., and Dukler, A.E., Modeling flow pattern transitions for steady upward gas-liquid flow in vertical tubes, *AIChE J.*, 26, 345–354, 1980.
Taitel, Y. and Dukler, A.E., A model for predicting flow regime transitions in horizontal and near horizontal gas-liquid flow, *AIChE J.*, 22, 47–55, 1976.
Tang, C.C., A study of heat transfer in non-boiling two phase gas liquid flow in pipes for horizontal, slightly inclined and vertical orientations, PhD thesis, Oklahoma State University, Stillwater, OK, 2011.
Tang, C.C. and Ghajar, A.J., A mechanistic heat transfer correlation for non-boiling two-phase flow in horizontal, inclined and vertical pipes, in *Proceedings of AJTEC 2011 ASME/JSME Eighth Thermal Engineering Joint Conference*, Paper No. AJTEC2011-44114, Honolulu, Hawaii, 2011.
Turner, J.M. and Wallis, G.B., The separate cylinders model of two phase flow, Technical Report No. NYO-3114-6. Thayer's School of Engineering, Dartmouth College, Hanover, NH, 1965.
Wallis, G.B., The onset of droplet entrainment in annular gas-liquid flow, General Electric Report No. 62GL 127, Schenectady, New York, 1962.
Weisman, J. and Kang, S.Y., Flow pattern transitions in vertical and upward inclined lines, *Int. J. Multiphase Flow*, 7, 271–291, 1981.

Woldesemayat, M.A. and Ghajar, A.J., Comparison of void fraction correlations for different flow patterns in horizontal and upward inclined pipes, *Int. J. Multiphase Flow*, 33, 347–370, 2007.

Wongs-ngam, J., Nualboonrueng, T., and Wongwises, S., Performance of smooth and micro-finned tubes in high mass flux region of R-134a during condensation, *Heat Mass Transfer*, 40, 425–435, 2004.

Wongwises, S. and Kongkiatwanitch, W., Interfacial friction factor in vertical upward gas-liquid annular two phase flow, *Int. Commun. Heat Mass Transfer*, 28, 323–336, 2001.

Xiong, R. and Chung, J.N., Size effect on adiabatic gas-liquid two phase flow map and void fraction in micro-channels, in *Proceedings of International Mechanical Engineering Congress and Exposition*, Chicago, IL, 2006.

Xu, Y. and Fang, X., A new correlation of two phase frictional pressure drop for evaporating two phase flow in pipes, *Int. J. Refrigerat.*, 35, 2039–2050, 2012.

Xu, Y. and Fang, X., Correlations of void fraction for two phase refrigerant flow in pipes, *Appl. Therm. Eng.*, 64, 242–251, 2014.

Zhang, W., Hibiki, T., and Mishima, K., Correlations of two phase frictional pressure drop and void fraction in mini-channel, *Heat Mass Transfer*, 53, 433–465, 2010.

Zivi, S.M., Estimation of steady state steam void fraction by means of the principle of minimum entropy production, *Trans. ASME J. Heat Transfer*, 86, 247–252, 1964.